Continuous non-invasive blood pressure monitoring via 3D force sensor and its applications in diagnostics

Sándor Földi

This dissertation is submitted for the degree of
Doctor of Philosophy

Supervisors:
Dr. György Cserey,
Dr. Péter Sótonyi

Roska Tamás Doctoral School of Science and Technology
Faculty of Information Technology and Bionics
Pázmány Péter Catholic University

Budapest, 2019

Összefoglaló

A szív- és érrendszer a teljes emberi szervezetet behálózza, ezért vizsgálatának fontos szerepe van az egészségügyben. A vér kémiai összetételének vizsgálatát széles körben alkalmazzák diagnosztikai célokra, de sokkal több információ is kinyerhető ebből a rendszerből. A vérnyomás és annak hullámterjedése egy jelenleg még kiaknázatlan diagnosztikai lehetőség és egyben alapvető a betegmegfigyelésben is. Manapság diagnosztikai célra leginkább a pillanatnyi vérnyomásértéket használják. Monitorozási célra csak egy széles körben használt megoldás van, az arany standard artériás kanül, mely egy invazív módszer. Ez a disszertáció egy újszerű nem-invazív folytonos vérnyomás monitorozási módszert mutat be, mely betegmegfigyelésre és diagnosztikai célokra is használható.

Ez az újszerű módszer egy 3D erőmérő érzékelőn alapszik. Ezt az érzékelőt a Pázmány Péter Katolikus Egyetem két végzett doktora fejlesztette ki. Nagyon kis erőhatásokat is képes érzékelni, akár az artéria falának mozgását is. Megoldásomban ezt az érzékelőt a csuklónál a radiális artéria fölé kell helyezni, ahol folytonos nyomás görbét képes rögzíteni, mellyel monitorozási és diagnosztikai célok is megvalósíthatók.

Jelen disszertáció két fő témakört mutat be, a folytonos vérnyomás monitorozás validálását és a rendszer pulzusdiagnosztikai alkalmazhatóságának vizsgálatát. A folytonos monitorozás validálása egy másik nem-invazív módszerrel, Millar tonométerrel és invazív artériás kanüllel történt. Utóbbinak két fő lépése volt, először a hullámforma összevetése, ahol csak a felvett görbék alakja számított szívciklusonként, majd a tényleges vérnyomás értékek összehasonlítása. A pulzusdiagnosztika esetében egy 175 alanyt magába foglaló adatbázis felvételét valósítottam meg.

Az eredmények erős korrelációt mutattak, mind a Millar tonométerrel, mind az artériás kanüllel szemben. Az átlagos korreláció 0,85 és 0,9 közötti. A vérnyomásértékek összehasonlításához Bland-Altman módszert alkalmazva a legtöbb érték az Association for the Advancement of Medical Instrumentation (AAMI) által felállított nemzetközi követelményeken belülre esett, ami 5 Hgmm átlagtól való eltérést és 8 Hgmm szórást jelent. Kivételt képzett a szisztolés érték az invazív kanülhöz hasonlítva. A diagnosztikai témakörben sikerült hullámforma jelölteket találni néhány egészségi állapotra, mely analóg az irodalomban megtalálhatókkal.

A disszertációm egy rövid bevezetéssel indul, majd az elméleti háttérrel folytatódik, bemutatva a szív- és érrendszer fiziológiai hátterét, a vérnyomásmérési módszereket és a pulzusdiagnosztikát. Három fő fejezet foglalja össze a munkámat, az általam alkalmazott módszereket és az elért eredményeimet. Az utolsó fejezet összefoglalja a tézis mondataimat és a bemutatott módszer alkalmazási területeit.

Abstract

Studying the cardiovascular system has a great importance in healthcare as it covers every organs. Besides the widely used diagnostic values acquired by chemical composition of the blood, the cardiovascular system carries much more diagnostic information. Blood pressure (BP) and its propagating waveform also have great potential in diagnostics and it is crucial for patient monitoring. Today, for diagnostics, mainly just the momentary BP value is used. For monitoring, there is only one widely used method, the gold standard arterial cannulation, which is an invasive method with risks. This dissertation introduces a novel non-invasive BP measuring method that can be used for both diagnostics and patient monitoring.

This novel method is based on a 3D force sensor developed by two former PhD students at Pázmány Péter Catholic University. This sensor is sensitive enough to be able to detect alterations of the arterial wall. In my solution, the sensor is attached to the wrist over the radial artery and it can continuously record the pressure waveform, providing information for monitoring and diagnostic purposes.

This dissertation focuses on two main applications of the mentioned novel method: continuous BP monitoring and pulse diagnostics. The continuous monitoring capabilities were validated with another non-invasive method, a Millar tonometer and with the invasive arterial cannula. The latter comparison had two main steps, first, only the waveform was compared, exact BP values were not taken into consideration, and the second, where even the exact BP value comparison was studied. A pulse diagnostic pilot study including 175 participants was conducted as well.

Results suggest a strong similarity compared to the Millar tonometer and the invasive arterial cannula. Average correlation of the compared BP signals were between 0.85 and 0.9. For BP values Bland-Altman plots were utilized, and most of the values, except for systole, when compared to the invasive arterial cannula were within the international requirements set by Association for the Advancement of Medical Instrumentation (AAMI), meaning the bias is within 5 mmHg and the standard deviation is within 8 mmHg. In the diagnostic study different health condition related characteristic waveforms published in previous studies can be detected.

My dissertation starts with a very short introduction and a theoretical background chapter, introducing physiological basis of the cardiovascular system, BP measurement methods and pulse diagnostics. My work, the methods I have applied and the results I have gained, is summarized in three chapters. The last chapter includes my Thesis sentences and the application areas of the presented methods.

Glossary

aorta – The largest artery, originating from the left ventricle of the heart.

arterial cannulation – An invasive method used for continuous arterial blood pressure monitoring in acute and critical care.

arteriole – A smaller artery segment which has more smooth muscle than large arteries. It ends in capillaries.

atherosclerosis – A chronic disease characterized by abnormal thickening and hardening of the arterial walls with resulting loss of elasticity.

atrioventricular valve – Heart valve between each atrium and ventricle.

atrium – A chamber of the heart receiving blood from the corresponding vein and forwards it to the ventricles.

beat-to-beat – Every cardiac cycle, each heartbeat.

brachial artery – The main artery of the upper arm. It divides into the radial and the ulnar arteries.

calcification – A process resulting in stiffening of the arteries. It is caused by the deposition of or conversion into calcium carbonate or some other insoluble calcium compounds.

capillaries – The smallest arterial elements with μm diameters.

dicrotic notch – Also called as *incisura*. The edge point of the *dicrotic wave*.

dicrotic wave – A forward wave in the blood pressure signal, a small uprise in the pressure waveform, which is created by the collision of the heart valves and the blood after the closure of the valves.

insicura – See *dicrotic notch*.

missbeat – An extra beat of the heart, which happens earlier than the end of the cardiac cycle, usually in the repolarisation phase of the heart muscles. As the heart ventricles cannot be filled with blood during this shorter time, the missbeat usually have a lower systolic blood pressure.

myocardial cell – Specialized muscle cells of the heart.

percussion wave – A forward wave in the blood pressure signal reflecting the systolic event.

pericardium – A cavity containing the heart.

precardial – In front of the heart, on the external surface of the chest.

pulmonary circulation – The passage of blood from the right side of the heart through arteries to the lungs where the oxygen absorption occurs and returning to the left side of the heart by veins.

pulmonary trunk – The pulmonary artery originating from the right ventricle of the heart. It forwards the blood from the heart to the lungs.

pulse diagnosis – A non-invasive diagnostic method based on the traditional Chinese medicine.

pulse diagnostics – A non-invasive diagnostic method analysing the blood pressure waveform.

pulse transit time – The time required by the blood pressure wave to arrive at the peripheral measurement point (usually at the wrist over the radial artery) from the heart.

radial artery – An arterial segment originating from the brachial artery located at the forearm.

reflected wave – A backward wave in the blood pressure signal, the reflection from the peripheral arteries.

single-period signal – In this thesis it is considered as the continuous blood pressure waveform of a single heartbeat.

systemic circulation – The passage of arterial blood from the left atrium of the heart through the left ventricle and the systemic arteries. It is connected to most of the organs, except the lungs. It ends in the right atrium.

tonometry – A continuous non-invasive blood pressure measuring method.

tunica externa – Also called adventitia. The outer layer of the blood vessel wall. It is composed of collagenous and elastic fibers.

tunica media – The middle part of the blood vessel wall consisting mainly of circular muscle fibers.

ventricle – A chamber of the heart which receives blood from a corresponding atrium. It forwards the blood to the arteries.

venules – Small vein elements which collect the blood from the capillaries and forward it to veins.

Contents

List of Figures

iv

List of Tables

Chapter 1

Introduction

Cardiovascular monitoring is crucial in patient monitoring, during surgeries, in the ambulance and in intensive care units. In some critical stakes, it is vital to know the blood pressure (BP) values at any moment for the practitioners to be able to take immediate actions when the condition of the patient changes suddenly. Today, the gold standard, widely used method for continuous BP measurements is the invasive arterial cannulation. So far, this method is the most accurate solution, however it has many risks such as haematoma formation, bleeding at the place of puncture and peripheral nerve injury [3].

The classic non-invasive BP measuring method was finalized by Korotkov in the early 1900s. This cuff based method is still widely used, and has not been developed much in the recent decades. The main development was the oscillometric measuring method that led to the usage of the currently most well-known and applied automatized BP measuring devices. However, this method cannot provide detailed information, only one systolic and diastolic BP value and the actual pulse rate at 40 seconds time frame.

There is a growing need for a continuous BP measuring device, due to its potential beneficial features for both practitioners and patients. There are several solutions available, but none of them have been used widespread. It is a great challenge to create a robust non-invasive solution. The most promising solutions are tonometric devices, Peñaz principle based devices and pulse transit time (PTT) based solutions. All of these devices will be introduced in details in the next chapter.

The question would arise, why are these continuous non-invasive BP monitors not used in everyday practice? Is there any other solution which could provide an easier, more robust, more accurate and comfortable option for healthcare workers? Can a non-invasive monitoring device reach the accuracy of the gold standard invasive method? In this Thesis, I attempt to provide answers to some of these questions by introducing a 3D force sensor based novel BP monitoring method.

The OptoForce 3D force sensor-based solution is advantageous, because the 3 dimensional vector can provide information about the relative position of the sensor and the artery. Knowing this relative position is useful during sensor placement, it can help the

user to find the best measuring position. This system can be also more robust during measurements, small position changes of the sensor on the wrist caused by patient movements would not require immediate repositioning, the signal can remain good quality.

Are there other ways how the continuous BP signal can be used? These signals are not only important in patient monitoring, but they can also be important in diagnostic procedures. The shape, characteristics of the signal can provide information about the cardiovascular system and according to the traditional Chinese medicine it can reflect to several internal organ related diseases. The method utilizing these information is called pulse diagnostics. These information can be extracted from the pulse, more specifically from the continuous BP waveform.

Today trends show that an easy to use, compact monitoring device would be a great tool for everyday use as well. There are smart watches, smart phone extensions that can provide information about heart rate, blood oxygenation level and even blood pressure. The accuracy of these devices are still questionable, but by using better and better sensors, it can improve a lot. Also, if there was a sensor, attached to a smart device, which can record the blood pressure waveform and analyse it, a new home diagnostic tool could be developed. This would be a great step forward in prevention by providing an early diagnostic suggestion.

In the following chapters, the theoretical background is summarized including physiology of the cardiovascular system, blood pressure measuring and the current technologies and the background of pulse diagnostics. Then, I introduce my work in three main sections, the applied 3D force sensor and its attachment to the wrist, the blood pressure monitoring and the pulse diagnostics. Afterwards, I conclude my Thesis with summarizing new scientific results and application possibilities of my work.

Chapter 2

Theoretical background

This chapter summarizes the principal theoretical background related to the main topics of Thesis, starting with the physiological knowledge of the cardiovascular system and moving to the current technologies and studies in the cardiovascular monitoring and diagnostics.

2.1 Physiology of the cardiovascular system

It is essential to summarize the basics of the cardiovascular system's physiology to understand the cardiac cycle and other processes that take part in creation of the blood pressure waveform.

2.1.1 Heart and circulation

Heart is the engine of the cardiovascular system, an organ in the chest covered by a double-walled sac, called the pericardium. The pericardium's walls are very close to each other, between them there is aqueous fluid, which is responsible for the protection of the heart during its beating movement [4].

Heart is the centre of the cardiovascular system, which divides this system into two parts, the pulmonary and the systemic circulation. It has four chambers, two atria and two ventricles as shown in Figure 2.1. (source of this figure: Wikipedia[1]). The left side of the heart is the part of the systemic circulation, the right side is part of the pulmonary circulation. The atria receives the blood from the veins and forwards it to the ventricles. Heart valves are the main rectifier elements of the cardiovascular system. There are four valves, two atrioventricular valves, which do not allow the blood to flow back from the ventricles to the atria, and a pulmonary and an aortic valve, which prevent the back flow from the pulmonary trunk and the aorta, respectively, to the ventricles. The opening and the closure of these valves are passive processes, caused by the pressure difference between the two sides of them. The ventricles are getting filled with blood and they

---

[1]https://commons.wikimedia.org/wiki/File:Diagram_of_the_human_heart_(cropped).svg

pump the blood into the arteries. The wall of the left ventricle is thicker than the right side's, because maintaining the systemic circulation requires more pressure, thus more heart muscle.
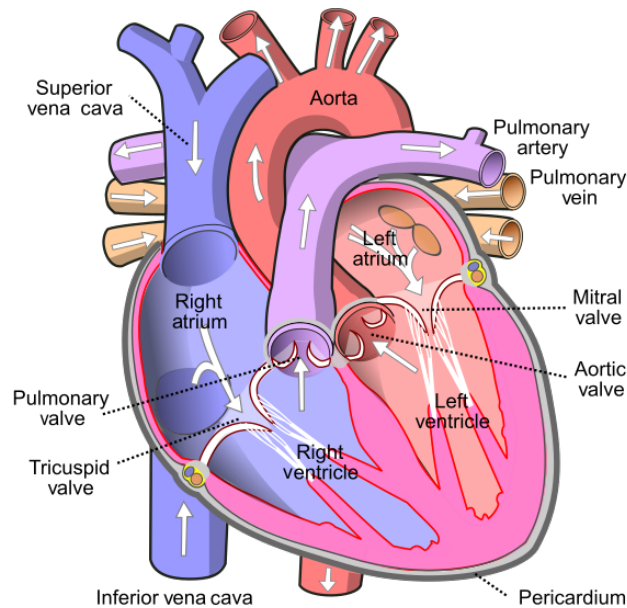
Figure 2.1: Structure of the heart.

Pulmonary circulation consists only of the lungs. It starts of the right ventricle of the heart and ends in the left atria. The main function of the pulmonary circulation is the gas exchange in the blood, the CO_2 leaves the blood cells, and oxygen attaches to it.

The heart consists mostly of myocardial cells, which is a specially differentiated muscle cell. These myocardial cells are connected with gap junctions which provides a very fast depolarization, thus a synchronized, almost simultaneous contraction [5]. Another important property of these cells is that they do not need to rest, they constantly work through the life. Some of these myocardial cells further differentiated creating the conduction system of the heart. This conduction system, shown in Figure 2.2. (source of this figure: Wikipedia[2]) consists of the sinus node, the atrioventricular node, the bundles of His and the Tawara branches.

In average, heart beats 72 per minute, it is called normal heart rate. If this rate is over 100 beats per minute (bpm), then it is called tachycardia and if it is below 50 bpm, it is called bradycardia. The heart has its own pacemaker function, but in a normal case, heart rate is controlled by the autonomous nervous system through signals sent to the sinus node. The electric signal travels through the wall of the atrium to the atrioventricular node. From this node, the signals get to the ventricles, propagating through the bundle

---

[2]https://commons.wikimedia.org/wiki/File:ConductionsystemoftheheartwithouttheHeart-en.svg
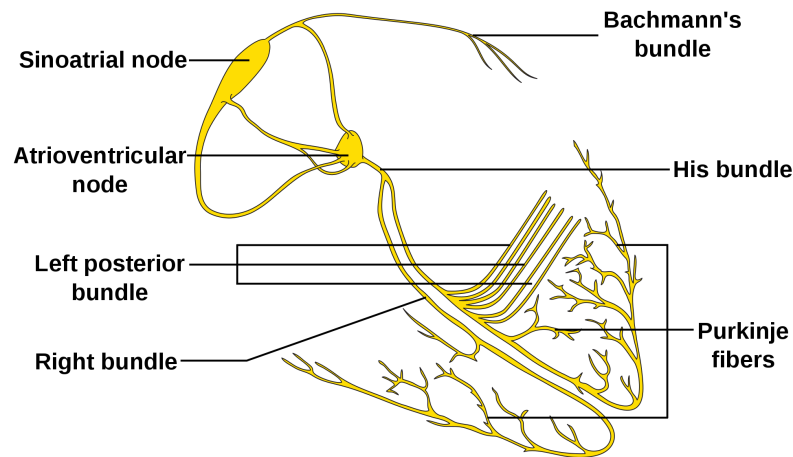
Figure 2.2: The conduction system of the heart.

of His, then the Tawara branches, reaching the ventricle's wall. By the spreading Tawara branches and the fast conducting of the ventricle wall, the myocardial cells are able to contract almost simultaneously.

The heart is usually examined by electrocardiograph (ECG), which measures the electric activity of the cardiac muscles. By ECG the potential changes can be measured. To measure this activity, electrodes are attached to the chest. The positions of the electrodes are shown in Figure. 2.3. (source of this figure: Wikipedia[3]). The muscle activity and thus the measurable electric signal reflects the events of the cardiac cycle, which is introduced in the corresponding subsection later in this dissertation.
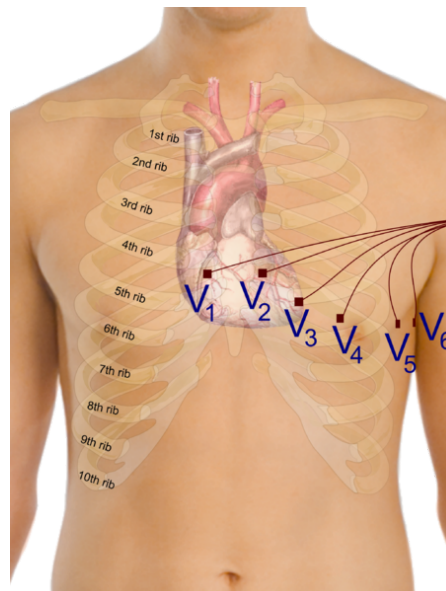
Figure 2.3: Positions of the precordial electrodes on the chest.

---

[3]https://commons.wikimedia.org/wiki/File:Precordial_leads_in_ECG.png

In this Thesis, the main focus is on the systemic circulation. This circulation covers the whole body, all the organs except the lungs. The main function of the systemic circulation is transporting oxygen and nutrient to the cells of the organs and the body while also collecting the metabolic by-products. Therefore, systemic circulation is connected and interacts with almost all cells of the human body, and therefore can store information about it.

2.1.2 Elements of the vascular system

The vascular system consists of the following elements: arteries, capillaries and veins. The arteries have a relatively large variety in their diameters. The aorta, the largest artery in the body, has an average diameter of 25 mm and wall thickness of 2 mm. The wall of the aorta is elastic and expandable, which is important, because it must bear the blood volume bursts from the left chamber. By the fast expansion and slow contraction, the aorta has a vital part in maintaining the pressure gradient through the diastolic phase in the arterial system. This property of the aorta is called the Windkessel effect.

Large arteries has a diameter between 1 to 10 mm and wall thickness around 1 mm. They are still elastic, but after a threshold pressure/extension, the collagen fibers start to be recruited, which lowers their maximal extension. The main function of the large arteries is transferring blood to the periphery. As the arteries tighten, the blood pressure is getting lower. Small arteries and arterioles are close to the periphery or the internal organs. This type of arteries have more smooth muscle, which is controlled by the autonomous nervous system. By smooth muscle contraction, these parts of the arteries can change their diameter, controlling the amount of blood flowing to the organs. For example, under stress or shock, more blood reaches the brain, but during digestion, stomach gets more blood.

Arteries end in the micro-vascular system. These small vessels' wall have only one layer. The metabolic processes happen here. The blood pressure in the microvessels is low, below 1 mmHg, and the blood flow is slow. The microvessels ends in the venules, small diameter veins which collect, merge the microarteries to root back in higher diameter vessels. The venules end in veins. The main function of the veins is to drive the blood back to the heart. To be able to do this, valves in the veins' walls have a crucial part, which prevent the back flow of the blood against the effects of the gravity. In the veins the blood pressure is between 3 to 6 mmHg. As a summary the connection between the elements of the vascular system is shown in Figure 2.4. (source of this figure: Wikipedia[4]).

The wall of the arteries typically has 3 layers: endothelial layer, tunica media and tunica externa, also called adventitia [4]. The innermost layer is the endothelial, which consists of a single cell layer. The main function of this layer is to provide a very smooth

---

[4]`https://commons.wikimedia.org/wiki/File:Illu_capillary.jpg`
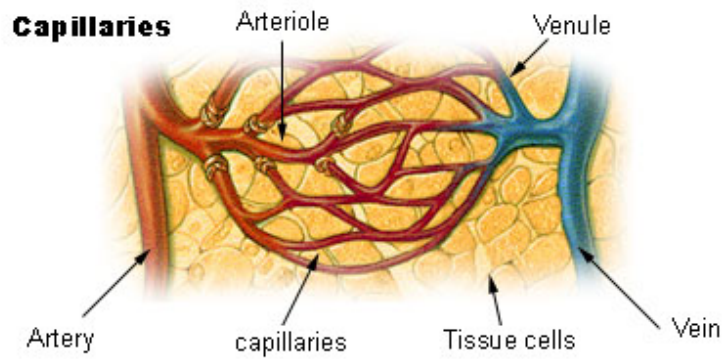
Figure 2.4: Connection between the elements of the vascular system.

surface, which prevents sedimentation and when the arteries is externally closed it prevents the sticking of the artery's wall. Tunica media is the middle layer. It consists of elastic fibers and smooth muscles. In larger arteries elastic fibers dominate, but in smaller arteries the proportion of smooth muscles increase. The adventitia mainly consists of collagen fibers, and vasa vasorums (vessels providing blood to the cells of the arterial wall). The main function of this layer is to provide nutrients and oxygen to the cells of the arterial wall, and prevent the arterial wall from injury by collagen fibers in the case of high blood pressure.

2.1.3   Cardiac cycle

The cardiac cycle is the source of the blood pressure wave formation. It can be divided into two main parts, systolic and diastolic events. Both parts can be divided further to an early and a late stage. At the start of the early systolic phase the ventricles are filled with blood, the semilunar (aortic and the pulmonary) valves are closed and the atria start to contract which pumps the blood from them to the ventricles. In the ECG signal this phase can be recognized by the P wave. Also the cardiac muscles of the chambers start to contract, the pressure in the ventricles increases, but the valves at the pulmonary trunk and the aorta are still closed. It refers to the start of the QRS complex in the ECG. In the beginning of the late systolic phase, the pressure inside the ventricles reaches the pressure in the arteries, thus the semilunar valves open and the blood flows to the arteries, while the cardiac muscles reach their peak contraction. As the blood pumped out from the heart ventricles, the pressure starts to fall and the semilunar valves close, the repolarization of heart muscles starts (T wave on the ECG).

The next phase is the early diastole, which is rather short. In this phase, the cardiac muscles start to relax, the atrial valves open and the ventricles start to fill with blood. In the late diastolic phase, the heart muscles completely relax and the ventricles continue to

fill with blood. The completion of the repolarization can be recognized by the isoelectric phase after the T wave in the ECG.

The physiological events during the cardiac cycle is presented in Figure 2.5 (source of this figure: Wikipedia[5]).
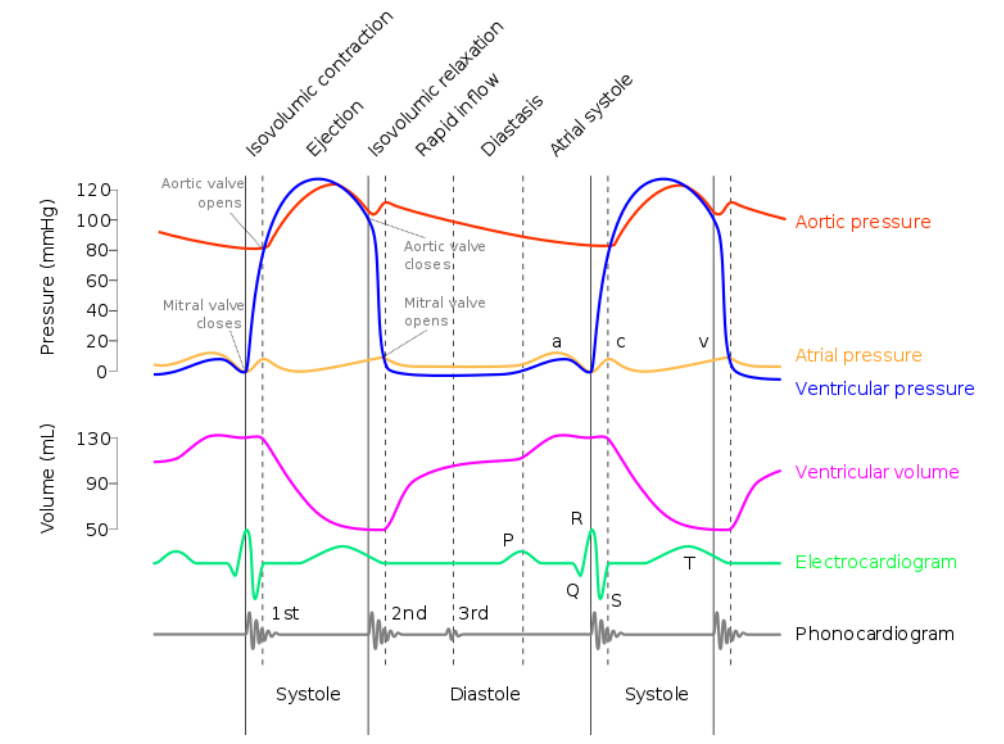
Figure 2.5: Events during a cardiac cycle with different modalities.

2.1.4   Pressure wave propagation and waveform

The repeated circulation of the systolic and the diastolic phase creates the blood pressure wave which propagates through the cardiovascular system. This pulsatile wave changes a lot throughout the vascular system.

Studying the propagation of the pressure waveform is part of the hemodynamics. Examining the blood flow usually several assumptions should be made. One of these is that the blood flow is considered laminar flow, which is a flow type having layers flowing on each other and the molecules in each layer can only move between layers by molecular diffusion. The blood flow usually considered as stationary flow, meaning the flow speed vector does not change in time any point inside the vessel. Another assumption is that the blood is considered Newtonian fluid meaning that the connection between shear stress and speed is linear. This latter assumption is almost true in large arteries.

---

[5]https://commons.wikimedia.org/wiki/File:Wiggers_Diagram_2.svg

A typical BP waveform at the radial artery at the wrist can be seen in Figure 2.6. This typical waveform consists of three waves, two forward propagating wave, the percussion wave and the dicrotic wave, and a backward propagating wave, the reflected wave. The initial point of each heart cycle is the onset point which refers to the diastolic point (lowest BP in a heart cycle). The percussion wave refers to the systolic event, by a fast uprise in BP amplitude. Reflected wave is the reflection of the blood flow from the peripheral arterial site. The arrival of this wave can significantly modify the characteristic of the blood pressure waveform, so it is crucial in pulse diagnostics. The dicrotic wave (dicrotic notch) refers to the closure of the aortic valves. The closure of the heart valves creates a vacuum effect at the initial aorta, which causes a small backflow. This backflow leads to a collision at the heart valves leading to a small pressure uprise. The sum of these three waves characterizes the shape of the blood pressure signal.
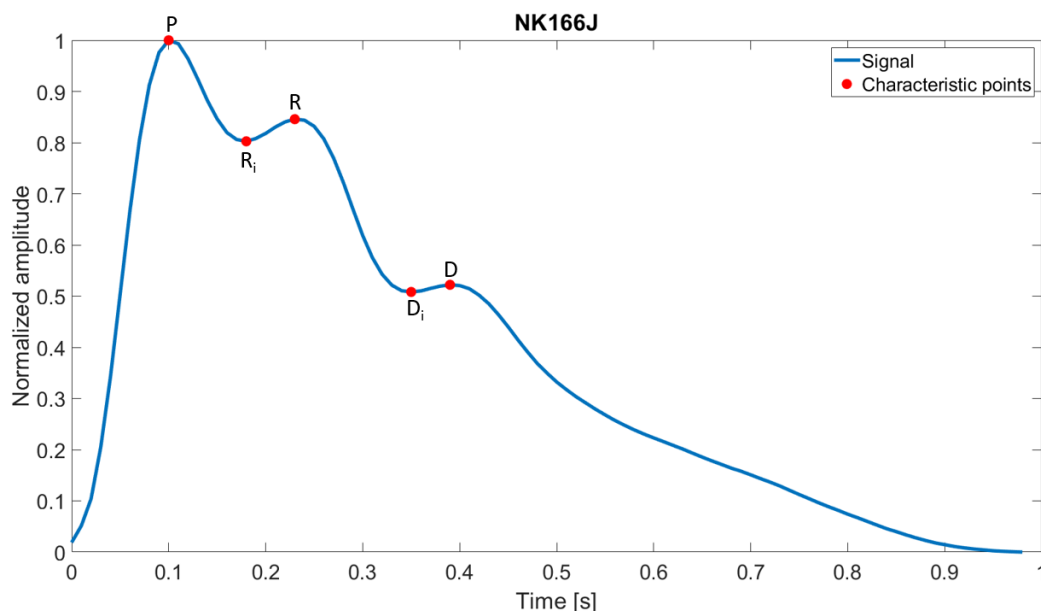
Figure 2.6: A typical healthy BP waveform with its characteristic points. P–peak of the percussion wave, R_i–Initial point of the reflected wave, R–peak of the reflected wave, D_i–initial point of the dicrotic wave, D–dicrotic notch.

The BP waveform can vary between different health conditions. For example, when the arteries are getting stiffer, the reflected wave can seemingly disappear by merging with the percussion wave, since in stiffer arteries the pressure wave propagation is faster. Usually elderly people's pulse signals show this waveform change. Similar distortion arises in hypertensive patients, where the reflected wave arrives earlier and with a much higher amplitude. These examples are shown later in the Pulse diagnostics chapter.

BP waveforms can be divided into three main categories based on the number of visually distinguishable waves: the TRIWave, where all the above mentioned waves are visually distinguishable meaning that five characteristic points can be defined; the DUOWave,

where these waves merge with one another, creating two visually distinguishable waves and three characteristic points; and those signals where seemingly there is only one wave with only one characteristic point, the peak of the percussion wave.

2.1.5 External and internal factors affecting the cardiovascular system

Due to its complex nature and connections throughout the whole body the cardiovascular system is affected by many internal and external factors. This very complex homeostatic system is controlled by both the autonomous nervous system and the endocrine system. Moreover, the cardiovascular system owns a reasonable role in maintaining the homeostasis of the body. Listing all the effects on the cardiovascular system is not an aim of this Thesis, only several examples will be briefly introduced.

Smoking is a well-known factor which greatly affects the cardiovascular system. Smoking increases the risk of atherosclerosis. As the consequence of this disease the arterial walls are calcified making it much stiffer compared to healthy arteries.

Another well known factor is the stress. Today, people are getting more and more stressed, being under pressure both in their work and personal life. This means that the body is continuously in an alert state, often meaning higher blood pressure. Having high blood pressure for a longer period of time harms the arterial wall, leading again to hypertension, which is a vicious circle. Also hypertension rises the possibility of stroke and heart attack, by having a greater chance of arterial or microvascular wall tearing.

Several other effects can be considered such as physical activity, nutrition and diet, socioeconomic state, social networks [6]. These all have effects on the states of the arteries, on their stiffness and thus the measurable blood pressure characteristics.

2.2 Blood pressure measurement

Studying the parameters of the cardiovascular system roots back to the ancient civilizations, where the pulse was considered as the sign of the life. For a very long period of history, only the pulse and the pulse rate could be examined by the medical practitioners. The first blood pressure measurement was conducted in the XVII. century by Stephen Hales, who measured the arterial blood pressure of a horse. In his experiment the arterial blood pressure of a horse was measured through an invasive procedure which caused the death of the horse.

Fortunately, since then, blood pressure measurement methods have been developed a lot. There are invasive methods which are no longer lethal to the patients of course and more and more non-invasive solutions are starting to appear. Measuring the blood pressure is a difficult task. The circulation is a closed loop system, which carries risks connected to the measuring device. In the next subsections, the currently applied blood pressure measuring and monitoring technologies and methods are introduced.

2.2.1 Invasive blood pressure monitoring

Invasive blood pressure monitoring includes arterial catheterization and arterial cannulation. Catheterization is primarily used for diagnostics, examination of the heart, ventricles or aorta. This is a very expensive method and the utilized sensor can be used only once for hygienic and safety reasons. It is able to measure the pressure waveform directly, mostly using a piezo-electric force/pressure sensor.

Currently, invasive arterial cannulation is considered as the gold standard for blood pressure measuring, only measuring the central aortic pressure can reach more accurate data [7]. By this method, the arterial blood pressure can be measured directly and continuously as it is connected through a fluid column to a pressure transducer [3]. Usually the cannula is inserted in the radial artery at the wrist, but in several cases, if the radial artery is not accessible, the brachial artery can also be used. It requires a trained professional to insert the arterial cannula and it is also important to have the adequate aseptic environment. It also means a greater hazard to the patient as it has many risks, like bleeding, haematoma formation, peripheral nerve injury, infection at the cannula site and embolism. Embolism can cause further harms leading to heart attack or stroke [3].

2.2.2 Non-invasive blood pressure monitoring methods

Non-invasive BP monitoring has two main categories, the intermittent and the continuous methods. Intermittent methods are widespread, but has not been developed significantly in the recent decades. However, continuous blood pressure measurement is an emerging area.

Intermittent non-invasive blood pressure measurement can be carried out using cuff-based devices. The most frequently used methods are the manual Korotkov method and the automatic oscillometric method. These methods can provide a systolic and a diastolic blood pressure value in a measurement lasting about 40 second. These devices are cheap, widespread, have an adequate accuracy, but low temporal resolution, meaning it is not continuous (intermittent blood pressure measurement).

Continuous non-invasive BP monitoring is an actively developed area. It has great temporal resolution, it can provide the pressure waveform of a single cardiac cycle. The main challenge is the robustness of these continuous BP measuring devices. They are sensitive to motions and other external effects on the measuring sensors.

For non-invasive blood pressure measurement, there is an international criterion set by the Association for the Advancement of Medical Instrumentation (AAMI) [8, 9]. This criterion set the maximal bias against a validated blood pressure measurement device at 5 mmHg and standard deviation at 8 mmHg. There are many different protocols for BP measurement validation set by the AAMI. Most of them have very high requirements, which is beyond the possibilities that were realistic during my PhD with the introduced

device. These rules were set for the validation of commercially available solutions. I was trying to focus on a good scientific and research quality, thus I chose the AAMI SP10 protocol mentioned in [10] which requires minimum 15 subjects and 10 BP reading pairs per subject. The criterion is the same as above, average difference should be below 5 ± 8 mmHg.

2.2.2.1   Intermittent BP monitoring

Intermittent methods can only provide one systolic and one diastolic BP value within approximately 30 to 60 seconds depending on the method and the manufacturer. The main advantages of these methods are being non-invasive, having low risk for the users and being cost-effective. Thus, these intermittent devices are widely used even at homes, because today's automatized measuring devices do not require any special training or trained personal, they are very simple to operate.

The development of these devices roots back to Scipione Riva Rocci (1863–1937), who was the first to use a cuff to temporarily stop the blood flow. He inflated the cuff above systolic blood pressure, thus closing the brachial artery, while checking the pulse at the wrist. After the pulse stopped, he deflated the cuff slowly. When the pulse reappeared at the radial artery, the systolic blood pressure could be recorded. So this method could only measure the systolic blood pressure, but this was a very important step in blood pressure measuring developments.

The next great development was made by Nikolai Korotkov (1874–1920), whose auscultatory method included an arm cuff and a phonendoscope. Like in Riva Rocci's method the cuff was inflated above the systolic blood pressure. At that point, no sounds can be heard. Slowly deflating the cuff and reaching the systolic pressure value, the so called Korotkov sounds appeared, like a continuously beating sound. The source of these sounds can be related to two phenomenon, the continuously opening and closing arteries or the sound of the turbulent blood flow. Both can be traced back to the partially blocked arteries. The latter is the older theory, which states that when the cuff flattens the artery, thus partially closes it, the blood flow becomes turbulent. The turbulent flow causes collisions between the arterial wall and the blood cells which generates the Korotkov sounds. The other, newer theory states that while the cuff pressure is between the systolic and the diastolic BP, there are periods during a heart cycle when the arteries are closed and periods when the arteries are open. This fluctuation between opened and closed state generates a clapping noise which could be matched to the Korotkov sounds. Further deflating the cuff, the sounds disappeared when the cuff pressure reached the diastolic pressure and the above causes of the sound disappears.

This Korotkov method is still widely and frequently used by practitioners. There were not any new significant development in this intermittent blood pressure measuring method until today. However, automatized versions of this cuff-based method are widely

available. The most frequently used is the oscillometric method. The oscillometric devices measure the oscillations in the blocked artery. The oscillations, like the Korotkov sounds, appear between the systolic and the diastolic blood pressure. These devices can measure the highest oscillation which appears at around the mean arterial pressure and calculate back the systolic and diastolic values. The calculation method differs between the manufacturers and are usually kept as a company secret.

There are other similar cuff-based solutions using different sensors such as ultrasound. By monitoring the rate of the arterial blockage, ultrasound is able to detect the systolic and diastolic values. Also using microphones, the auscultatory method can be automatized.

2.2.2.2 Continuous BP monitoring

BP monitoring is considered continuous when the frequency of the provided BP values are at least beat-to-beat, meaning that for every cardiac cycle, a systolic and a diastolic BP value can be determined. However, more detailed signal (acquired with higher sampling frequency) carries more diagnostic information. In the following subsections, several continuous blood pressure monitoring methods are introduced.

Sphygmograph Sphygmograph is the first continuous non-invasive blood pressure waveform measuring device, developed by E. J. Marey in 1860 [11]. It consists of levers, which are connected to the measuring sensor and the recording pen. The pen is able to draw the continuous pressure waveform on a moving paper by following the movement of the attached sensor. Marey's measuring device is shown in Figure 2.7. (source of this figure: Wikipedia[6]). Although this device foregoes the cuff based blood pressure measurement method, it could not spread widely, since it was not able to give information about the exact blood pressure values, showed only the contour of the blood pressure waveform, which was not useful enough at that time. However, later this device inspired the development of applanation tonometry.
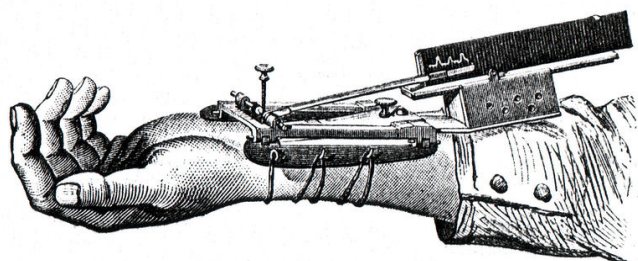
Figure 2.7: E. J. Marey's sphygmograph.

---

[6]https://en.wikipedia.org/wiki/File:Marey_Sphygmograph.jpg

Applanation tonometry   Applanation tonometry is based on the movement of the arterial wall that can be measured by partially closing the artery by pressing it to a solid surface like a bone [12]. The most commonly chosen artery for it is the radial artery at the wrist. Tonometric devices for BP monitoring usually have a pressure stamp, which can sense the small motions of the arterial wall. The location of the sensor is crucial, it has to be placed exactly over the artery in order to get good quality signal. The concept of tonometric sensor positioning is shown in Figure 2.8. Another challenge is the calibration, which can last several minutes. Movement of the patient can also be a problem, because after some movement the system must be recalibrated. Hence, these devices mostly used on anesthetized patients. Tonometric devices can be divided into two categories, the supervised and the unsupervised method.
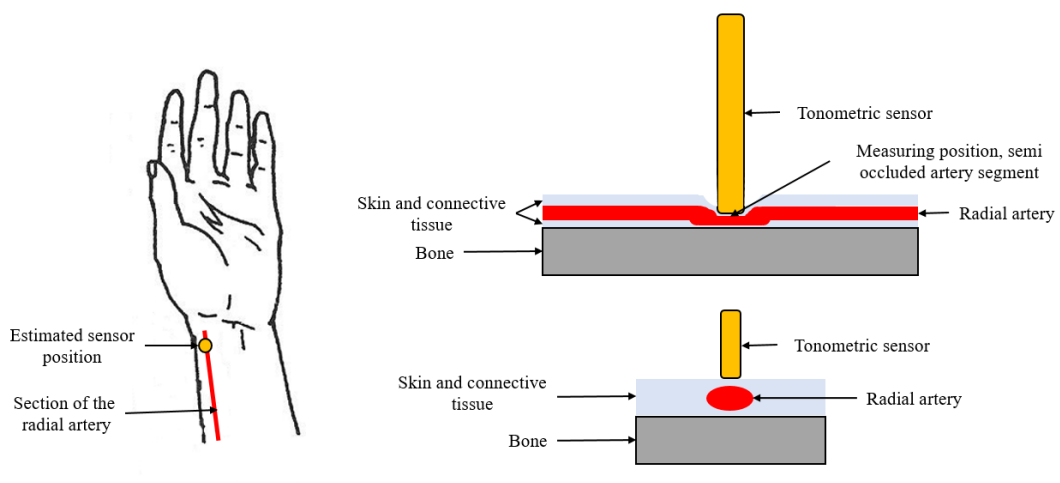
Figure 2.8: The basic concept of tonometry. The measuring position is at the wrist over the radial artery. The tonometric sensor must be pressed to the artery and then the artery have to be pressed to the bone to become semmi-occluded.

The supervised method means that a medical professional holds the sensor at the desired position during the whole time of the examination. These tonometric devices usually have a pen-like structure. In the tip of this pen the measuring transducer, usually a pressure sensing stamp can be found. Examples for such supervised tonometric devices are the Millar tonometer [13], PulsePen device [14] and the SphygmoCor system (also using Millar transducer) [15]. In general the measuring protocol is the following. The patients asked to take a resting position, which could mean a sitting or a lying position. A soft, comfortable support is put under the examined wrist. Then, the medical professional tries to find the best measuring position over the radial artery. If the position is considered adequate, the recording of the signal is started. During the measurement, which is usually one-minute long, the professional tries to hold the sensor at the same position with the same applanation force. The recording is stopped after the decided measurement

length. This protocol can be supplemented by a cuff-based blood pressure measurement for calibration to the current blood pressure of the patient.

This supervised method is great for short term waveform analysis, but cannot be used for a long term monitoring. The supervised nature is advantageous, because the frequency of patient's movement artefacts can be minimized. However, another noise source is integrated in this method – the movement or inaccurate sensor holding of the medical professional.

The other type of applanation tonometric devices is the unsupervised version. These devices require a trained personal only for the sensor installation. During the signal recording or monitoring, the device is attached to the wrist. The usual measuring protocol is the following. First, by touching the wrist the trained personal determines and marks the position of the radial artery of the patient. Then, the measuring device is attached over the marked area and the device starts to adjust its position to the best measuring position by continuously searching for the best quality signal possible. When the adjustment is finished, a calibration takes place. There are two main ways for that, using a cuff-based blood pressure monitor, or using a recorded database which estimates the blood pressure through antropometric characteristics of the patient [16]. After calibration the continuous monitoring can be started.

The main challenge in the unsupervised tonometric method is the displacement of the sensor. This can happen easily during patient movements, but can arise in other situations as well, for example if the professional accidentally pushes the sensor's holder. If the sensor's position changes, the position adjustment and the recalibration must be started over again. It means that the monitoring can be interrupted for minutes. Thus, these tonometric devices usually applied on anaesthetized patients where the patient's movements are unlikely.

The most frequently studied tonometric device is the Tensys TL series [17, 18, 19, 20, 21, 22, 23]. It has a great accuracy as compared to the invasive arterial cannulation, which is promising for a continuous non-invasive blood pressure measuring technique. Moreover, even in the special case of morbidly obese patients it has an acceptable accuracy [24].

Peñaz principle-based BP monitoring   Peñaz principle-based devices have good accuracy in beat-to-beat blood pressure measurements [25, 26, 27, 28, 29, 30]. These devices have one or two finger cuffs each including a photoplethysmograph (PPG) sensor that can measure the blood oxygenation level. This method is also called vascular unloading technique. The main idea behind vascular unloading is to measure the blood oxygenation level continuously on the index and/or the middle finger and by a finger cuff set the measurable signal to a constant line. In details, the blood oxygenation level reflects the events of the cardiac cycle. The measured signal is similar to the arterial pressure waveform, but it is less detailed. It also has to be mentioned that the signal waveform is

also altered by the measuring position, meaning that the finger artery is much smaller in diameter than for example the radial artery. There is a back control loop, which changes the pressure of the finger cuffs to press the finger arteries as much as to keep the PPG signal as a constant line. Therefore, the control loop provides the blood pressure values. The idea behind this measuring method is summarized in Figure 2.9 (source of this figure: Wikipedia[7]).
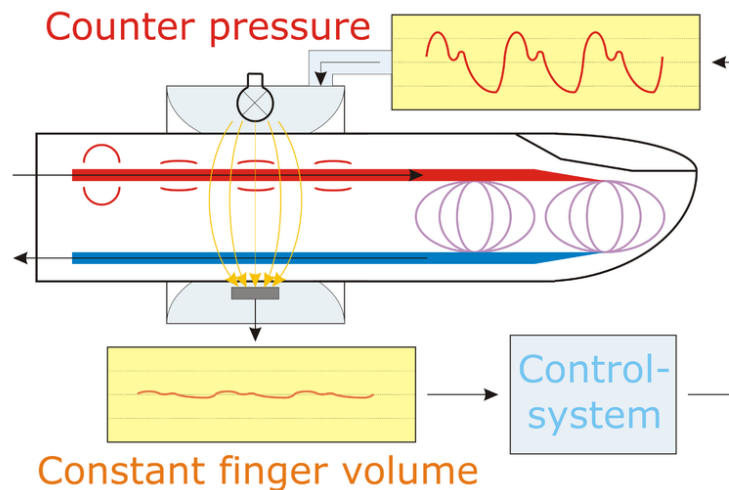
Figure 2.9: Summary of the Peñaz principle-based non-invasive continuous BP monitoring method.

As mentioned above, the finger arteries are much smaller in diameter than the radial or brachial artery, so the measured blood pressure values must be corrected. This correction can be done by precalibration with a brachial oscillometric blood pressure monitor or by a transfer function. When the brachial BP is used, the measuring protocol is similar to the one introduced at the tonometric BP measurement. After the finger cuff is put on, the medical professional measures the brachial BP by the oscillometric device, and calibrate the output of the Peñaz principle based device to that pressure. The other solution is using a transfer function to calculate the radial arterial BP from the BP of the smaller finger arteries. This transfer function based calibration is easier in practice, because it does not require any additional device, but the transfer function is not clearly defined, the parametrization or even the function itself can alter between patients.

Based on the number of utilized fingers this method can be divided into two categories. The one finger version, i.e. BMEYE's Nexfin/Edwards Lifesciences' ClearSight device [27, 31, 32, 33, 34, 35, 36, 37], continuously measures and therefore oppresses the given finger. The two finger version, i.e. CNSystems' CNAP monitor [38, 39, 40, 41, 42, 43, 44], can alter between fingers. By altering between the two fingers at every heart beat, it can

---

[7]https://commons.wikimedia.org/wiki/File:Vascaular_unloading.png

provide smooth blood flow for a short period of time in both fingers. Due to constant oppression of the finger arteries, these devices have a temporal limit for safe use. The recommended time for the one-finger version is 12 hours and for the two finger version is 24 hours.

Most of the limitations of the Peñaz principle based system are given by the utilized PPG sensor's limitations. The factors effecting the accuracy of a PPG include body and air temperature, skin color, condition of the finger arteries, outer light conditions, sweat and age. Some of these effects can change in a longer monitoring period, so the quality of the measured signal can differ during measurement. Also the blood oxygenation level itself should be taken into account. A standard plethysmograph measures the alterations of oxygenation level accurately, while it is above 70%. If it is below that level, the measured signal cannot be considered accurate. In most cases it is not a big problem, but in some patient group such as during a surgery or in the case of heavy smokers, it can cause issues.

Pulse Transit Time   Pulse Transit Time (PTT) is getting popular recently, mainly due to the smart devices used for health applications. This method has a wide variety in the sense of measuring techniques. Basically the typical PTT system consists of an ECG and a measuring device that can give information about the heart cycle at the periphery. For the latter purpose, the most frequently used device is the finger plethysmograph. The idea behind the PTT is to measure the time difference of a given heart beat from initiation to the appearance at the periphery. To do that an ECG and a peripheral pulse waveform measurement must be recorded simultaneously. The PTT can be calculated from the time of the R peak of the ECG to the time of the initial point of the corresponding pulse waveform at the periphery. From PTT and the distance between the heart and the peripheral sensor, the pulse wave velocity (PWV) can be calculated.

Another possible PTT measuring method is to use transducers in two different positions at the periphery. A frequently used solution for that is when two pressure sensors are attached to the forearm, one at the end of the brachial artery at the elbow pit and the other over the radial artery at the wrist. In this case, the distance between the two sensors can be easily measured and because of the same measured modality, the initial phase of the signal is also a bit easier to annotate. But in this case the temporal resolution of the sensors must be very good, the sampling frequency should be at least 1000 Hz.

PWV is proportional to the arterial blood pressure [45], thus a good approximation of the BP can be calculated [46]. This provides a cuffless beat-to-beat blood pressure measuring method, which is very advantageous. Portability is also an advantage. Nowadays, the PTT based BP monitoring method is utilized in almost all the smart devices. Mainly in smart watches [47] and smart phones. These smart devices measure ECG signal and a

peripheral pressure waveform using a simplified plethysmograph. This simplified plethysmograph can be the camera of a smart phone extended with its flash, but of course it is much less accurate than a professional device with red and infrared light.

The limitation of the PTT method is the lack of personalization. The existing functions that converts the PWV to BP are only for estimation and there are not any general parametrization. It is the bottleneck of this method and requires a lot of studies to create a personalizable function that can be used for individualized measurements.

Arteriograph TensioMed's Arteriograph is a Hungarian development. This works as a combination of several above mentioned methods. It uses an oscillometric cuff on the upper arm and a PPG sensor on one finger of the same arm. It combines the two measurements taking reflected waves into account [48]. Due to the detection of the reflected wave, the device can calculate the PWV. The measured blood pressure value by the cuff is used for calibration [49].

2.3   Automatized pulse diagnostics

Pulse diagnostics roots back to the traditional Chinese medicine [50, 51] called as traditional pulse diagnosis. Pulse diagnosis is a non-invasive, painless method without side-effects that can give information of several internal organ's and the cardiovascular system's health and diseases [52]. The main idea behind it is that the cardiovascular system is connected to the whole body, interacts with every organs, and the effects of these interactions appear in the pulse waveform. The pulse waveform is the continuous blood pressure waveform without the actual blood pressure values. This method has not yet been accepted by the western medical practice. But as several other traditional Chinese medicine methods, like acupuncture, it has the potential to become partially accepted. Below, I introduce the automatized pulse diagnostic method, which considers several ideas from the traditional pulse diagnosis, but relies on quantitative measurements.

Automatized pulse diagnostics is based on several different methods, but the main idea is the same behind all of them, which includes measuring a continuous pulse waveform at the wrist, filtering the signal and analysing the data. The measuring technique has a relatively wide range of variability. Several of them can also be used for continuous blood pressure monitoring, like tonometric devices, but there are several other solutions that can measure the waveform itself without taking the exact BP values.

The advantages of the automatized method are the following, it is objective, the diagnostic accuracy can be evaluated, the examination time can be shorter, taking only several minutes. The more reliable diagnosis can also help in popularizing the method, which would be a great step in prevention of several cardiovascular diseases like hypertension.

It is interesting that for pulse waveform measurement not the usual continuous blood pressure monitoring solutions are used, but other devices that are able to record a continuous pulse wave contour or a little modified version of the continuous BP measurement devices. This fact is based on the different requirements for pulse diagnostics. To this diagnostic method, blood pressure itself is not as crucial, it is only a parameter which is beneficial to know, but the signal shape is more critical. The length of the diagnostic measurements is much shorter than it is required for patient monitoring. Thus, any sensor is good for the task which is able to detect arterial wall movement, or blood flow with adequate accuracy. Below, several examples are introduced briefly.

An example for sensors used for pulse diagnostics is ultrasound [53, 54]. Ultrasound can measure blood wave velocity, thus the blood flow at a short section of the artery. Blood flow corresponds to the pulse wave, therefore it can be used for waveform analysis. By ultrasound a spectrogram can be measured, so a preprocessing step is required to get the analysable pulse waveform. The preprocessing step consists of an envelope graph fitting according to the intensity borders.

Another widely used sensors are the piezo-electric pressure transducers [55], pressure sensor arrays [56] and devices based on strain gauges [57, 58]. These are similar to the pressure stamp based tonometric devices, but are usually less accurate, less robust. It is not rare that these measurements have high frequency and low amplitude noises. Also the movement artefacts are a serious challenge, so an adequate signal processing method is required for these signals. Although it has many challenges, this type of transducers are frequently used, because they provide a usable signal quality with a relatively cheap and widely available sensor. Furthermore, sensors can be arranged into a sensor array due to their small size. The sensor array is advantageous, because it can detect the best measuring position. In practice it means that from the sensor array an algorithm chooses the signal with the highest amplitude and this chosen signal is to be processed.

Continuous pulse waveform recording can be done by laser-based distance sensors too. In a pilot study, red laser light was used to detect the movement of the arterial wall at the wrist [59]. This is a contactless measurement method, which makes it very comfortable for the patient. It applies a triangulation method to record the arterial wall movement. The resolution of arterial wall movement detection by this system is better than 4 μm. The device has considerable size, however, for diagnostic purposes it is not an issue.

The signal processing of pulse waveforms generally consists of the following steps:

1. preprocessing, if the measuring method requires it,

2. noise filtering,

3. signal averaging to get the continuous waveform of a single cardiac cycle,

4. feature extraction and classification.

Preprocessing step includes a data representation process, in which the measured modality is transformed into a continuous wave signal. This step is required for example if the signal was recorded by an ultrasound device, but it is not required if the continuous waveform was measured directly for example piezo-transducer based methods.

Noise filtering is crucial, because detailed, clean signal is important for diagnostic decisions. Filtering high frequency noise is a relatively easy task for pulse diagnostic purposes, because wrist pulse signal is a low frequency signal. Thus, filtering the low frequency noises is much more challenging. The main challenge in it that the noise itself can happen with nearly the same frequency as the pulse signal. These low frequency noises can be because of normal breath movements, slow tremor, small finger or hand movements. Noises of a longer or a stronger hand or arm or body movements make even lower frequency noises.

Filtering low frequency noises is even harder when the blood pressure value is also considered as an important information, and not just the signal waveform. It is because diastolic BP and some low frequency noises, mainly breathing movements, are strongly connected. By breathing the signal fluctuates because of two reasons. Once, during breathing the whole body has a small movement. Secondly, during inhale phase the heart is a bit pressed by the lungs and the moving chest, thus causing a slight blood pressure drop. Therefore, the noise generated by breathing cannot be filtered out from blood pressure waveform without losing diastolic information.

When the BP values are not considered important, the baseline wander can be filtered. To do this filtering, zero-phase filters [60], wavelet decomposition filters [61, 62, 63] and classic frequency filters can be applied. An important aspect for the filtering that the pulse waveform should not be distorted, therefore, the parameters of the filters should be carefully set. Zero phase filtering is advantageous, because it has no phase distortion, but it requires more computation time. The frequency filters are easy to be applied, but can distort the signal in some cases such as anomalies in the signal caused by phase shift or the frequency to be filtered is too close to the frequency of the pulse wave signal.

Wavelet decomposition filters for biological signals become more and more popular. Since the early 2000s, the number of studies using wavelet decomposition filtering increases. Wavelet decomposition filtering is beneficial because it provides information not only from the frequency spectrum of the signal, but it also keeps the information about the time domain. In practice, wavelet decomposition filters use a so called mother wavelet function, which must create an orthonormal basis. Using this mother wavelet function and convolution, the signal can be decomposed for a signal approximation and details on a specific level. To gain more information about the signal, continuous wavelet transformation can be used. Applying this method, the time-frequency spectrum can be created for the signal. This is a great help both in finding the best filter parameters and both in checking, whether the applied filter is good enough.

After filtering the signal, the next step is the onset point detection. Onset point is the initial point of each heart beat. There are several techniques to detect onset points, namely, the slope sum function-based method [64], the Hilbert transformation based method [65] or the adaptive windowing method [60]. These methods will be introduced in details in the Pulse diagnostics chapter of this thesis.

When all the onsets are marked, the signal is segmented according to this marks. By the segmentation, the single-period signals are created. The single-period signals are the waveforms of one cardiac cycle. To get the personalized single-period signal, all the single-period signals are averaged. The averaging is made only if the given single-period signals are close to each other. The definition of "close" can differ, depending on the metrics applied. It can mean the absolute difference, or the root mean squared difference, or more generally the distance measure defined by the dynamic time warping algorithm [66]. If there are more distinguishable single-period signal groups with a relevant number of signals, then all these signal groups are specific for the given person.

After the personalized, averaged single-period signal is obtained, feature extraction has to be made. Features include time domain, frequency domain, spatial and relative features. Time domain features are the corresponding time of each characteristic point, presented above in the *Pressure wave propagation and waveform* subsection, of the given pulse signal. Frequency domain features are the strongest frequencies of the frequency spectrum, that can be easily obtained by FFT. Spatial features include the absolute amplitude value, which can be identical to the blood pressure values if it is measured, and the amplitude levels of each characteristic point. Relative values are the ratio of the aforementioned features. These are the basic features of a time series. However, there are other type of features such as autoregressive models [67, 68], feature vector created by independent or principal component analysis and different transformations of the signal, like Hilbert-Huang transformation [69].

To obtain features, the first challenge is to find the characteristic points. For this purpose, there are a lot of solutions. One of the easier algorithms is the derivative based extremum search [70]. This method can work quite well if the signal is lack of major noises, and all the characteristic points appear distinguishably. The derivative based characteristic point search can be improved by analysing slope variability [71]. Another solution is the utilization of wavelet transformation and apply it as a characteristic point detection algorithm [1, 72]. This algorithm uses discrete wavelet decomposition with the adequate decomposition level and by the calculated detail parts, an estimation can be made for the characteristic points. The strength of this method is that it is able to deal with signals, where the peak of the reflected wave is not obvious, not easily distinguishable.

Another commonly used feature extraction method is the independent [73] and the principal component analysis [74]. Both methods create a feature vector from the nor-

malized single-period pulse signals. Description of features can also be done by defining a Gaussian model. Lu et al. [75] presented a three-term weighted Gaussian function, which reached a better classification accuracy than the two-term Gaussian methods [53]. A well parametrized Gaussian model is also useful, because it can provide signal smoothing as well.

In the case of feature extraction, one of the main challenges is the size of the feature set. It has to be optimized by finding the minimum number of features excluding one or more of the strongly correlated ones. For this optimization, statistical analysis is required, usually by cross correlating all the features to one another [53]. A well defined feature set is crucial for an accurate classification.

The last step of pulse diagnostics is classification. There are a wide range of classification methods applied in literature, here only a brief listing is presented. The less accurate methods include different k-nearest neighbour techniques [74, 76, 77, 78] and the support vector machine methods [68, 79]. The more accurate ones are connected to neural networks, the fuzzy neural networks [80], where the knowledge of the practitioners is tried to be involved by fuzzy logic, wavelet networks [81], complex networks [82] and the recently very popular deep or artificial neural networks [83, 84, 85, 86]. A bit different approach is the classification by edit distance with real penalty [55]. This method utilizes the whole single-period signal, thus if the recorded signal has a good quality, then it can reach quite a good accuracy.

Chapter 3

Blood pressure waveform measurement using 3D force sensor

This chapter introduces the 3D force sensor, summarizes my sensor attachment design and protocol.

3.1 OptoForce/OnRobot sensor

OptoForce/OnRobot OMD-20-SE-40N tactile force sensor [87] can measure both the magnitude and the direction of the force applied to its surface. The sensor has a hemispherical dome as shown in Figure 3.1. This device can measure the deformation of its silicone dome by light reflection. In the middle of the sensor there is an infra LED, which emits light. Around the infra LED, there are four light sensing photodiodes in a circle at every 90° from the centre. These photodiodes measure the current generated by the reflected light from its silicone dome. After amplification, the photodiodes' output signals are converted by a 24 bit ADC. The output representation is a 16 bit data, which is sent to the PC via a USB port [88].

During the measurement as the dome deforms, the light intensity on each photodiode changes, thus the measured current also changes. Using these data, a 3D vector can be calculated, which identifies the direction of the force that is applied on the surface of the silicone dome. The calculation method is the intellectual property of OptoForce/OnRobot. An example of the calculation method for 3 photodiodes (an earlier version of the sensor), where the angle between them is 120°, is presented in [89]:

$$F_x = \left(\frac{(S_2 - \beta_2) + (S_3 - \beta_3)}{2} - (S_1 - \beta_1) \right), \tag{3.1}$$

$$F_y = ((S_2 - \beta_2) - (S_3 - \beta_3)), \tag{3.2}$$

$$F_z = \left(\frac{\sum_{i=1}^{3} (S_i - \beta_i)}{3} \right), \tag{3.3}$$

where F_x, F_y and F_z are the 3D vectors' components, β_i is composed of the sensor offset (the measured value of the photodiode without infrared light emission) and the calibration value (the measured value of the photodiode with infrared light emission at no force applied) and S_i is the measured photodiode output value [88].

To read out the OptoForce sensor data from a PC, the OptoForce Data Visualization software can be used. Using this software the sampling frequency and the low pass filtering frequency can be set and the data can be saved to a comma separated values (csv) text file with a user specified file name.

The utilized OptoForce sensor in my work is the OMD-20-SE-40N version. The diameter of its dome is 2 cm. This 3D force sensor is sensitive, it is able to detect a 0.01 mm deformation of its dome and it is also robust, and tolerates a 600% overload compared to its nominal capacity of 40 N. The sampling frequency of the sensor goes up to 1000 Hz, but with specialized hardware it can be increased even further.

The measuring principle is based on infrared light reflection, so the sensor does not emit any harmful radiation. Moreover, the sensing surface is made of silicone rubber, which is a hypoallergenic material and feels comfortable on skin contact. Due to its material, the sensor's disinfection is easy. The sensing method of the sensor is based on the deformation of its dome. Due to external effects, forces on the sensor, the silicone dome deforms. This deformation causes changes in the amount of light detected on each light sensing element.
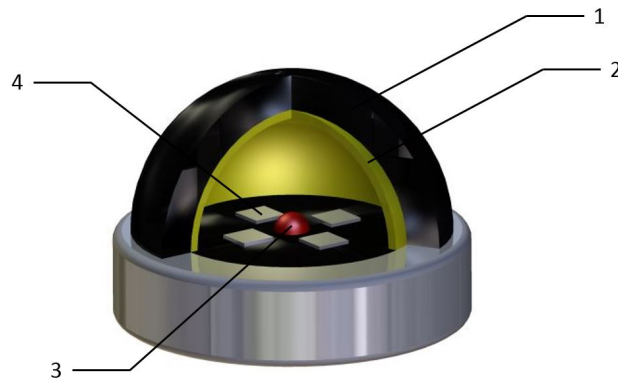
Figure 3.1: Schematic figure of the OptoForce sensor. 1 – sensing surface, 2 – reflective layer, 3 – light emitter, 4 – sensing element.

3D sensing has numerous applications in the field of robotics such as robotic hand or walking robots. Inserting the sensor in the fingertips of a robotic hand leads to advantageous grabbing solutions. It can solve tasks such as grabbing an egg or a bulb without breaking it, like other force sensors, but by 3D sensing it is capable of grabbing and holding a glass even during filling the glass with water. This is possible due to the 3D

sensing. The shear forces appearing as the weight of the glass increases can be detected. An adaptive algorithm can be created for the robotic hand to apply more grabbing force, thus prevent the glass from slipping out of the robotic hand.

Another example from robotics is balance. When this 3D force sensor is utilized in a walking robot's sole, using the 3D force sensing a balancing algorithm can be created for the robot. This balancing algorithm can make the robot capable of walking on rough or imbalance terrain like a broken stair.

The sensing is so sensitive that this 3D force sensor is capable of measuring biological parameters, including muscle contraction and the pulsatile behaviour of the arterial walls, which is the topic of this thesis. In the next section of this dissertation, the main steps of the development is introduced about the target application of this sensor for blood pressure waveform measurement.

3.2 The measurement environment and the protocol based on the 3D pressure sensor

For my work I used the OptoForce/OnRobot 3D force sensor introduced above. This choice was made due to the beneficial attributes of this 3D sensor, compared to other force sensors in the market. In the 2.2.2.2. subsection tonometry was introduced. Most of the tonometric devices utilize different piezoresistive pressure sensors. These sensors can be sensitive enough to measure the pulsatile behaviour of the radial artery. They are relatively cheap and easy to integrate. They can be also small, which is beneficial, because the average diameter of the human radial artery is around 2.2 mm. But as these sensors can measure only the magnitude of the applied force, the positioning of these sensors over the radial artery is crucial. Moreover, slight changes of the sensor position over the radial artery can cause false measurements. In the case of OptoForce 3D force sensor, slight changes of the sensor position can still have good quality signals. This is based on the 3D sensor's measuring concept, it can measure on the whole surface of its dome, if the radial artery is not under the tip of its dome, it can still sense the signal in another point of its dome.

The other promising sensor group which can be applied to record arterial wall alterations is the array sensors. In these sensors the pressure sensing elements are very small so the area around the radial artery can be covered with several of them. An example is introduced in [56]. Using the array, the strongest pulsating point under the array can be identified, and selected as the BP signal, which then can be recorded and further processed. In spite of its great potential, I did not find many occasions where array sensors were used to measure BP signals during my work. This array based method is an interesting concept, which would require more investigation, but it was not the aim of this study.

First, the attachment of the 3D force sensor had to be developed. The first version utilized velcro and a two-sided tape attached to the sensor's bottom. The idea behind it was that the velcro provides wide variability for different wrist sizes which the sensor can be attached to. But this version was not robust enough, the velcro could loosen during measurements and the position of the sensor could change after the movements. For more stability, instead of velcro a strong band was applied with a buckle, which was able to ensure the stability during the measurement. But this solution led to a new challenge, namely during attachment it was difficult to keep the sensor in the desired position, as the sensor's dome usually fell over a bit, not much, but enough to measure much worse signals. Therefore, a sensor holder was designed, using a 3D designer software, Autodesk Inventor Professional (Student version). The designed sensor holder was then printed by a 3D printer (Stratasys Objet24 3D printer). This sensor holder granted more stability for the sensor and also a way to adjust the sensor position after the buckle was closed. My experiences suggest that this sensor attachment method can be easily learned how to use, and provides good stability and it is suitable for different size and shape of wrists. The final design is shown in Figure 3.2.
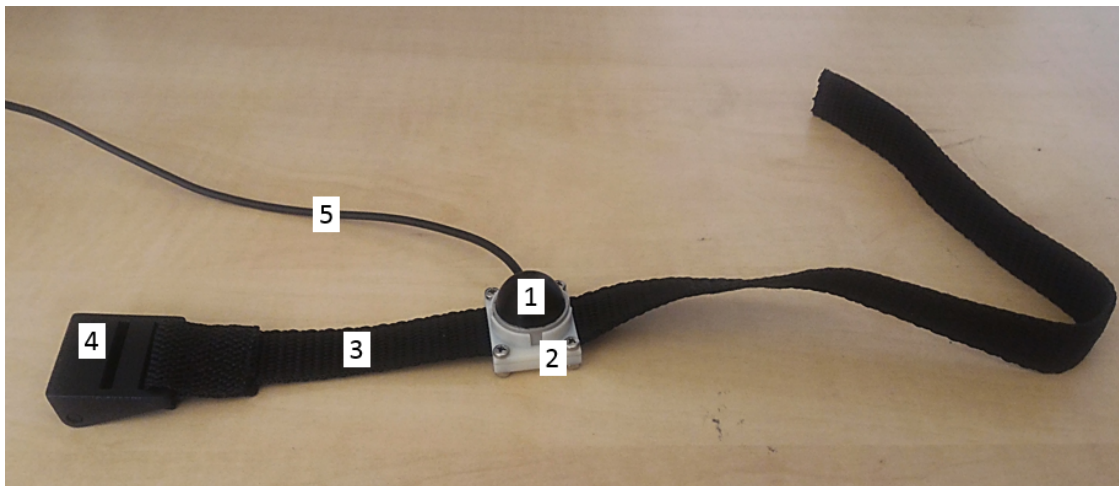
Figure 3.2: Final version of the sensor attachment. 1 – OptoForce OMD-20-SE-40N sensor, 2 – sensor holder, 3 – band, 4 – buckle, 5 – wire of the sensor

To measure good quality signals, the sensor has to be attached at the wrist over the radial artery. Three factors can help to find the best position and evaluate the quality of the signal. First is the 3D force vector, which is better if it is closer to $90°$ from the xy-plane (the basement plane of the sensor). My experiences suggest, that the optimal range of the 3D vector angle from the xy-plane is between $50°$ and $130°$. In this range, the measurable signal can be good quality. The second factor is the difference between the minimal and the maximal amplitude. For the sensor channels (measured values for each light sensing element) it has to be at least 100 units. And the third is the characteristics

of the measured waveform which is currently a visual based decision made on the site, but after well defined quality measures it can be done by a measurement software. This quality measure is still under development.

For sensor installation at the wrist, the following steps must be done:

- The observer attempts to find the radial artery at the wrist by palpation.

- At a strongly pulsating point the sensor is attempted to be attached. The tip of the sensor's dome is put over the strongest pulsating point, then the band is fixed using the buckle.

- A check should be done whether the amplitude of the signal is over 100 units for every channel and the 3D force vector is close to the 90°, if so, the sensor placement is completed. Otherwise, the position of the sensor has to be adjusted by moving the sensor holder on the band or the band must be tightened. In several cases the initial position of the sensor has to be changed, using palpation again to find the strongest pulsating point and trying to position the sensor over it, again.

The installed sensor at the wrist is shown in Figure 3.3.
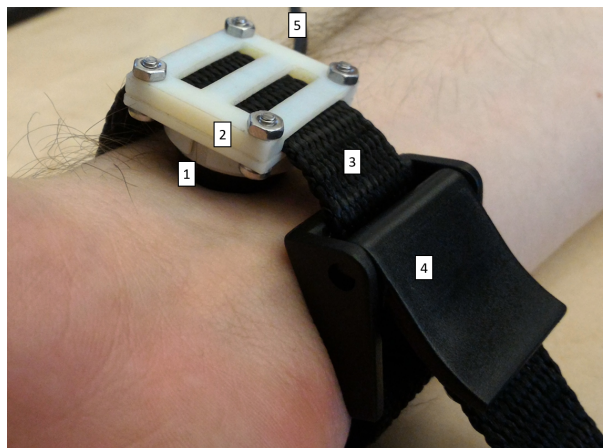
Figure 3.3: The placement of the presented system at the wrist. 1 – OptoForce OMD-20-SE-40N sensor, 2 – sensor holder, 3 – band, 4 – buckle, 5 – wire of the sensor

The required pressing force differs for each individual. It is based on the individual attributes of the examined person. For thin women, the stretching force should be quite gentle, because their radial artery can be closed easier than an average man. It also depends on the actual blood pressure values, naturally in the case of higher blood pressure, measuring good quality signals is easier. However, during my work the lowest BP value, when good quality signals could be recorded, was around 50 mmHg.

3.3   Repeatability of sensor attachment

A repeatability study was conducted in order to test the above defined measurement environment and sensor attachment protocol. I asked one of my colleagues to participate in this test. First, I attached the sensor to her left wrist 20 times in a row, applying the defined protocol. Then, it was repeated it to her right wrist, again 20 times in a row. The readable BP waveform's amplitude had to be at least 100 units and the 3D vectors angle had to be in the above mentioned optimal range from the xy-plane of the sensor $(50° - 130°)$. After the sensor was attached to the wrist, a two minutes long signal was recorded with 100 Hz sampling frequency for each trial. Figure 3.4. shows the averaged single-period signals for each trial.
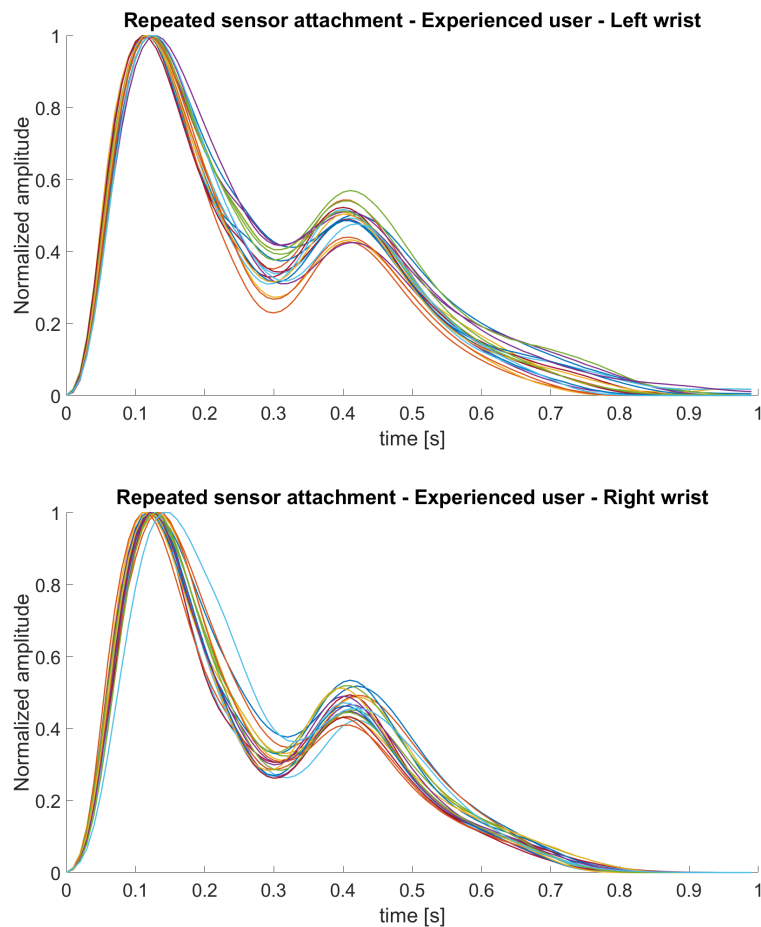
Figure 3.4: Averaged and normalized single-period signals as results of repeated sensor attachment by an experienced user.

The average correlation was 0.9932 ± 0.0045 between the single-period signals of the left arm and 0.9910 ± 0.0103 between the single-period signals of the right arm. The slight differences can occur, due to the dynamical changes of the participant's heart rate and BP during the study. The average difference and standard deviation of the angle between the 3D force vector and the sensor's central (z-)axis was $20.83 \pm 9.01°$ for the

left wrist measurements, and $22.63 \pm 8.30°$ for the right wrist measurements.

In the next phase, the participant was asked to make measurements on me, applying the same protocol. After a short (several minutes) practice, the same measurement procedure was repeated with 10-10 trials on each of my wrist. Figure 3.5. shows the results of these trials.
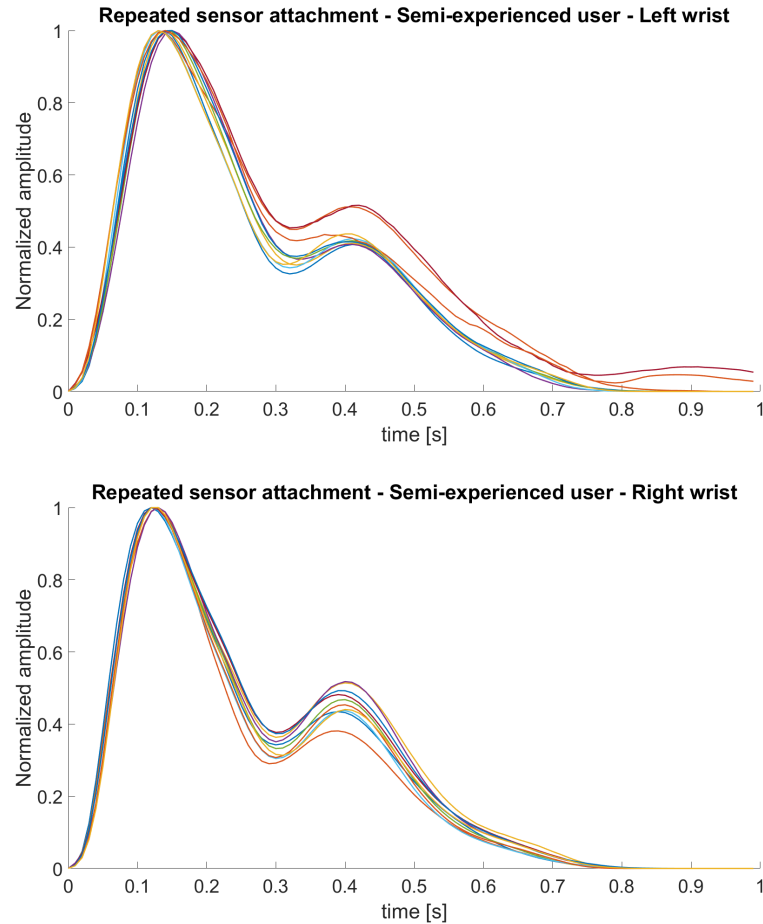
Figure 3.5: Averaged and normalized single-period signals as results of repeated sensor attachment by a semi-experienced user.

The average correlation was 0.9940 ± 0.0042 between the single-period signals of the left arm and 0.9964 ± 0.0030 between the single-period signals of the right arm. The average difference and standard deviation of the angle between the 3D force vector and the sensor's central (z-)axis was $26.09 \pm 10.73°$ for the left wrist measurements, and $21.38 \pm 10.45°$ for the right wrist measurements.

As a conclusion, the sensor attachment and its protocol is easy to learn and the measurement is repeatable by following the above defined criteria. Also, as the angle of the 3D vector differed in each measurement, a region on the sensor surface can be defined, where good quality signals can be recorded.

Chapter 4

Novel non-invasive continuous blood pressure monitoring

This chapter summarizes my work in the topic of continuous non-invasive blood pressure monitoring and the results obtained.

4.1 Validation by Millar tonometer

This section introduces the validation measurements using another non-invasive blood pressure waveform measuring system, a supervised tonometric device, the Millar tonometer. In the following subsections, the measurement devices, the measuring protocol, the characteristics of the participants, the applied signal processing and statistical analysis steps and the results will be introduced.

4.1.1 Measurement devices and protocol for non-invasive validation

Data collection was conducted at the Faculty of Information Technology and Bionics of Pázmány Péter Catholic University (Budapest) under ethical license no. 186/2013. The tonometric measurements were conducted by a trained professional, Dr. Tamás Horváth and the 3D force sensor measurements were conducted by me.

The proposed OptoForce OMD-20-SE-40N tactile force sensor [87] based method was compared to an applanation tonometry system, the pencil-shaped Millar SPT-301 non-invasive, handheld tonometer (Millar Instruments, Houston, Texas, USA) as reference measurement. The analogue output of the tonometer sampled by an ADInstruments PowerLab 4/35 data acquisition system. The sampled signals were processed, displayed and stored with a LabChart data analysis software (LabChart v.7.3, ADInstruments, Bella Vista, Australia). The 3D force sensor's signal was recorded with the OptoForce Data Visualization software. During the recording sessions, ECG was collected from Lead-II. Blood pressure was measured simultaneously on both arms by double-cuff, oscillometric blood pressure monitor (Microlife WatchBP Office ABI).

First, the participants were informed about the measurement. During that phase the participants were in sitting position, so it also served as a resting period. After ECG electrodes and upper-arm blood pressure cuffs were applied to the participants, all measurements were carried out in a supine position with straight, parallel legs in two turns. There was also a 3 – 5 minutes resting time, while the non-invasive sensor were positioned over the radial artery. Within each turn, a one minute long recording session was acquired 3 times by both the OptoForce sensor and the Millar tonometer. Before and after the sessions simultaneous, bilateral upper-arm blood pressure readings were taken. Between the recordings there was a 2 – 3 minutes long resting phase. In the first turn the OptoForce sensor was positioned above the left- and the Millar tonometer over the right radial artery. In the second turn both sensors were repositioned on the contralateral side. In the end, a total of six one minute long measurement pairs were taken with each participant. The sampling frequency of the continuous measurements was 1000 Hz. The protocol is summarized in Figure 4.1.

4.1.2 Characteristics of the participants for non-invasive validation

Our study included 30 participants: 8 women and 22 men. Table 4.1 shows their main anthropometric characteristics.

Table 4.1: Characteristics of participants

	Range	Mean±std.
Age (years)	20–30	24.4±2.5
Height (cm)	155–191	175.2±8.4
Weight (kg)	44–95	69.3±11.1
BMI (kg/m^2)	18.3–28.7	22.5±2.6

4.1.3 Data analysis for non-invasive validation

The first step of the signal processing was the synchronization of the two signals, which were recorded on different computers, by matching the systolic peaks. In order to find the systolic peaks, first, the onset point of each heartbeat was detected using a windowed and weighted slope sum function-based algorithm [64]. This algorithm will be introduced in details in the next chapter. Then, the systolic peak points were detected by searching for the global maximum points between the onset points. For compensating the measurement noise, such as motion artefacts, a moving average filter was applied. The window of this filter was 3 seconds, an empirical choice to avoid the distortion of the diastolic information in the signal.
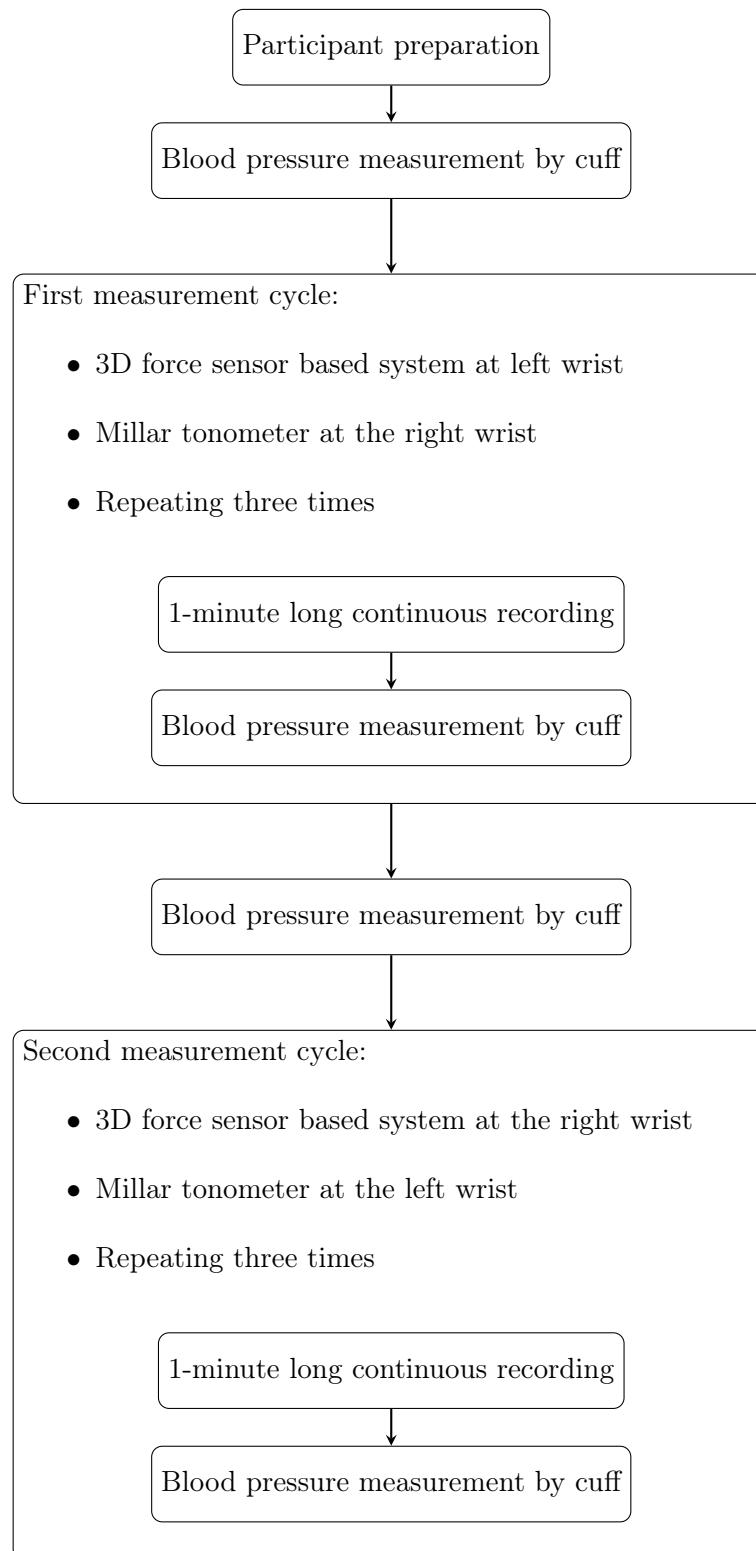
Figure 4.1: Summary of the measuring protocol.

For comparison, the middle 70% of each one minute long measurement was selected ($\sim$42 sec) in order to exclude the possible noise at the beginning and at the end of the recordings. There were 12 cases where the width of the examined window had to be shortened due to significant motion artefacts.

Average blood pressure was calculated by averaging the cuff-based measurements made before and after each recording. The average mean arterial pressure (MAP) was calculated as well using the following equation:

$$MAP_{avg} = \frac{1}{3} \cdot SYS_{avg} + \frac{2}{3} \cdot DIA_{avg}, \tag{4.1}$$

where SYS_{avg} is the averaged systolic blood pressure and DIA_{avg} is the averaged diastolic blood pressure.

Both continuous non-invasive blood pressure monitoring systems require calibration. I applied the same calibration method for the two signals, compensating for the linear gain and average offset values:

$$Gain = \frac{MAP_{avg} - DIA_{avg}}{U_{avg} - U_{dia}}, \tag{4.2}$$

$$CBP(t) = Gain \cdot (U(t) - U_{dia}) + DIA_{avg}, \tag{4.3}$$

$CBP(t)$ is the continuous blood pressure at time (t), U_{avg} is the averaged, U_{dia} is the averaged minimum values of the raw, uncalibrated signal $U(t)$ recorded by each sensor.

Last, the averaged single-period signals were calculated. For this, the recorded signals were segmented by their onset points. Afterwards all the single-period signals were averaged. Since we set the averaged signal length according to the longest single-period signal's length, all signals shorter than that were padded with their last value.

4.1.4 Repeatability analysis for non-invasive validation

First, a repeatability test of the Millar tonometer system was conducted to be sure that the applied reference system is a reliable base for comparison. For this purpose the above mentioned averaged single-period signals were used. The root mean square error (RMSE) was calculated between all recordings made on the same participant on the same wrist. Low RMSE values suggest repeatable and reliable measurements acquired by the Millar tonometer. The averaged RMSE value on each arm was calculated as follows:

$$RMSE_{avg} = \frac{RMSE_{1v2} + RMSE_{1v3} + RMSE_{2v3}}{3}, \tag{4.4}$$

where $RMSE_{1v2}$ is the RMSE value of the first and the second measurement for the same participant at the same wrist, $RMSE_{1v3}$ is the same for the first and the third and $RMSE_{2v3}$ is the same for the second and the third.

4.1.5   Statistical methods for non-invasive validation

To compare the continuous blood pressure signals of the two non-invasive systems, the correlations between them were calculated, as well as the RMSE values. This comparison included the above mentioned 70% segments of each recordings. These two methods could give an initial estimation about the concordance between the two systems of the two systems' recording, but further investigation was required.

For further comparison, the averaged single-period signals were examined. Bland-Altman plots [90] were created for systolic, diastolic and incisura pressure values of each signal – determined by a simple derivative based local extremum search and the MAP calculated as the area under each single-period blood pressure signal. Bland-Altman plot is a data plotting method used for comparing two measuring methods. It graphs the mean of the two system's recordings (S_x) against the difference between them (S_y) with the mean values and 1.95-times the standard deviation lines. Compared to a reference the system is considered accurate, when the average difference (S_{y_avg}) is close to zero, and precise when all points are located within $\pm$ 1.95 standard deviation range. The Bland-Altman plot was carried out for each systolic, diastolic, MAP and incisura value comparing the following pairs:

- Simultaneous measurements: the two sensors are on different sides, but measured at the same time,

- Same side measurements: the two sensors are on the same wrist, but in different times.

In the case of simultaneous measurements, the within subject variation of repeated measurements were taken into consideration by using modified Bland-Altman analysis for repeated measurements within one individual [91]. This version of Bland-Altman analysis compensates the limits of agreement lines using the within subject variation of repeated measurements. Furthermore, for the simultaneous measurements the blood pressure difference (BP_{diff}) between the two arms as measured by cuff was took into consideration, and was compensated. The same principle was applied in the case of the same side measurement comparison, but with blood pressure difference between two given times. The incisura point was compensated using the difference in the MAP. The plotted values were calculated as follows:

$$S_x = (S_o + (S_t - BP_{diff}))/2, \tag{4.5}$$

$$S_y = S_o - (S_t - BP_{diff}), \tag{4.6}$$

where S_o and S_t represent the systolic, diastolic, MAP or incisura blood pressure values measured by the 3D force sensor based system and by the Millar tonometer, respectively. BP_{diff} is the difference in systolic, diastolic blood pressure or MAP between the two

arms (simultaneous measurements) or in different moments (same side measurements), as measured by cuff.

Our study is summarized in Figure 4.2.
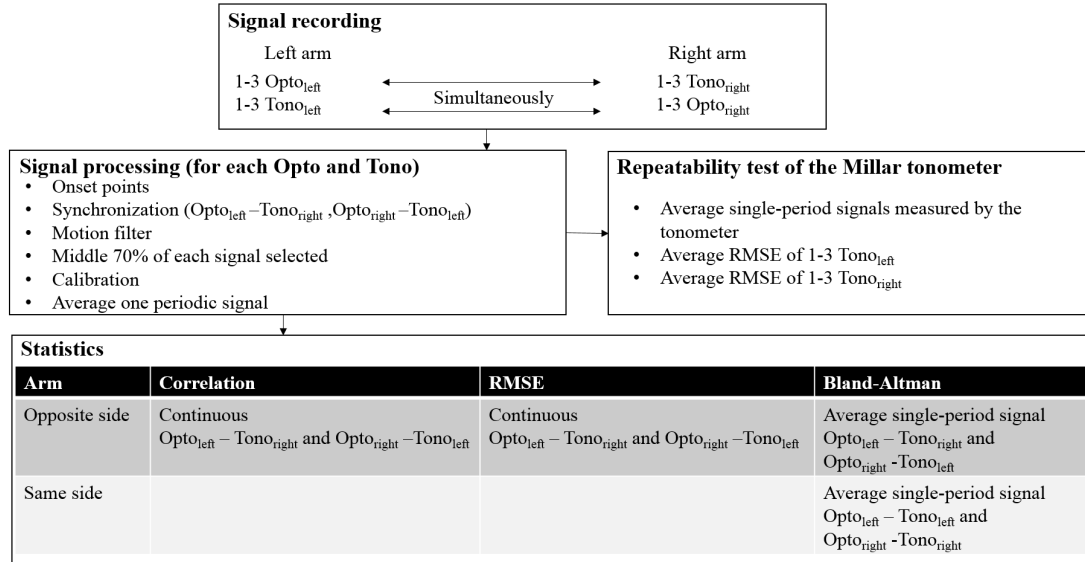
Figure 4.2: Summary of our study. Opto refers to the 3D force sensor based system based on OptoForce sensor, and Tono refers to applanation tonometry based on Millar tonometer.

4.2 Results of non-invasive validation

The results concerning the repeatability of the tonometer measurements are summarized in Table 4.2. It contains the RMSE values ($RMSE_{avg}$) defined in subsection 4.1.3. The average RMSE value for the right arm was 2.52 ± 1.11 mmHg, while for the left arm it was 3.14 ± 1.14 mmHg.

The average correlation between the simultaneously measured signals was 0.8933 ± 0.1307, and the average RMSE value was 7.25 ± 4.03 mmHg. These values are summarized for each participant in Table 4.3.

There were some outliers with significantly lower correlation (< 0.7), mostly due to motion artefacts. Excluding these (12 out of 180; 6.67%), the average correlation between the simultaneously measured signals increased to 0.9213 ± 0.063, and the average RMSE value decreased to 6.58 ± 3.08 mmHg. Figure 4.14 shows a highly correlated signal pair. Figure 4.4 shows the averaged single-period signal for the worst (after exclusion of the 12 outliers by the less than 0.7 correlation value criterion), the best and an average correlated recording pairs. The correlation values of these signals are related to the complete continuous waveforms. It has to be considered that averaging the single-period signals can reduce the noise.

Table 4.2: Repeatability of tonometer measurements.

	Average RMSE values [mmHg]	
	right arm	left arm
Participant 01	2.30	4.05
Participant 02	0.97	2.15
Participant 03	2.68	3.56
Participant 04	4.03	2.53
Participant 05	1.43	1.90
Participant 06	3.82	1.43
Participant 07	3.08	2.10
Participant 08	1.31	4.47
Participant 09	1.20	3.89
Participant 10	2.05	2.34
Participant 11	2.30	4.73
Participant 12	2.51	3.34
Participant 13	2.51	2.67
Participant 14	2.96	3.82
Participant 15	2.66	5.23
Participant 16	2.10	4.44
Participant 17	5.46	4.85
Participant 18	3.25	1.88
Participant 19	2.04	3.68
Participant 20	4.23	2.05
Participant 21	1.44	1.68
Participant 22	1.84	3.79
Participant 23	3.76	3.56
Participant 24	2.47	2.15
Participant 25	1.95	1.48
Participant 26	2.64	4.67
Participant 27	1.63	1.64
Participant 28	4.58	2.94
Participant 29	1.44	3.62
Participant 30	1.06	3.57

Table 4.3: Correlation and RMSE between simultaneously recorded non-invasive continuous blood pressure signals in the time domain. Average of measurement 1–3: the 3D force sensor based system on the left arm, tonometer on the right arm. Average of measurement 4–6: the 3D force sensor based system on the right arm, tonometer on the left arm.

	Correlation		RMSE [mmHg]	
	Measurement 1–3	Measurement 4–6	Measurement 1–3	Measurement 4–6
P01	0.8825 ± 0.0548	0.9676 ± 0.0202	7.12 ± 1.17	6.66 ± 2.03
P02	0.6481 ± 0.2336	0.8711 ± 0.0477	12.17 ± 3.34	9.47 ± 2.31
P03	0.9166 ± 0.0397	0.7683 ± 0.1801	4.84 ± 0.80	9.60 ± 6.91
P04	0.7594 ± 0.1541	0.9254 ± 0.0106	11.21 ± 3.02	5.99 ± 0.27
P05	0.7240 ± 0.0599	0.8779 ± 0.0542	15.10 ± 3.24	8.56 ± 1.85
P06	0.7048 ± 0.1148	0.8902 ± 0.0684	18.63 ± 4.82	8.64 ± 1.50
P07	0.8360 ± 0.0916	0.8746 ± 0.0478	10.34 ± 2.52	10.00 ± 1.46
P08	0.8251 ± 0.1070	0.9356 ± 0.0274	10.50 ± 2.82	5.03 ± 1.69
P09	0.9287 ± 0.0163	0.8905 ± 0.1078	8.73 ± 2.83	6.53 ± 2.46
P10	0.9676 ± 0.0104	0.9481 ± 0.0246	4.22 ± 0.18	4.26 ± 1.17
P11	0.9845 ± 0.0038	0.9508 ± 0.0119	5.84 ± 0.65	5.68 ± 0.80
P12	0.9008 ± 0.1251	0.9829 ± 0.0059	4.40 ± 3.00	2.34 ± 0.52
P13	0.9829 ± 0.0059	0.9142 ± 0.0595	5.69 ± 1.31	9.46 ± 1.67
P14	0.8877 ± 0.0747	0.7973 ± 0.2089	11.33 ± 1.81	8.88 ± 4.59
P15	0.3936 ± 0.4612	0.8017 ± 0.0991	16.08 ± 8.75	12.72 ± 2.96
P16	0.9505 ± 0.0284	0.8291 ± 0.1939	5.36 ± 0.91	8.87 ± 4.16
P17	0.9005 ± 0.0337	0.7219 ± 0.2407	9.53 ± 0.88	11.42 ± 4.91
P18	0.9700 ± 0.0129	0.9747 ± 0.0111	3.57 ± 0.63	3.46 ± 0.78
P19	0.9542 ± 0.0209	0.9320 ± 0.0333	4.76 ± 0.99	5.60 ± 1.37
P20	0.9237 ± 0.0359	0.9664 ± 0.0196	6.65 ± 0.70	3.90 ± 1.05
P21	0.9657 ± 0.0040	0.9471 ± 0.0190	4.04 ± 0.19	5.12 ± 1.51
P22	0.8947 ± 0.0622	0.8905 ± 0.1053	9.39 ± 2.17	7.33 ± 3.37
P23	0.8914 ± 0.0522	0.9690 ± 0.0079	7.87 ± 1.17	3.18 ± 0.47
P24	0.9424 ± 0.0430	0.9399 ± 0.0382	6.27 ± 1.18	4.93 ± 2.00
P25	0.9709 ± 0.0102	0.8639 ± 0.1743	4.57 ± 0.43	6.25 ± 4.84
P26	0.9630 ± 0.0140	0.9121 ± 0.0376	3.45 ± 0.56	5.67 ± 1.03
P27	0.9289 ± 0.0376	0.9665 ± 0.0187	6.58 ± 1.79	6.35 ± 1.04
P28	0.9748 ± 0.0106	0.9532 ± 0.0135	1.91 ± 0.53	3.76 ± 1.24
P29	0.9631 ± 0.0163	0.9319 ± 0.0228	5.64 ± 1.40	11.53 ± 1.11
P30	0.9325 ± 0.0514	0.9756 ± 0.0171	5.12 ± 1.16	2.92 ± 0.82
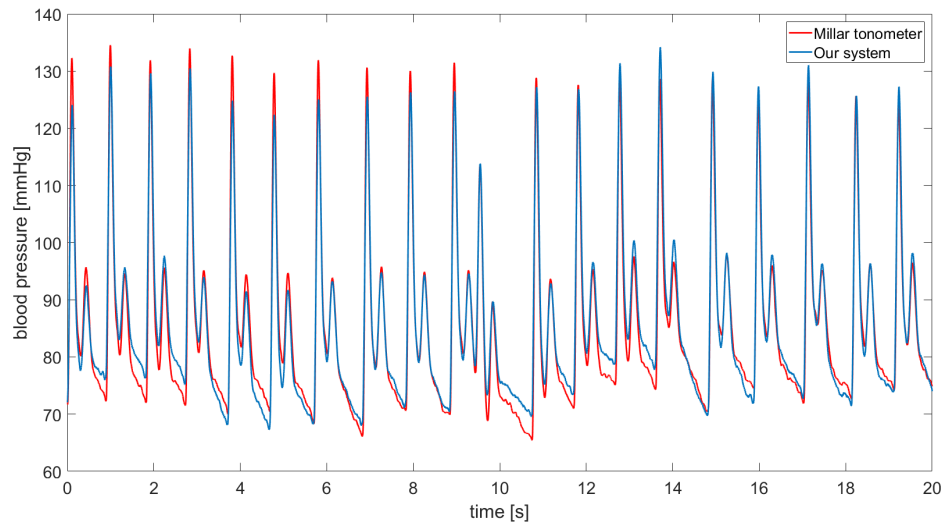
Figure 4.3: 20 seconds-long section of the best correlated signal pair without compensation of the blood pressure difference between the two arms (correlation coefficient is 0.9889)
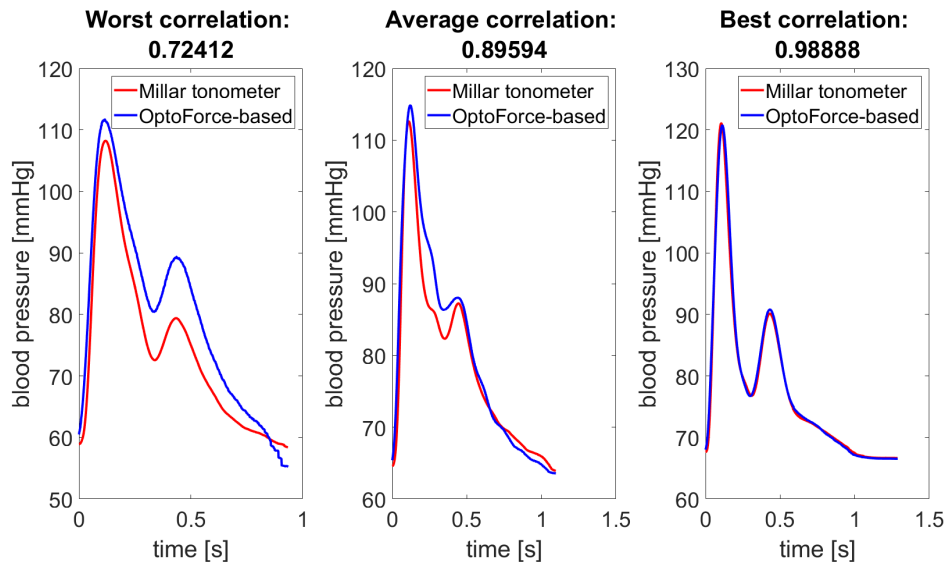
Figure 4.4: The averaged single-period signals of the worst (after exclusion of the 12 outliers), the best and an average correlated signal pair. Correlation values refer to the complete continuous 1-minute long measurements.

The Bland-Altman plots of the simultaneously measured averaged single-period signals' systolic, diastolic, MAP and incisura values are represented in Figure 4.5, Figure 4.6, Figure 4.7 and Figure 4.8, respectively. The same Bland-Altman plots of the same side measurements are shown in Figure 4.9, Figure 4.10, Figure 4.11 and Figure 4.12, respectively. Table 4.4 summarizes the average bias and standard deviation values for systolic, diastolic, MAP and incisura pressure presented in Figure 4.5–4.12.
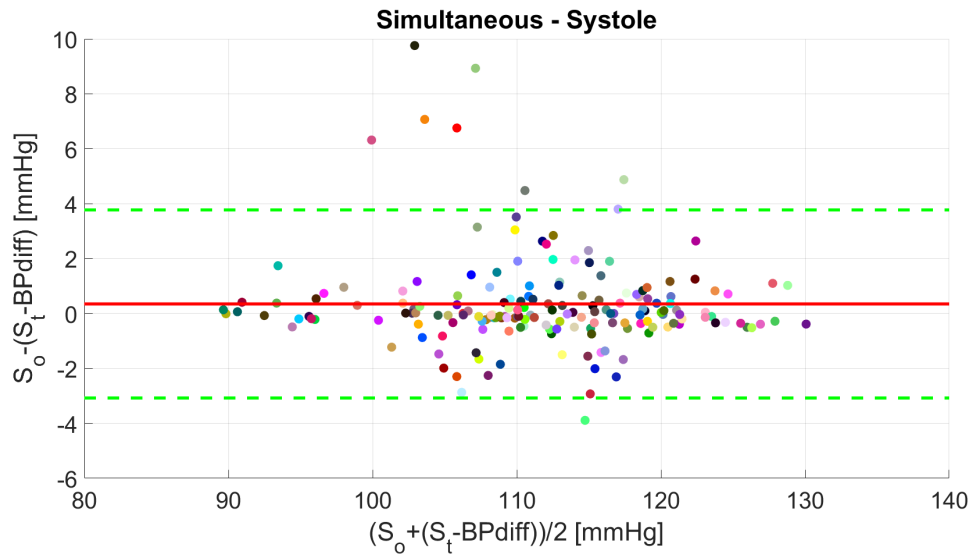
Figure 4.5: Bland-Altman plot of the simultaneously measured signals' systolic pressure. The red line is the mean difference, and the dashed green lines are the limits of agreement (1.95×standard deviation) compensated with the within subject variation of repeated measurements. The mean systolic difference and standard deviation is 0.35 ± 1.75 mmHg.

Table 4.4: Summary of average bias and standard deviation values for systolic, diastolic, MAP and incisura pressure presented in Figure 4.5–4.12.

	Simultaneous [mmHg]	Same hand [mmHg]
Systolic pressure	0.35 ± 1.75	0.42 ± 1.77
Diastolic pressure	0.02 ± 0.19	0.02 ± 0.74
MAP	2.88 ± 2.42	3.02 ± 2.26
Incisura pressure	3.84 ± 3.90	3.85 ± 3.43
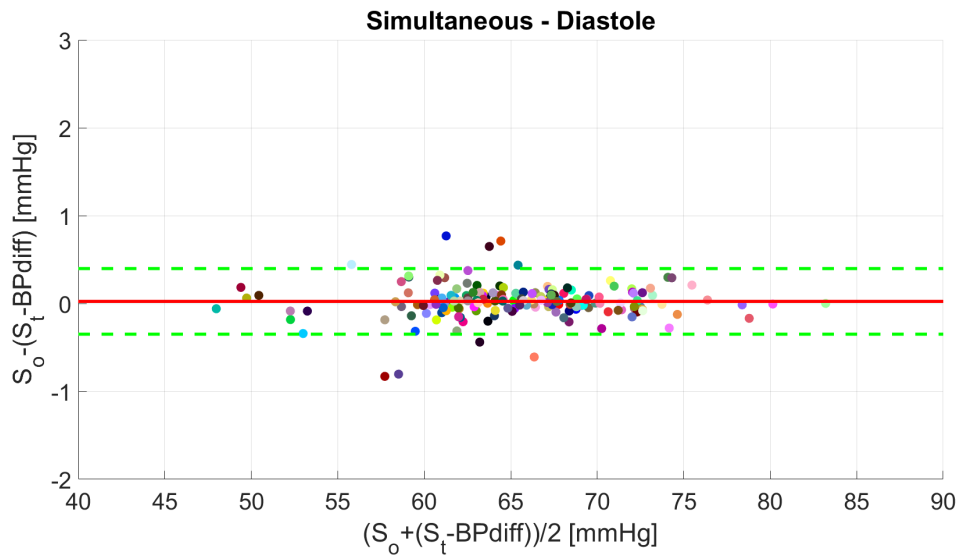
Figure 4.6: Bland-Altman plot of the simultaneously measured signals' diastolic pressure. The red line is the mean difference, and the dashed green lines are the limits of agreement (1.95×standard deviation) compensated with the within subject variation of repeated measurements. The mean diastolic difference and standard deviation is 0.02 ± 0.19 mmHg.
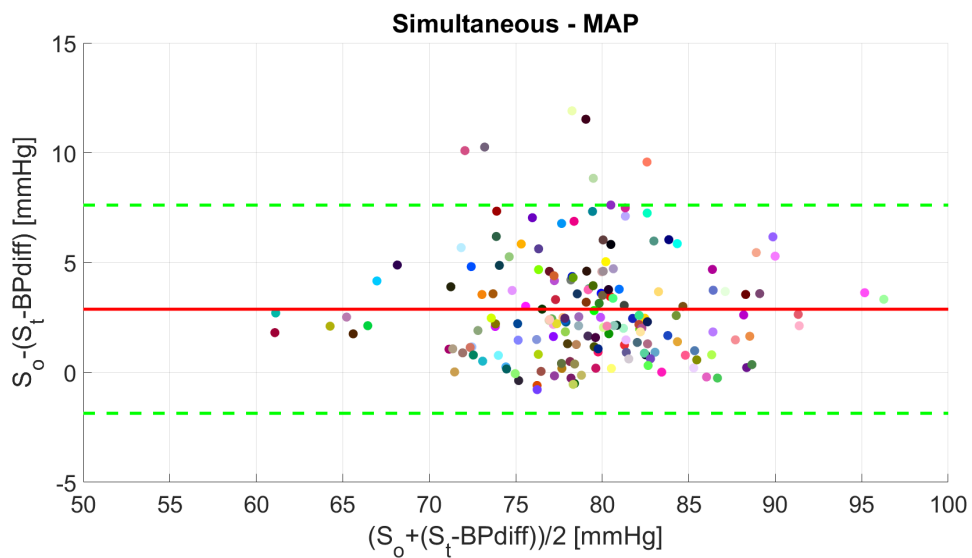
Figure 4.7: Bland-Altman plot of the simultaneously measured signals' MAP. The red line is the mean difference, and the dashed green lines are the limits of agreement(1.95×standard deviation) compensated with the within subject variation of repeated measurements. The mean MAP difference and standard deviation is 2.88 ± 2.42 mmHg.
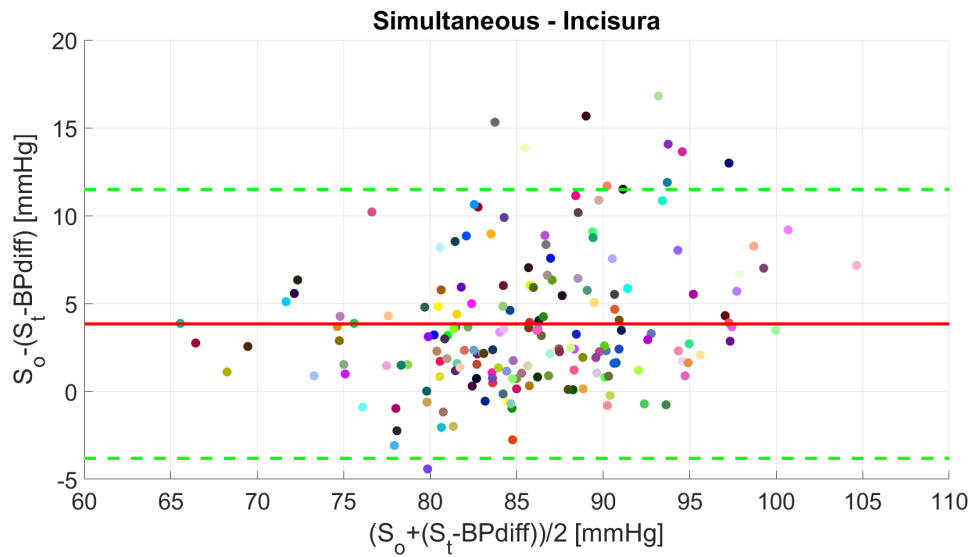
Figure 4.8: Bland-Altman plot of the simultaneously measured signals' pressure at the incisura peak. The red line is the mean difference, and the dashed green lines are the limits of agreement (1.95×standard deviation) compensated with the within subject variation of repeated measurements. The mean difference in incisura pressure and standard deviation is 3.84 ± 3.90 mmHg.
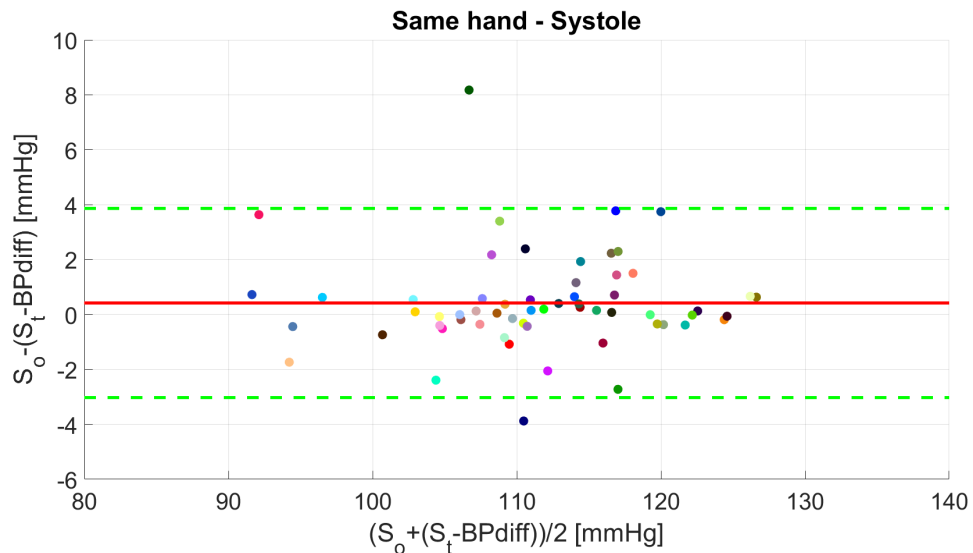
Figure 4.9: Bland-Altman plot of the signals' systolic pressure measured on the same arms. The red line is the mean difference, and the dashed green lines are the limits of agreement (1.95×standard deviation). The mean systolic difference and standard deviation is 0.42 ± 1.77 mmHg.
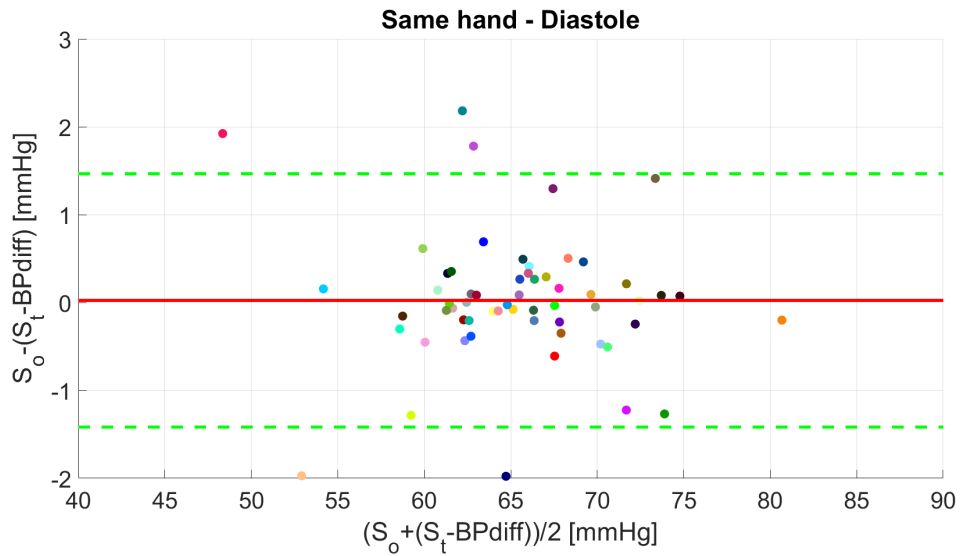
Figure 4.10: Bland-Altman plot of the signals' diastolic pressure measured on the same arms. The red line is the mean difference, and the dashed green lines are the limits of agreement (1.95×standard deviation). The mean diastolic difference and standard deviation is 0.02 ± 0.74 mmHg.
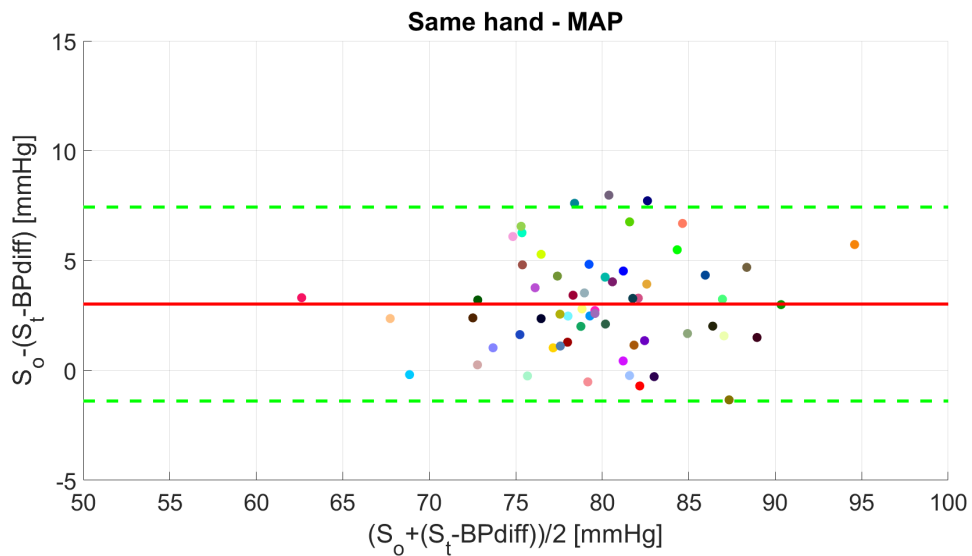
Figure 4.11: Bland-Altman plot of the signals' MAP measured on the same arms. The red line is the mean difference, and the dashed green lines are the limits of agreement (1.95×standard deviation). The mean MAP difference and standard deviation is 3.02 ± 2.26 mmHg.
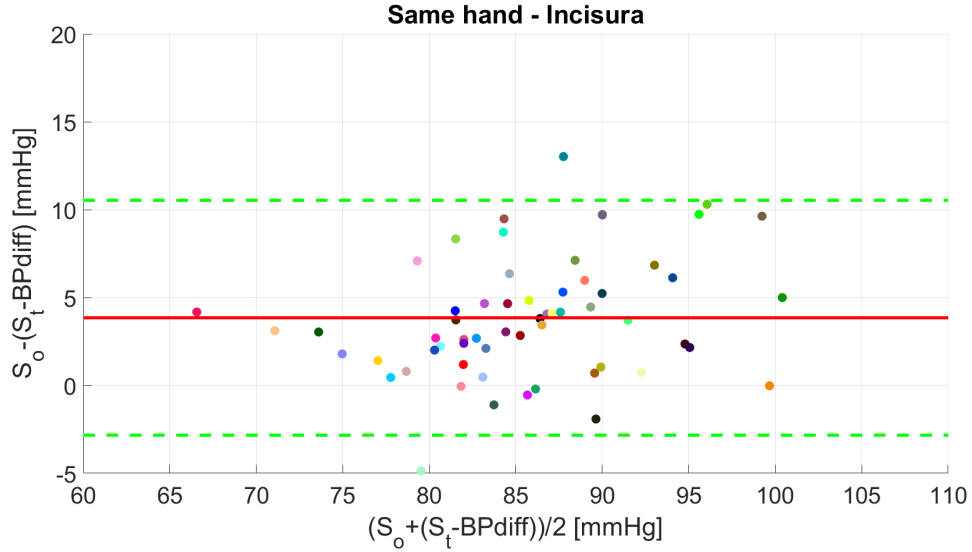
Figure 4.12: Bland-Altman plot of the signals' pressure at the incisura peak measured on the same arms. The red line is the mean difference, and the dashed green lines are the limits of agreement ($1.95 \times$ standard deviation). The mean difference in incisura pressure and standard deviation is 3.85 ± 3.43 mmHg.

4.3 Discussion for non-invasive validation

The results of the tonometer repeatability test suggest that the method is repeatable with reasonable accuracy. The small differences in the RMSE values could arise from changes in the participants' blood pressure with time. According to our results, the comparison of the two non-invasive systems is appropriate.

The 0.8933 average correlation value in the time domain is acceptable. It further improves (0.9213), if we exclude the outliers (< 0.7 correlation). The RMSE values suggest that there are small differences in the waveform of the measured signals. Evaluating the results some assumptions have to be made. First of all, since the tonometric method is not considered as the gold standard method for blood pressure measurements, the difference of the two sensors does not indicate that values measured by the 3D force sensor based system are less closer to the intra-arterial blood pressure values. The tonometric method, however, allowed us to determine whether the 3D force sensor based system is capable of measuring a continuous blood pressure signal with acceptable accuracy. As to the difference, it has to be taken into consideration that blood pressure waveforms can differ between the left and right sides due to the side-difference in the vascular anatomy.

As mentioned above, there were 12 outliers out of the 180 measurements (< 0.7 correlation coefficient). In these cases, the poor measurement quality was attributed to patient movement. During data acquisition the 3D force sensor based system was more susceptible to subject motion compared to tonometry. After an initial positioning, the 3D force

sensor based system was completely unsupervised, while on the contralateral side, the tonometer operator was able to stabilize the hand, therefore preventing the appearance of unwanted motion-artefacts. In most measurements the participants' movements were not significantly affects the results, with the exception of the 12 outliers where even the presented filtering algorithm cannot produce a reasonable continuous waveform.

Additional to time-domain comparison, harmonic analysis in frequency-domain was performed between the non-invasive pressure signals. First, the FFT spectrum of each signal was determined, and the correlation and RMSE values between the spectra were calculated. For the frequency spectrum, the average correlation was 0.9994 ± 0.0008 and the average RMSE value was 0.54 ± 0.07. So, the correlation coefficients were almost equal to one, which means the frequency spectra of the signals measured by the two methods are basically identical. In practice, it means that the 3D force sensor based system was able to record every frequency component of the continuous blood pressure waveform recorded by the Millar tonometer.

For further comparison, Bland-Altman plots were applied. First, the simultaneously measured signals were compared. Again, for a more general comparison, the blood pressure difference between the two arms was taken into consideration. As Figure 4.5 shows, there is a very small offset in systolic pressure between the two measurement systems (0.35 mmHg), and most results were within the 4 mmHg range. Most of the outliers are the same as above. The results were very similar for diastolic blood pressure (Figure 4.6), but it has an even smaller offset (0.02 mmHg) and a very narrow interval. The same calibration method applied for both measuring systems can indicate the high similarity as well. It could be also concluded that in higher blood pressure regions the reliability is better than in lower blood pressure regions both for systolic and diastolic pressures. For the MAP, the bias of the difference is 2.88 mmHg that is within the clinical limit (Figure 4.7). also the outliers here are the same as in systolic case. This proves the potential of the device's clinical applicability.

For the incisura, the results show a significant difference (Figure 4.8). Incisura pressure was chosen to study, since it gives information about the waveform. Blood pressure signals measured by the 3D force sensor based system show a significantly higher incisura pressure. Some considerations should be made here. First, cuffs offer no information about incisura pressure. Therefore, the MAP was used to compensate for the pressure difference between the two arms. Second, we were unable to ascertain which system's results are closer to the actual waveform of the incisura pressure. Moreover, the waveform of the incisura pressure may also differ in each arm, which could account for our findings.

All the results mentioned above satisfy the AAMI criterion, which is currently requires that the bias of systolic, diastolic and mean arterial blood pressure must be below 5 mmHg and the standard deviation below 8 mmHg. Based on these results, another study needs to be conducted to validate the 3D force sensor based system against an invasive arterial

cannula, in order to determine the system's accuracy compared to blood pressure values measured by the gold standard method.

Concerns mentioned above led us to examine the difference in the measurement results of both systems on the same arm. The blood pressure difference in terms of time needed to be compensated, as the elapsed time between two measurements could be as much as 10-minutes, during which the participant's blood pressure might have changed significantly. It was not possible for us to pair the continuous 1-minute long measurements, because as the two measurements does not happened simultaneously, the pulse rate could have changed between the two measurements and the heart cycles cannot be matched to each other. So for each measuring cycle, the single-period signals were averaged to get a signal characteristic to the given participant. The results of the Bland-Altman plots suggest the same as above: the results of the two measuring systems are almost the same in terms of systolic and diastolic blood pressure (Figure 4.9 and Figure 4.10, respectively). Again, in higher blood pressure regions the reliability is better than in lower blood pressure regions for systolic pressure. For MAP, the bias of the difference is a bit higher, 3.02 mmHg, but it still suggests a good similarity (Figure 4.11). For incisura pressure, the results were also very similar (Figure 4.12): incisura pressure measured by the 3D force sensor based system is significantly greater (on average around 4 mmHg) than the one measured by the Millar tonometer.

4.4 Validation by invasive arterial cannula

Validation was done in two steps. First, only the waveform was validated, whether the characteristic feature of the invasive signal and the non-invasive signal are similar. The second experiment concentrated both on the signal waveform and the blood pressure values.

4.4.1 Waveform comparison study

The measurements were made at the Department of Vascular Surgery, Semmelweis University, Budapest under clinical license no. 186/2013. The experiment was conducted on those patients who had to undergo carotid surgery. All participants received written and oral information about the experiment, and after their approval, a written informed consent was obtained. In this study, there were 13 patients (7 men and 6 women), but due to bad quality signal, 4 of them had to be excluded (3 men and 1 woman). These exclusions had to be made, because during measurements the participants have made significant movements with their hands, which moved the sensor away, from the desired measuring position. Unfortunately, the time available for the experiment, no evaluable signals could be recorded on these participants. The characteristics of the remaining patients can be seen in Table 4.5.

Table 4.5: Characteristics of participants

	Range	Mean±std.
Age	57–77	65.2±7.7
Height (cm)	148–173	161.2±8.6
Weight (kg)	50–82	69.1±9.9
Heart rate (bpm)	57–90	72.4±10.1
Systolic BP (mmHg)	106–178	132.7±20.3
Diastolic BP (mmHg)	51–78	58.7±8.1

The aim of this study is to compare the invasive continuous arterial BP waveform to the one that can be measured by our system. Since all participants underwent a carotid surgery, invasive BP monitoring was a must. Our measurements were made after the successful surgery. During the measurement, the patients were awake, and they were monitored by trained nurses. The patients were asked to try to stay still as much as possible. Motion affected the non-invasive signal more than the invasive signal.

Patient monitoring was done by a GE™Dashboard 4000 patient monitor system, which recorded the invasive BP signal. During each experiment, the invasive and the non-invasive continuous BP waveforms were recorded simultaneously by a PC which was connected to the patient monitor and the 3D force sensor by USB cables. The invasive catheter was inserted in the radial artery of one arm, and our non-invasive system was put on the contralateral wrist. The measuring position on each arm was nearly the same. The measurements were 20-30-minutes long. The data from the GE patient monitor was acquired by Datex-Ohmeda S/5™Collect software. The non-invasive signal was acquired by the OptoForce Data Visualisation software. The sampling frequency in both cases was 100 Hz. After the measurement, the raw signals were processed.

During our experiment reproducibility was also tested. For 4 individuals two measurements were made consecutively by repositioning the non-invasive sensor on the wrist. Then the results of the two measurements were compared by their average correlation values.

4.4.1.1 Steps of analysis for waveform comparison study

To be able to compare the two waveforms, the same signal processing method had to be followed. For continuous arterial BP waveform's signal processing a cascaded adaptive filter was applied. It can filter the baseline wander from the signal. This signal processing method consists of two parts, a discrete Meyer wavelet decomposition filter and a spline estimation filter [62, 63]. Wavelet decomposition filters are based on signal and noise estimation on different decomposition levels. In this study the continuous BP wave was

approximated by the 1st level discrete Meyer wavelet decomposition, and the noise was estimated by the 7th level, in a similar manner to [63].

To completely remove the baseline drift, the spline estimation filter was applied. This method requires the onset points of the arterial BP signals. The onset point is a local minimum point appearing at the start of the heart cycle, which was determined by the same algorithm introduced in 4.1.3. subsection. In our study the cubic spline data interpolation was used. By fitting the cubic spline curve on these onset points, the baseline wander can be removed. These onset points can also be used for signal segmentation to create the single-period signals, which describe each heart cycle. The signal processing steps are summarized in Figure 4.13.
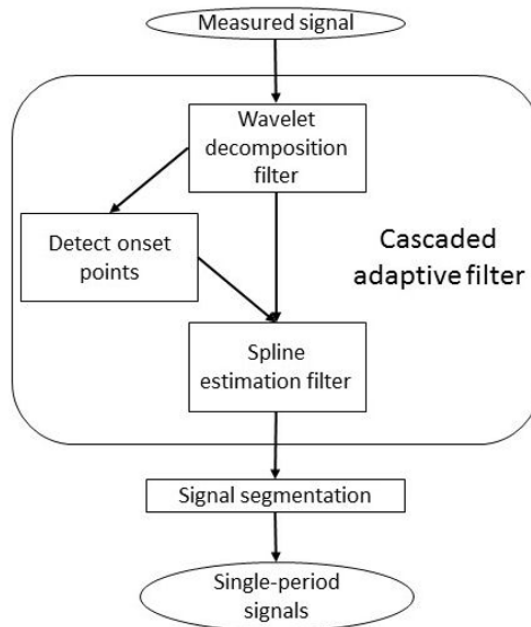
Figure 4.13: Summary of the signal processing steps. The measured signal is filtered with a cascaded adaptive filter, which has two main parts: wavelet decomposition filter and Spline estimation filter. Then the filtered signal is segmented into single period signals.

After signal processing, each single-period signal was normalized to 1 for both the invasive and non-invasive signals separately so that the waveform of the invasive and non-invasive measurements could be compared. This step was required, because the data from the invasive and non-invasive system had different units. The comparison was done by cross correlation. Those single-period signals that were corrupted by movement were excluded from the comparison if the movement could not be filtered via signal processing. To decide whether this exclusion was necessary or not, the length of each single-period signal was considered. If the length of the non-invasive single-period signal differed by more than 20% from the corresponding length of the invasive single-period signal, the

segments in question were excluded. The rate of the excluded single-period signals was always below than 10% of the corresponding continuous BP signal.

4.4.1.2 Results for waveform comparison study

The mean and standard deviation values for each participant's signals can be seen in Table 4.6., as well as the maximum, the minimum and the median correlation values between the corresponding single period signals. The highest correlation value and the standard deviation was 0.986 ± 0.024. Most of the resulting correlation values were above 0.9. This means, most of the invasive and non-invasive single-period signals were identical in more than 90%. Figure 4.14. shows an example of a highly correlated signal section.

Table 4.6: Correlation of single-period signals

Individual	Mean correlation±std.	Min.	Max.	Median
#1	0.939 ± 0.142	-0.479	0.998	0.981
#2	0.968 ± 0.055	0.240	0.992	0.980
#3	0.986 ± 0.024	0.617	0.997	0.990
#4	0.960 ± 0.090	0.176	0.999	0.991
#5	0.893 ± 0.187	-0.590	0.990	0.945
#6	0.949 ± 0.079	0.100	0.993	0.969
#7	0.960 ± 0.111	-0.397	0.998	0.987
#8	0.935 ± 0.073	-0.073	0.993	0.951
#9	0.984 ± 0.064	0.112	0.999	0.992
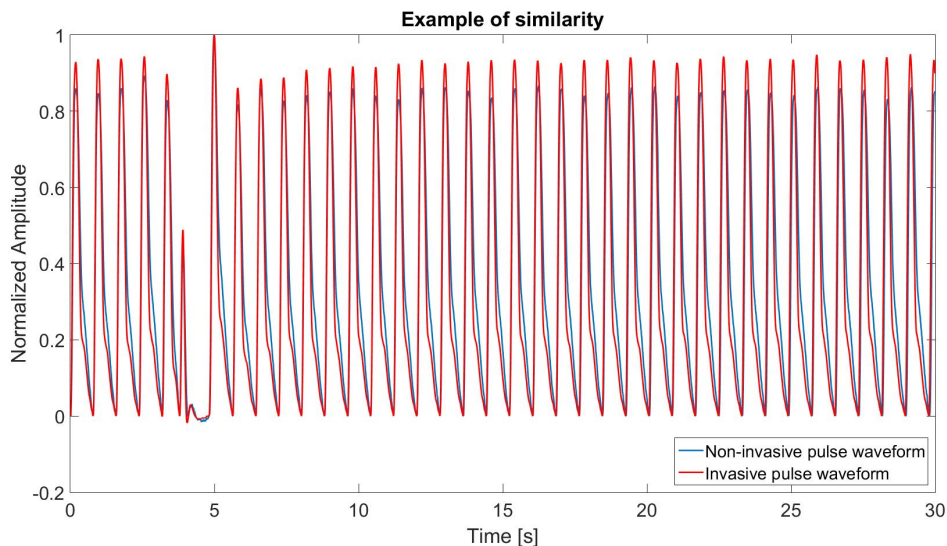
Figure 4.14: An example of a well correlated invasive and non-invasive continuous BP signal section. In this figure for better visibility, the normalization was made to the highest amplitude invasive signal in the presented segment.

For each individual there were some less correlated signal sections, which can occur as a result of movements. Figure 4.15. shows an example of a signal section for a low correlated pair.
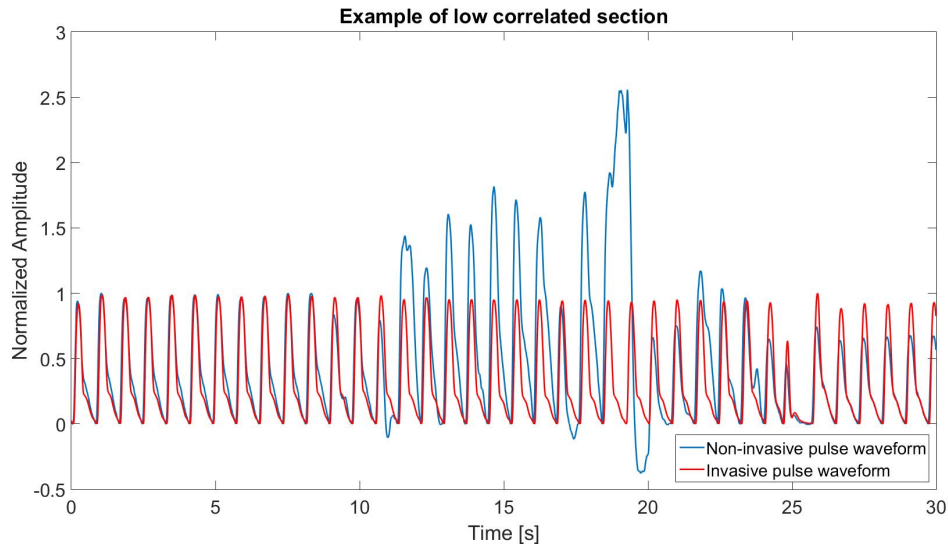
Figure 4.15: An example of a low correlated invasive and non-invasive continuous BP signal section. In this figure for better visibility, the normalization was made to the highest amplitude invasive signal in the presented segment before the movement noise.

Concerning reproducibility, for each measurement pair the mean correlation value of the corresponding invasive and non-invasive single-period pulse waveforms were: (0.939±0.142, 0.971±0.096); (0.968±0.055, 0.977±0.022); (0.986±0.024, 0.969±0.076); (0.935±0.073, 0.954±0.032), respectively.

4.4.1.3   Discussion for waveform comparison study

The results presented in Table 4.6. show that all the correlation values between the corresponding invasive and non-invasive single-period BP signals are high, sometimes almost identical (Figure 4.14). In both signals, a missbeat could be identified clearly which makes it visually clear, how similar the two signals to each other. Although in most of the cases the minimum correlation values were high, in some cases these were below zero. This means that there were parts in the signal where one of the signals increased, while the other decreased at a given moment. But according to the standard deviation and the median of the correlation values, the low correlated single-period signals were not significant.

These rare low correlation values could occur due to several reasons. One reason is that the participants were awake during the measurement and sometimes made movements. Those segments of the signals that could not be processed were excluded from

the examination. However several segments, where the signal was affected by movement, could still be processed. These segments lead to those single-period signal pairs in which the waveforms significantly differ from each other due to the effect of movements (Figure 4.15.). Another reason for low correlation values could be an outside effect, for example the nurse could push the arm accidentally. These effects occurred rarely in our experiments.

There are some other factors that should be considered for signal comparison. The non-invasive measurements were made on the contralateral wrist than the position of the invasive catheter. If the sensor position on each arm is not at the same height small time shift between the two signals can occur. This factor is also important in waveform similarity, because the two waveforms can be different due to disease or differences between the conditions of the arterial wall of the two sides. For example, in two patients the difference between blood pressure in the two arms was more than 20 mmHg. This can cause a significant difference in waveform as well. The inclusion of these patients should be considered, but due too the low number of participants, I have decided to include them with mentioning the fact here, in the discussion.

A limitation of this study is the measured BP value itself. The comparison was done between the processed and normalized invasive and non-invasive continuous BP signals, because our experiment focused on the waveform similarity. This means that the difference of the noise characteristic between the two measuring methods was not considered. Our signal processing method is able to filter out most of the noises from both systems, except long term or very high amplitude motion noises. This signal processing cannot be applied for comparing actual BP values since the filtered signal only preserves the pulse pressure (difference between systolic and diastolic BP values). It is not a problem in diagnostics, but the signal processing method must be modified for monitoring purposes.

Examining the reproducibility of the non-invasive measurements, **high correlation values were obtained for the consecutive measurements**. The results of the repeatability test suggest that the method is repeatable with reasonable accuracy. This feature is important in its application both as a monitoring device and as a diagnostic device.

Consequently, our results are promising and our experiments show that our non-invasive system is capable of measuring the continuous BP waveform accurately.

4.4.2 Continuous blood pressure comparison study

In this subsection, the comparison of invasive and non-invasive continuous BP measurements are presented, where not only the signal waveform similarity was studied, but also the BP values.

4.4.2.1 Measuring devices for continuous blood pressure comparison study

The non-invasive signal was recorded by OnRobot^{TM}OMD-20-SE-40N 3-axis sensor (developed by OptoForce^{TM}) connected to PC via USB. The signal was recorded by the OptoForce Data Visualization software. The sampling frequency was 100 Hz.

The proposed method was compared to an arterial cannulation device as part of the GE^{TM}Dash 4000 patient monitor connected to the same PC as the above mentioned non-invasive sensor via USB. The signal was recorded at 100 Hz using the Datex-Ohmeda S/5^{TM}Collect software.

4.4.2.2 Measurement protocol for continuous blood pressure comparison study

The data collection were conducted by me at the Department of Vascular Surgery of Semmelweis University (Budapest) under ethical license no. 186/2013. All participants received written and oral information about the measurements and signed an informed consent form.

Our study included 21 participants: 6 women and 15 men. Table 4.7. shows their main anthropometric characteristics. Most of the participants were elderly people after a surgical procedure. Twelve of the participants had a carotid artery surgery, four had heart transplantation, and the other participants had stent graft surgeries. All participants had an arterial cannula inserted in their radial artery as part of normal post-surgical care. Therefore, none of the participants experienced additional invasive procedures to participate in the study. During the study, 4 of the participants were still anesthetized while the remainder of the participants (17) were awake.

Table 4.7: Characteristics of participants

	Range	Mean±std.
Age (years)	34–87	63.8±11.2
Height (cm)	148–190	169.4±27.1
Weight (kg)	50–123	78.1±14.3
BMI (kg/m^2)	23–34	27.1±3.6

The 3-axis sensor based system was attached to the arm contralateral to the arterial cannula. In 12 cases the sensor was attached to the left wrist. The duration of the measurements differed for each participant. The length of the analysed signal depended

on the presence of motion artefacts and the condition of the patient. In average, the analysed signal length was 409.03 ± 230.31 seconds, range from 98.22 to 988 seconds.

In the case of 5 participants out of the 21, there were two consecutive measurements, therefore altogether 26 simultaneously recorded invasive and non-invasive signals were processed and statistically analysed.

4.4.2.3   Data analysis for continuous blood pressure comparison study

For signal processing and statistical analysis, Matlab R2018b software was used.

The non-invasive signal measured by the 3-axis sensor was affected by artefacts, mainly at awake participants. To filter these noises, first a moving average filter was applied. The length of the averaging windows was set to 3 seconds (300 data points). This length filtered the low amplitude oscillations that appeared in the 3-axis sensor during a long term measurement, but still kept the diastolic information.

To filter out the motion artefacts, a Daubechies wavelet with maximum 8 vanishing moments (db8) decomposition filter was applied. There are several examples in literature where wavelet decomposition filters were applied during noise filtering of BP waveforms, i.e. [1, 63], because the appropriate wavelet decomposition filter is an efficient tool to filter out aperiodic, low frequency noises like motion artefacts. The basic principal of the wavelet decomposition filtering is to approximate the signal and the noise on different decomposition levels. In our case, the signal was approximated on the 1st level, and the noise was approximated on the 6th level, then by the following subtraction, the desired, filtered signal's approximation could be acquired:

$$A_{filtered} = A1 - A6, \tag{4.7}$$

where $A1$ is the 1st level approximation, $A6$ is the 6th level approximation and $A_{filtered}$ is the approximation of the filtered signal. Then, this $A_{filtered}$ must be recomposed, by the db8 recomposition and the filtered BP signal is produced.

The invasive signal measured by the GE patient monitor is considered a filtered signal. None of the measured invasive signals contained any visible artefacts, therefore no noise filtering was applied on them, except the moving average filter with the 3 seconds long window to achieve similar phase shifts in both signals.

The last step of signal processing was to find all the systolic and diastolic points in the signal. The diastolic points are the onset points of each cardiac cycle. First, an open source slope sum function-based onset point detection method was applied [64]. After the onset points were found, a maximum search was conducted between each onset point which gave all the systolic points.

4.4.2.4 Calibration of the non-invasive signal for continuous blood pressure comparison study

The non-invasive BP measuring device must be calibrated. Only the invasive arterial BP values were available, therefore the calibration had to be made using the invasively measured values. Therefore, only the contralateral side's BP was known for every participant. Thus, it should be considered in the discussion of the results.

For the calibration, the average invasive BP values were applied, where the averaging was conducted to every systolic, diastolic and mean arterial pressure (MAP) value. The MAP was calculated as the integral of the signal between each onset point (area under the curve). This calculation of the MAP is more accurate than the sum of third of systolic and two thirds of diastolic BP and it also represents the waveform more. The calibration algorithm is the same as presented in the earlier study above, which is the following. First we calculated a gain as follows:

$$Gain = \frac{MAP_{avg} - DIA_{avg}}{U_{avg} - U_{dia}}, \tag{4.8}$$

where MAP_{avg} and DIA_{avg} are the average MAP and diastolic value calculated from the invasive BP signal, respectively. U_{avg} is the average area under curve in the non-invasive uncalibrated signal between each cardiac cycle, and U_{dia} is the average measured value by the non-invasive sensor in each diastolic point. After the gain is specified, the calibrated BP values were calculated, as follows:

$$NICBP\left(t\right) = Gain \cdot \left(U\left(t\right) - U_{dia}\right) + DIA_{avg}, \tag{4.9}$$

where $NICBP(t)$ is the non-invasive continuous BP at time (t), U_{avg} and U_{dia} are the same defined above. $U(t)$ is the uncalibrated recorded value by the non-invasive sensor.

4.4.2.5 Statistical methods for continuous blood pressure comparison study

The invasive and non-invasive BP signals were compared via the correlation between the signals and the root mean squared error (RMSE) values. For further comparisons, the Bland-Altman plot method was applied to check the agreement between two measuring techniques [90]. To create the graph, the mean of the two systems' recordings (S_x) and the average difference between the simultaneously recorded values (S_y) had to be calculated. For the Bland-Altman plots, limits of agreement were set to ±1.95 standard deviation.

For all the recordings, Bland-Altman plots were depicted, and the mean differences and limits of agreement were calculated. There were 12820 simultaneously recorded systolic and diastolic pressure, and MAP values measured, but 660 points were considered as outliers and were excluded. Therefore, 12160 measurement pairs were included in the analysis. The criterion for outlying were specified by the interquartile range (IQR) outlier finding method. The lower limit of the criterion was calculated as follows:

$$L = Q_1 - 1.5 \cdot IQR, \tag{4.10}$$

where Q_1 is the first quartile and L is the lower limit. Similarly, the upper limit was calculated as:

$$H = Q_3 + 1.5 \cdot IQR, \tag{4.11}$$

where Q_3 is the third quartile and H is the upper limit. The outlier limits for the diastolic values were -8 and 8 mmHg, and for the systolic values -30 and 15 mmHg, respectively. The ratio of outliers was 5.15%.

In the case of 5 participants, two measurements per participant could be made, therefore in these cases the modified Bland-Altman analysis for repeated measurements within one individual was applied, which made us to be able to take the within subject variation of repeated measurements into consideration [91]. This version of Bland-Altman analysis alters the limits of agreement by the within subject variation of repeated measurements.

The similarity between the invasive and non-invasive signal's frequency domain was also analysed by creating each signal's Fast Fourier Transform (FFT) and calculating the correlation between the two spectra using the whole frequency range (0–50 Hz).

4.4.2.6 Results for continuous blood pressure comparison study

The average correlation between the 26 simultaneously recorded invasive and non-invasive BP signals was 0.9001 ± 0.0588 which indicates a high similarity in the waveforms. Even the least correlating signals had a correlation value more than 0.7, which is considered as a fair similarity. The average correlation between the frequency domain of each simultaneously recorded invasive and non-invasive signals was 0.9988 ± 0.0009 that implies the identity of the frequency components.

The average RMSE values for the systolic and diastolic BP and MAP simultaneously recorded signals were 10.72 ± 7.81 mmHg, 3.12 ± 1.35 mmHg and 2.64 ± 1.22 mmHg, respectively. The distribution of these RMSE values for systolic BP, diastolic BP and MAP are shown in Figure 4.16. The average RMSE values for diastolic BP and MAP, 3.12 ± 1.35 mmHg and 2.64 ± 1.22 mmHg, respectively, suggest a strong agreement. Even the greatest diastolic RMSE value was below 7 mmHg (6.07 mmHg). For MAP, the greatest RMSE value was 7.18 mmHg, all the others were below 5 mmHg. However, the average RMSE value for the systolic BP was 10.72 ± 7.81 mmHg, which was significantly worse than the RMSE values for diastolic pressure and MAP. The maximum RMSE for the systolic pressure was 35.8 mmHg, which is a significant difference. This suggests that the non-invasive measuring method using the described calibration algorithm is less accurate considering the systolic pressure values as compared to the diastolic pressure values.

The agreement between the two methods was also studied using Bland-Altman plots for systolic, diastolic and MAP values shown in Figure 4.17., Figure 4.18. and Figure 4.19, respectively. In the top of these figures for each participant the mean difference
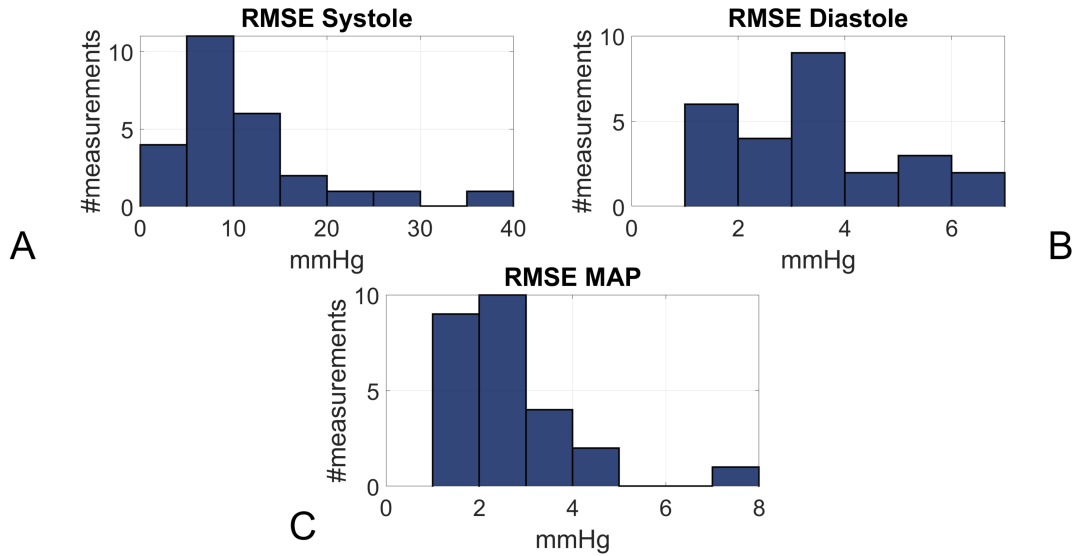
Figure 4.16: The distribution of RMSE values for simultaneously recorded invasive and non-invasive BP signals' systolic (**A**), diastolic (**B**) and MAP (**C**) BP values.

with the respective limits of agreement is depicted. In the bottom of these figures all the included simultaneously recorded non-invasive and invasive systolic, diastolic and MAP pairs are shown, respectively.
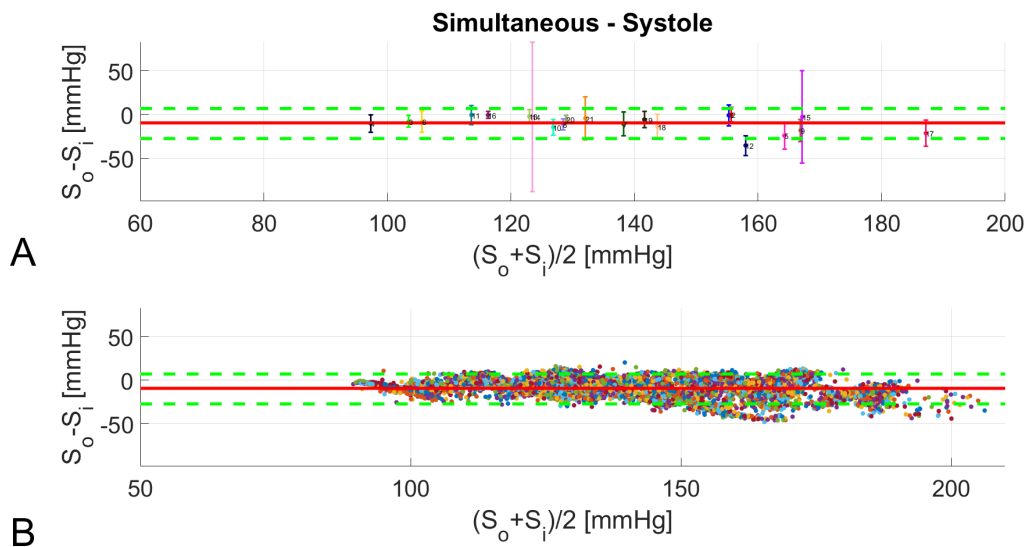
Figure 4.17: (**A**), Bland-Altman plot of the simultaneously measured signals' systolic pressure for each participant with the mean and limits of agreement. The red line is the mean difference for every participant, and the dashed green lines are the average limits of agreement ($1.95\times$ standard deviation). The mean systolic difference with standard deviation is -9.53 ± 4.69 mmHg. (**B**), the same Bland-Altman plot with all the simultaneously measured invasive and non-invasive systolic pairs.
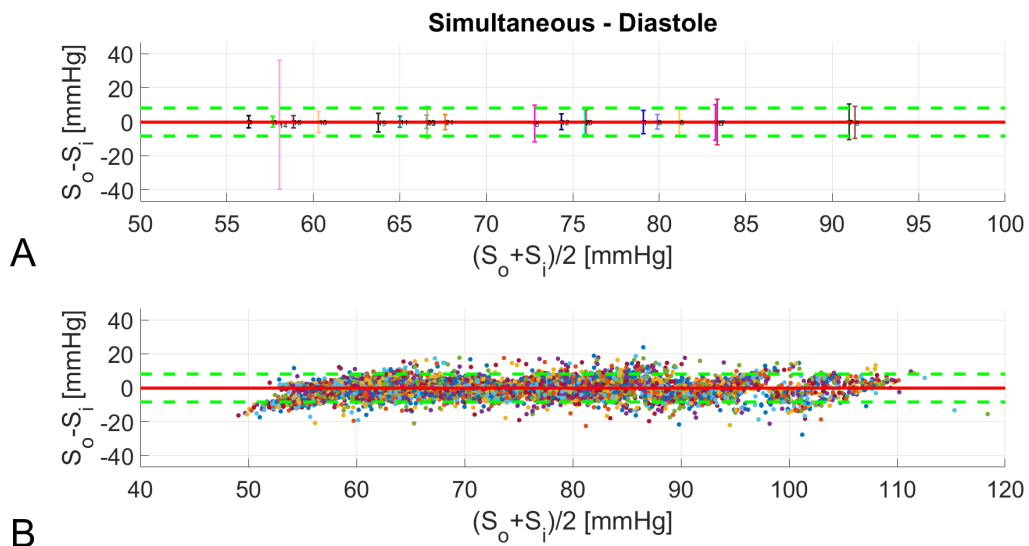
Figure 4.18: (**A**), Bland-Altman plot of the simultaneously measured signals' diastolic pressure for each participant with the mean and limits of agreement. The red line is the mean difference for every participant, and the dashed green lines are the average limits of agreement ($1.95\times$ standard deviation). The mean diastolic difference with standard deviation is -0.26 ± 3.06 mmHg. (**B**), the same Bland-Altman plot with all the simultaneously measured invasive and non-invasive diastolic pairs.
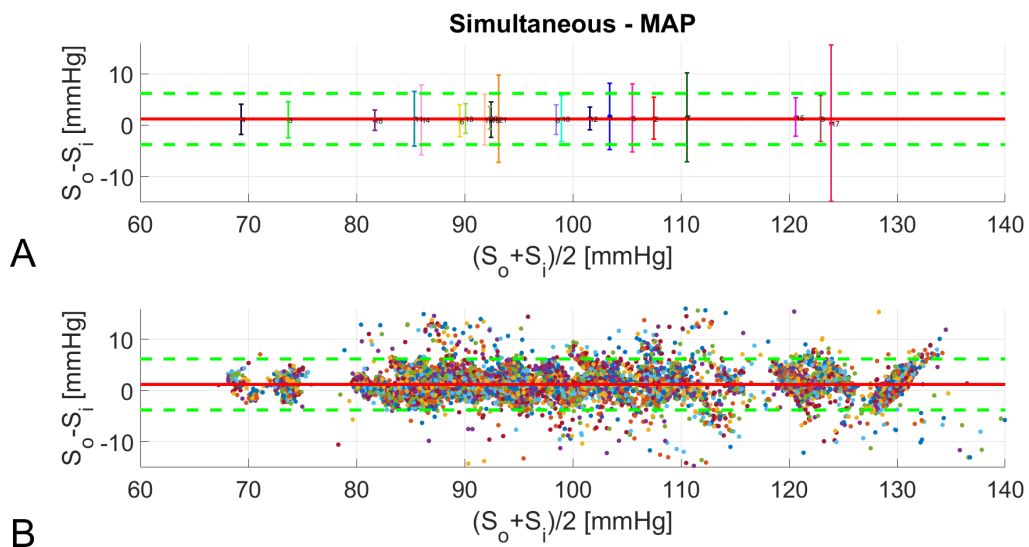
Figure 4.19: (**A**), Bland-Altman plot of the simultaneously measured signals' MAP for each participant with the mean and limits of agreement. The red line is the mean difference for every participant, and the dashed green lines are the average limits of agreement ($1.95\times$ standard deviation). The mean MAP difference with standard deviation is 1.25 ± 2.26 mmHg. (**B**), the same Bland-Altman plot with all the simultaneously measured invasive and non-invasive MAP pairs.

In the case of diastolic BP the mean difference between the simultaneously recorded invasive and non-invasive signals was -0.26 ± 3.06 mmHg, which satisfies the AAMI criterion. If the individual participants are considered, the greatest deviation of the mean diastolic pressure differences was 1.8 mmHg. The mean differences and limits of agreement are shown in Figure 4.18. For the studied 12160 invasive and non-invasive diastolic BP pairs, 11691 were inside the mean limits of agreement, where the mean limits of agreement ranged from -7.58 mmHg to 7.19 mmHg. 96.14% of the measured values are inside the mean limits of agreement. The widest limits of agreement was for Participant no. 14 from -34.31 mmHg to 33.86 mmHg, in which case there were several very short, high amplitude sudden motion artefacts in the signal.

In the case of MAP the mean difference between the simultaneously recorded invasive and non-invasive signals was 1.25 ± 2.26 mmHg, which also satisfies the AAMI criterion. For the individual participants, the greatest deviation of the mean MAP differences was 1.67 mmHg. All the mean differences and limits of agreement are shown in Figure 4.19. For the 12160 invasive and non-invasive MAP pairs, 11672 were inside the mean limits of agreement, where the mean limits of agreement ranged from -3.74 mmHg to 6.23 mmHg. It means that 95.99% of the measured values are inside the mean limits of agreement. The widest limits of agreement was for Participant no. 17 from -12.4 mmHg to 15.12 mmHg, in which case the non-invasive signal is like an envelope of the invasive signal. This means that in the invasive signal there were two separable peaks in one heart cycle, the systolic peak and the dicrotic notch, while in the non-invasive signal the dicrotic notch did not appear, it enveloped it, which causes a greater difference in the area under the two curves.

For the systolic pressures, the results show weaker similarity. The mean difference between the simultaneously recorded invasive and non-invasive systolic values was -9.53 ± 4.69 mmHg, which is out of the 5 mmHg bias range allowed by the AAMI criterion. For 8 out of 21 results of each participants satisfies the 5 mmHg bias range. All the mean differences and limits of agreements are shown in Figure 4.17.

4.4.2.7 Discussion for continuous blood pressure comparison study

Our results suggest that the presented continuous non-invasive blood pressure monitoring method has potential in clinical monitoring. Further developments should be made, but the results prove that the presented method is viable.

As considering the limitations of continuous blood pressure monitoring, measuring under low blood pressure conditions (like hypotension) it seems to be a great challenge. According to our experience, the utilized sensor could detect blood pressure signals from around 40 mmHg, but the quality of these signals was poor. Good quality signals could be recorded from around 50 mmHg depending on the characteristics of the measured

person. The minimal diastolic blood pressure measured during our study was around 48 mmHg.

Comparing this study to other recently published studies using the summary of Lakhal et al. [8] that summarizes the results of 41 recent publications, our results are promising. For a fair comparison, here we analyse only small size studies (patient number was always under 25). For diastole and MAP, we got better results than studies using Peñaz principle-based devices with lower mean bias difference and standard deviation. Balzer et al. [33], Heusdens et al. [34] and Hofhuizen et al. [92] found a mean bias difference around 5 mmHg and standard deviation between 5 and 13 mmHg which are significantly higher than our results. For systole, however, these studies show significantly lower mean bias difference (between -5.2 and 2.7 mmHg) than our results but with a higher mean standard deviation (between 10 and 16 mmHg).

Comparing to tonometric studies published by Lin et al. [22], Meidert et al. [21, 93], Dueck et al. [20], Szmuk et al. [94] and Janelle et al. [95], the mean bias difference values and standard deviation values for diastolic pressure and MAP are generally almost the same as what we found: mean bias difference was between 1 and 5 mmHg and standard deviation was between 4 and 7 mmHg. For systole, these studies showed better results by having the mean bias difference between -3.3 and 2.3 mmHg and standard deviation between 5.9 and 15 mmHg.

Based on aforementioned results from similar studies we can conclude that the blood pressure monitoring method presented in our study, which is still in an early stage of development, could achieve comparable results to commercially available devices. However, further studies should be made to confirm this statement in a wider patient group probably even in participants with presumably more healthy arterial system.

The significantly worse results of the systolic value could arise from two effects. First thing to be considered is the calibration method. The calibration method uses the MAP, which is calculated as the area under curve. If the non-invasive signal behaves as the envelope of the invasive signal, like in the case of participant no. 17, the calibration could lead to lower systolic values. As we proved in our earlier study above, in healthy, young people the 3-axis sensor could measure very accurate and detailed non-invasive continuous BP signals. In the current study, mainly elderly participants were measured with serious cardiovascular diseases. According to our experiences in most cases on elderly people the non-invasive signals were less detailed, mainly were an envelope of the invasive signal. This difference could arise from the measurement technique itself, because by the non-invasive technique only the movement of the arterial wall can be measured. In elderly, presumably more atherosclerotic people the arterial wall is stiffer, and is more so for individuals with cardiovascular disease. This could lead to distortion between the invasive and non-invasive signals. The other reason, why the systolic results were significantly worse, is also connected to the previous idea. If the signal remains

detailed, the systolic peak could be lower in non-invasive measurements, thus the arterial wall movement is less significant in the sense of diameter, it could not carry these detailed parts of the signal.

Another factor that should be considered in the sense of the accuracy in systolic BP is that there were no information of the BP difference between the two arms for each participant during the measurements. This fact is not the most probable factor in the difference, because this should affect the accuracy of MAP values too, but still has to be considered.

To improve the results, a non-linear calibration algorithm should be developed that can solve the theoretical differences in invasive and non-invasive blood pressure measurements. Also, a validation study with invasive arterial cannulation on younger people without severe cardiovascular diseases should be made to prove that the results for systolic pressure is due to the alterations in the arterial wall stiffness. If this is the case, then a mathematical model should be created, how the calibration method should be altered according to the condition of the arteries.

Chapter 5

Pulse diagnostics

This chapter summarizes the results achieved during my work in the field of pulse diagnostics. This includes the steps of creating a strong signal processing algorithm based on the literature. To be able to create a pulse diagnostic system, thousands of continuous pulse waveforms are required. This issue was the major limitation of this project since there were no available databases which include continuous non-invasive pressure waveform and corresponding patient's case history.

In this chapter, pulse waveform means the arterial BP waveform without BP information (filtered and normalized).

5.1   Signal processing

For noise filtering, a cascaded adaptive filter was applied. It consists of a wavelet decomposition filter, an onset point detection algorithm and a spline estimation filter as introduced in the previous chapter 4.4. Validation by invasive arterial cannula section. The wavelet decomposition filter utilizes the discrete Meyer wavelet transformation. The Meyer wavelet is linear-phase and orthogonal. Its function $(\psi(\omega))$ can be defined as follows [63]:

$$\psi\left(\omega\right) = \begin{cases} (2\pi)^{-1/2} \times e^{j\omega/2} \times sin\left(\frac{\pi}{2} \times \nu\left(\frac{3}{2\pi}\left|\omega\right| - 1\right)\right) & \text{if } \frac{2\pi}{3} \leq \left|\omega\right| \leq \frac{4\pi}{3}, \\ (2\pi)^{-1/2} \times e^{j\omega/2} \times cos\left(\frac{\pi}{2} \times \nu\left(\frac{3}{4\pi}\left|\omega\right| - 1\right)\right) & \text{if } \frac{4\pi}{3} < \left|\omega\right| \leq \frac{8\pi}{3}, \\ 0 & \text{if } \left|\omega\right| \notin \left[\frac{2\pi}{3}, \frac{8\pi}{3}\right], \end{cases} \quad (5.1)$$

where $\nu\left(a\right)$ is an auxiliary function defined as:

$$\nu\left(a\right) = a^4 \times \left(35 - 84 \times a + 70 \times a^2 - 20 \times a^3\right), \, a \in [0, 1]. \quad (5.2)$$

The approximation level of the signal is the first level and the approximation of the noise is the seventh level.

For onset point detection both the adaptive windowing technique [60] and the slope sum function-based method [64] are utilized. The adaptive windowing technique requires an initial window size. This can be set by using the pulse rate of the subject, if it is

available or can be determined by the strongest element of the FFT spectrum. After the initial window is set, the algorithm consists of the following steps:

- Initialization phase:

  - From the beginning of the signal using the initial window, the global maxima inside the given window have to be found.

  - The closest local minimum left from the peak found have to be marked. This is the first onset point of the signal.

- From the first onset point, using the initial window, the global maximum point inside the window have to be found.

- The onset point left from the peak point gained from the previous step have to be found as the closest local minimum.

- The adaptive window have to be set as 1.5× the difference between the last two onset points.

- The above steps have to be repeated while there are points in the signal.

This method is good for both a frequent and a slow pulse rate and it can deal with several small amplitude noises. But problem arises, when the signal contains a noise of greater amplitude like arm movement or tremor during the measurement, or if something unexpected, but physiologic occurs, like sudden extra beat or beats occurred in the case of arrhythmia.

The other onset point searching algorithm is the slope sum function method. First, the derivative of the arterial waveform signal must be calculated. Then, in a predefined window, the derivative of the signal points must be summed as follows [64]:

$$z_i = \sum_{k=i-w}^{i} \Delta u_k, \qquad \Delta u_k = \begin{cases} \Delta y_k : \Delta y_k > 0 \\ 0 : \Delta y_k \leq 0 \end{cases} , \qquad (5.3)$$

where z_i is the slope sum function at time i, w is the window size and Δy_k is the derivative of the signal at time k. If the window is defined correctly, this summed function have local maxima points almost exactly at the onset points. This position must be corrected a bit. For this purpose, another window size must be defined. Within this window around the assumed onset point, a global minimum point must be found, this will be the correct position of the onset point.

This slope sum function method performs well in the case of noisy signals and it can also deal with missbeats or extrabeats. Only very frequent or slow pulse rates can lead to higher chance of incorrect onset points. So, in this case the window parameters must be optimized. The other considerable problem is the amplitude of the signal. If the

amplitude is too low, then the difference between two consecutive points can be a small value. Therefore, the sum of the differentiated signal can be distorted, the derivative-based extremal search can found incorrect onset point candidates. To avoid this incorrect indication, the signal should be stretched by multiplying it with an adequate positive integer.

To complete the filtering of the baseline wander, a spline estimation filter is utilized. This method fits an estimated spline curve on the onset points and subtracts it from the wavelet filtered signal. The piecewise cubic spline function is the following:

$$S\left(x\right) = \sum_{k=0}^{3} a_k x^k + \sum_{i=1}^{L} b_i \left(x - X_i\right)_+^3 , \tag{5.4}$$

$$\left(x - X_i\right)_+^3 = \begin{cases} \left(x - X_i\right)^3 & \left(x \geq X_i\right), \\ 0 & \left(x < X_i\right), \end{cases} , \tag{5.5}$$

where a_k and b_i are the coefficients of the polynomial, $(X_i, F\left(X_i\right))$ is the knot of the cubic spline, $k = 0, 1, 2, 3$ and $i = 1, ...L$, L is the total number of knots [63].

Using a spline curve for filtering is advantageous, because it creates a smooth curve along the onset points, as its second derivative is continuous. Therefore it distorts the signal less than a higher order polynomial. The result of the spline estimation filter is a pulse signal without baseline wander, meaning that all onset points are on a vertical line.

Why is it important to remove the baseline wander in pulse diagnostics? It is difficult enough to find the small, but crucial differences between two pulse waveforms. If the baseline wander presents in the signal, it expands the differences between two waveforms. This difference refers to the blood pressure fluctuations, which is less significant information in the field of pulse diagnostics.

5.1.1 Graphical User Interface

During my work, I created a graphical user interface (GUI) for signal processing in Matlab. Utilizing more freedom in design, it was completely designed in a Matlab script, not with the built-in Matlab GUIDE. It has three main windows. The first window is an Open signal function shown in Figure 5.1. During my work, there were several different methods how the force sensor's software saved the signal, thus the opening method must be selected. Also, it can load the already processed and saved signals. The sampling frequency can also differ between measurements, so all the viable sampling frequency options can be chosen (100, 333 and 1000 Hz).

The second window is the core of this GUI, the signal processing window shown in Figure 5.2. Here, all the signal processing steps can be tuned, for the best performance. After changing each parameter, the result is shown in the plot on the right. There is a fast signal processing button, which performs all the signal processing steps automatically
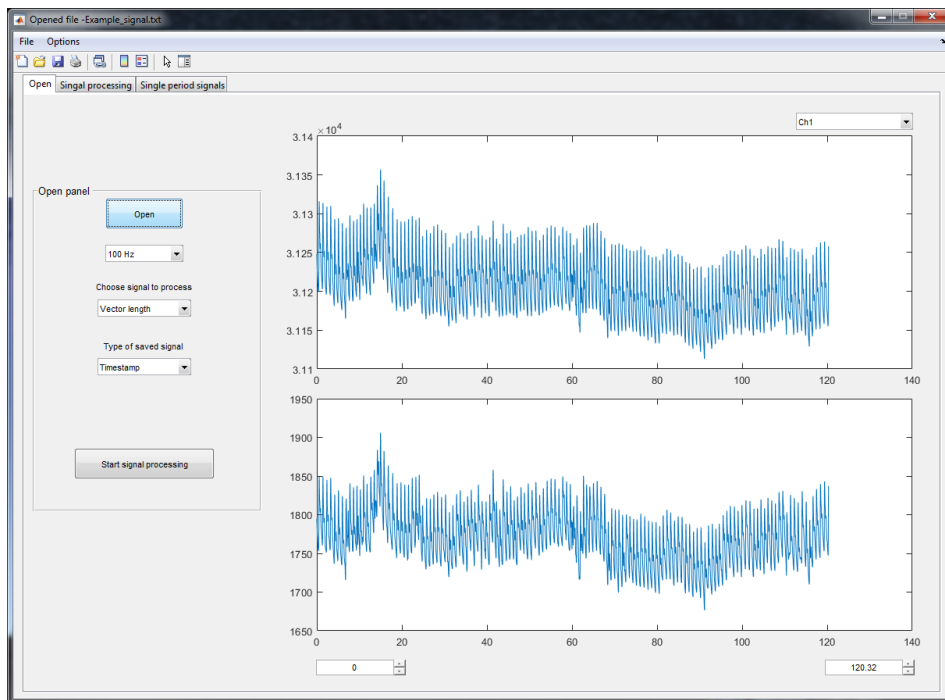
Figure 5.1: The Open tab of the GUI. In the upper panel, the raw sensor output of the first light sensing element can be seen. In the bottom panel, the vector length is depicted, calculated from the raw sensor data. For both panels, the x-axis is the time in seconds.
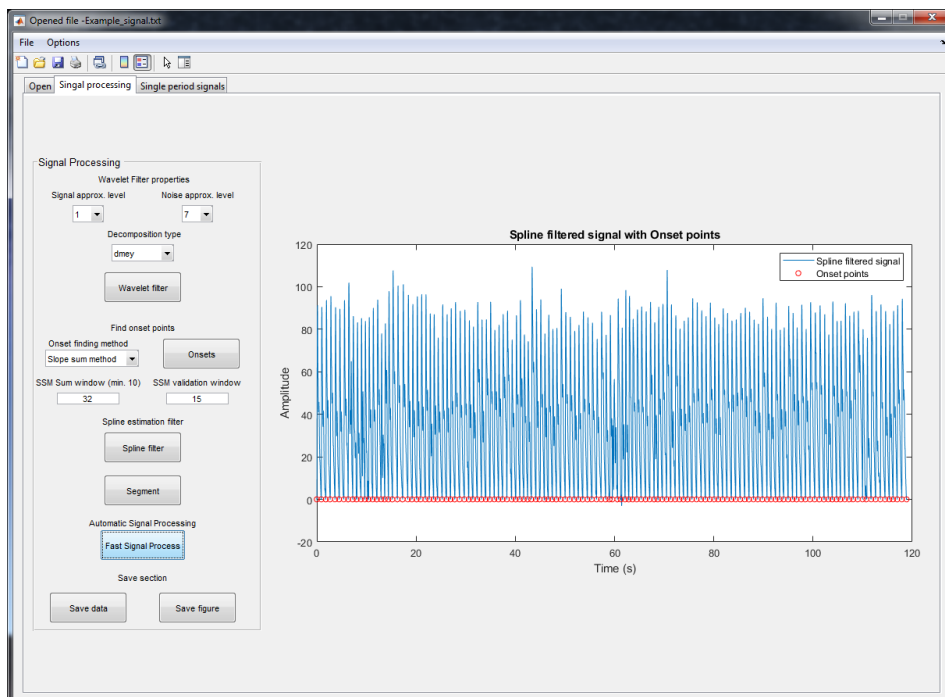
Figure 5.2: The signal processing tab of the GUI.

with the previously set default values, which were optimized during my work. For wavelet decomposition filter it can be set which wavelet transform method should be used such as Discrete Meyer, Daubechies, Symlets and Haar wavelet decomposition method. The appropriate wavelet approximation level for the signal and the noise can be set as well.

For the onset point search, the two options are the Slope sum function-based method and the adaptive windowing method. For the Slope sum function-based method, the window size for summation and for the onset point correction can be set to be able to optimize for fast or slow pulse rates. For the adaptive windowing method there is no need for parameters, the only parameter required is the sampling frequency, but that is known from the Open signal tab. The Spline filter button does the baseline drift removal by applying the Spline estimation filter. The Segment button segments the filtered signal along the found onset points. It also jumps to the Single-period signals tab.

There is a Fast Signal Processing button, which is a single-button signal processing function, doing automatically all the above steps using the default parameters. It can be used for most of the signals providing a fast tool for the user. The Save data button saves everything to a .mat file. It includes the original signal with all the originally measured parameters such as the values of each individual channel of the sensor and the original x-, y- and z-coordinates.
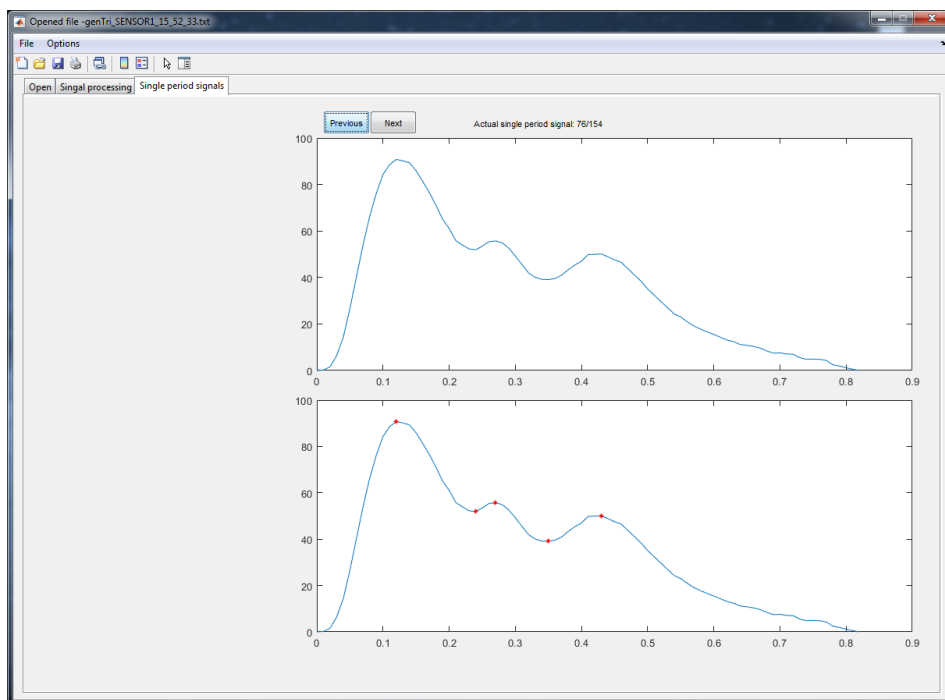
Figure 5.3: The Single-period signal tab of the GUI. In both panels the selected single period signal is shown, in the bottom, the characteristic points are also marked. The y-axis is the signal Amplitude after signal processing, the x-axis is the time in seconds.

In the Single-period signal tab, shown in Figure 5.3., all the single-period signals can

be checked. Also in the bottom axis, the characteristic points of the single-period signal are shown. The characteristic point search algorithm is based on the local extrema search using the derivative of the signal. This algorithm works well if the three waveforms can be distinguished visually. This local extrema search is also fine tuned with the search for pseudo-zero crossing points in the derivative of the signal. Here, instead of the zero line, the -0.02 line is taken into account. Thus, the pseudo extrema points can be found, which in many cases are considered as characteristic points.

There are many development ideas for this GUI. One of them is the integration of a scaling parameter for the Slope-sum function method. Experiences suggest, that with higher amplitude, even for bad quality signals, the onset point detection is better. Therefore, using a scaling parameter, a wider range of signals can be processed. The improvement of the single-period signal tab would require much more development. This tab should be expanded with a feature extraction button, a selection part, where the user can choose from the features which he or she would use. And in the final version, I would like to include a Diagnostic tab with the classification of the signals, and according to the determined class, a GUI would suggest a diagnosis.

5.2   Measurements

Measurements were conducted under ethical license no. 186/2013. All the participants got oral and written information about the measurements. All the measurements were recorded by me with the help of Flóra Zieger, who also helped in database recording and systematization. All information of the participants were recorded anonymously.

The measurements were conducted in sitting position with both hands parallel on a table at heart height. Before the start of signal recording, there was a several minutes long resting phase. The measurement protocol was the following:

- First, the 3D force sensor was attached to the right or left wrist.

- A cuff-based blood pressure measurement was made on the same side as the sensor.

- When the cuff is fully deflated, a 3-min-long measurement was started with the force sensor.

- After the 3 minutes, another cuff-based measurement was made.

- All the above steps were repeated on the contralateral wrist.

During the measurements, a finger PPG sensor was also attached to the same side, where the force sensor was and the pulse rate at the start and at the end of the 3-min-long measurements was recorded in the database. For the cuff-based blood pressure measurements an Omron M1 Compact semi-automatic device was utilized.

There were 175 participants, their characteristics are shown in Table 5.1. One aim was to have participants in each age group to be able to study the effects of ageing. Figure 5.4. shows the proportion of men and women in different age groups. Also there were several participants with different kind of diseases as shown in Table 5.2. It is important to mention that the participants' medical history was taken as self-assessment, so this must be considered later in forming conclusions.

Table 5.1: Characteristics of the participants

	Total	Men	Women
Number of participants	175	67	108
Age (years)	45.12 ± 12.04	42.64 ± 12.43	46.66 ± 11.59
Height (cm)	170.34 ± 9.74	179.9 ± 6.81	164.4 ± 5.73
Weight (kg)	76.18 ± 16.11	87.07 ± 15.23	69.42 ± 12.6
BMI (kg/m^2)	26.15 ± 4.63	26.49 ± 5.81	25.67 ± 4.48
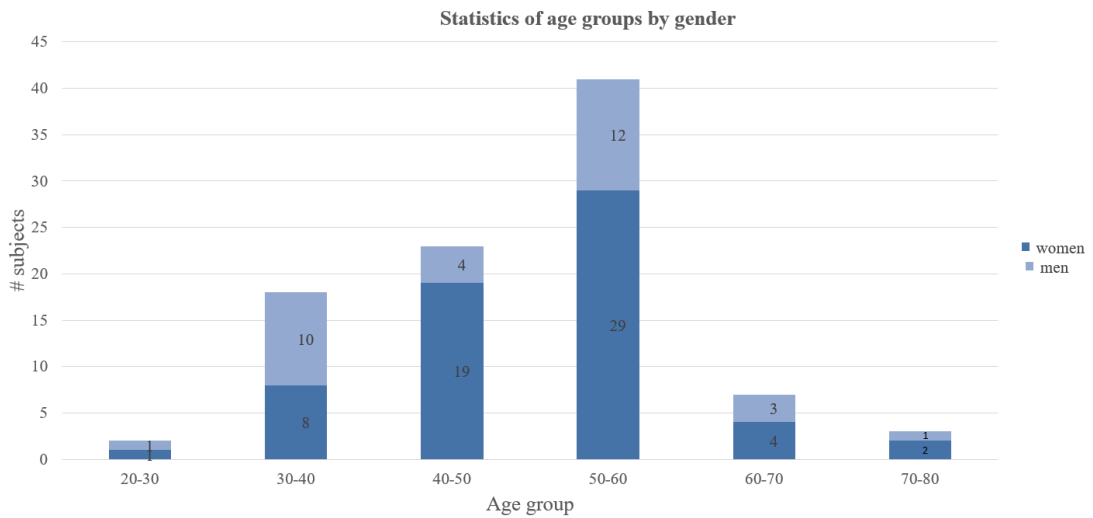
Figure 5.4: Proportion of men and women in different age groups in the recorded database.

A Table 5.2. suggests that the healthy and the hypertensive conditions had a significant presence in our recorded signals. Thus, these two groups could be examined further.

The measurement protocol is summarized in Figure 5.5.

Table 5.2: Statistics summarized according to health conditions of the participants

Condition	Male	Female	Age (years)	BMI (kg/m^2)
Healthy	44	60	44.59 ± 11.29	25.68 ± 4.78
Hypertension disease	16	33	53.73 ± 9.86	28.87 ± 4.68
Diabetic disease	5	7	53 ± 4.92	31.53 ± 4.86
Heart diseases	3	11	53.36 ± 12.63	26.95 ± 4.33
Kidney diseases	1	3	47 ± 15.55	26.66 ± 3.14
Liver disease	3	3	46.33 ± 4.58	23.31 ± 4.11
Abnormal cholesterol	6	11	54.65 ± 12.04	28.57 ± 4.23
Vascular diseases	2	4	53.83 ± 11.37	25.69 ± 2.51
Smoking habit	5	17	47.95 ± 9.52	26.22 ± 4.52

Inform the participant

↓

Collect data by a questionnaire anonymously

↓

Measurement protocol repeated for both arms:

- 3D force sensor based system attachment at the wrist

- BP cuff an plethysmograph attachment on the same arm

- BP measurement by cuff

- After complete deflation of the cuff with a one minute resting phase, a 3-min-long recording with the 3D sensor

- After the 3 minutes, another BP measurement by cuff

Figure 5.5: Summary of the measuring protocol for pulse diagnostic measurements.

5.3   Feature extraction

To describe the signal waveform for the classification or clustering algorithms, features have to be defined. The features should describe the signal obviously, but they should also have the smallest dimension possible, therefore for feature extraction observations should be taking into account. These observations mean how our brain recognize different waveforms, how we can distinguish for example ECG signals from pulse waveforms.

Features in general have three main groups, absolute, relative and derived features. The easiest for human understanding are the absolute features. These features include the amplitude and time features of the signal. The absolute features includes the characteristic points of the signal including its amplitude and time. The width of the signal in different height can also be important. Absolute features are shown in Figure 5.6.
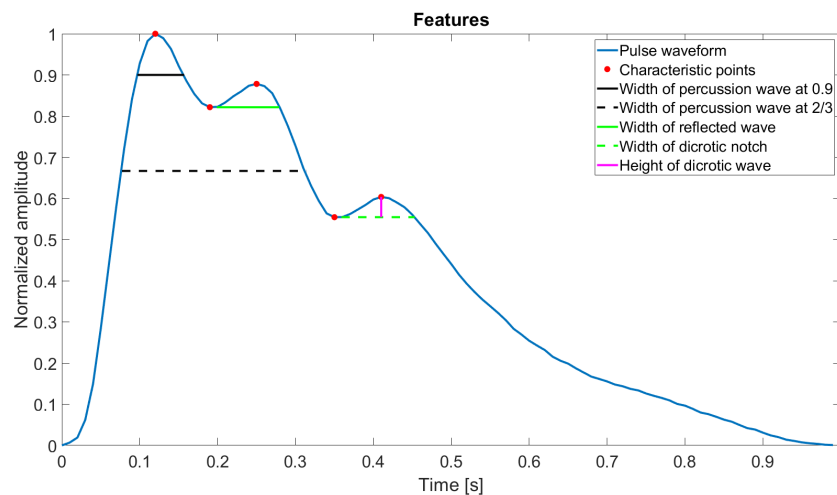
Figure 5.6: Absolute features of a pulse signal.

Absolute features include the following:

- amplitude features:

    - percussion peak

    - initial point of the reflected wave

    - reflected peak

    - initial point of the dicrotic wave

    - dicrotic peak

    - height of the dicrotic wave as the difference between the amplitude of the dicrotic peak and the amplitude of the initial point of the dicrotic peak

- time features:

    - percussion peak

- initial point of the reflected wave

- reflected peak

- initial point of the dicrotic wave

- dicrotic peak

- width of the percussion wave at the amplitude of 0.9

- width of the percussion wave at the amplitude of 2/3

- width of the reflected wave (start point is at the initial point of the reflected wave)

- width of the dicrotic wave (start point is at the initial point of the dicrotic wave)

- width of the signal

Not all the pulse waveforms have distinguishable reflected or dicrotic waves, therefore several features can be missing. In these cases the given features are considered 0.

The other feature type is the relative features. These can be calculated as the proportion of different absolute features. The most commonly used relative features in the case of pulse waveforms are:

- the relative height of each characteristic point:

  - ratio of the reflected peak and the percussion peak

  - ratio of the dicrotic peak and the percussion peak

  - ratio of the dicrotic peak and the reflected peak

- the relative length in time:

  - ratio of time of the reflected peak and time of the percussion peak

  - ratio of time of the dicrotic peak and time of the percussion peak

  - ratio of time of the percussion peak and pulse signals duration

  - ratio of time of the dicrotic peak and pulse signals duration

The relative features can be advantageous, because they have no dimensions, and they can compress the information. But also due to its relative nature, similar proportions could occur for significantly different signals.

The third type is the derived features. These features can be gained by different mathematical functions or transformations of the signal, like integrate of the signal or Fourier or Hilbert-Huang transformation [67]. A typical derived feature is the area under the waveform, which can be calculated for the whole signal or just a part of it. By Fourier transformation frequency features can be obtained, like the frequency of the heart beat.

The size of the presented database was too low and diverse to find the best features for signal description. But for future studies, it was important to become familiar with the topic of feature extraction.

5.4 Clustering

The presented database is too small to create a classification algorithm. Also, its size is not enough to create many clusters to separate different conditions. So, I concentrated only on the healthy and hypertensive signals and I tried to separate them by clustering using only the information gained from the waveform. The evaluation is based on the database information. To validate the results, I applied two different algorithms, a k-means algorithm and a competitive neural network.

For this clustering the number of features should be minimal to make the dimension of the problem low, thus making it easier for the algorithms to identify differences how to separate the two groups. One feature is based on the observations about the signal shape in different health conditions. In the case of hypertensive signals, the width of the percussion wave is usually much longer, as the reflected wave arrives earlier and merges with the end of the percussion wave. This feature can be described more precisely by taking the numeric integral of the upper 10% of the signal, because the amplitude decreases slowly in a typical hypertensive signal. This can be one of the main differences between the hypertensive signal waveform and the healthy signal waveform of elderly people. The other feature was selected from the absolute features. I took the average and the standard deviation of each absolute feature in the healthy and in the hypertensive group. Then, I searched for the greatest difference between the average features taking the standard deviation into account. The latter is required, because standard deviation can give an interval around the average and I tried to find the least overlapping intervals. The result was not surprising, the greatest difference between the healthy and hypertensive group occurred in the height of the dicrotic peak. The selected features for the clustering is shown in Figure 5.7.

For the clustering 104 healthy participant's signals (44 men and 60 women) and 24 participants (8 men and 16 women) with only hypertension disease were selected according to database information. Overall this includes 256 single-period pulse signals.

I utilized two different algorithms to check whether the results are the same, thus checking the separating capabilities of the chosen features. Both cases I used the built-in functions of Matlab R2019a. The k-means clustering algorithm partitions observations into k cluster by selecting the nearest mean serving as a prototype of the cluster that is also called as the centroid element of the cluster. This algorithm requires the number of clusters, which is in this study equals to two and a distance function. For the distance function the Euclidean distance was applied. The aim of this algorithm is to minimize
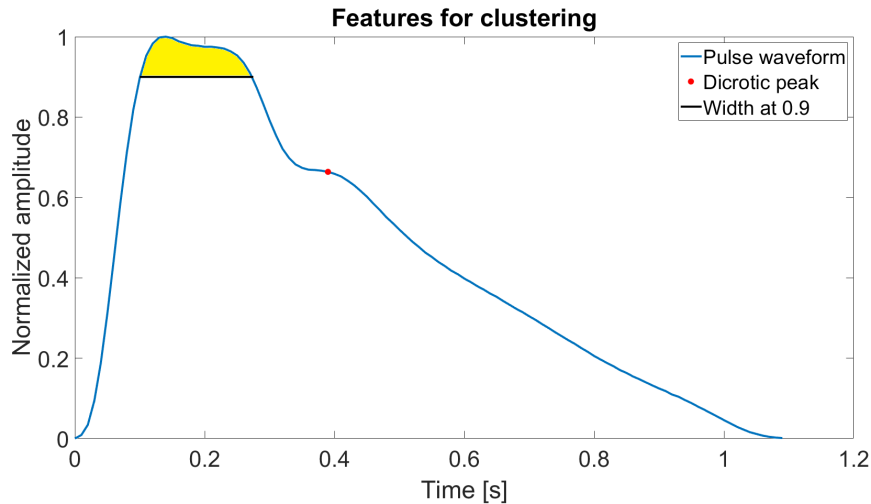
Figure 5.7: Features for pulse signal clustering into healthy and hypertensive groups.

the within cluster distance from the cluster centroid. In each iteration all the distances between each observation and cluster centroid are calculated and according to these distances the observations are separated into two groups. Then, the centroid element of each cluster is set by the average of within cluster observations. And again all the distances between centroid elements and observations are calculated and the observations are separated into two groups. This algorithm continues as long as no more observations change cluster after the centroid element is recalculated.

The other clustering algorithm is based on a competitive neural network. Machine learning and neural networks are very popular tools in every classification and clustering problems. These networks can find patterns in the features, thus they can explore some connections between the data points. I chose the competitive neural network method, because it is commonly used for clustering. In competitive neural networks the neurons are competing to be activated. Thus, during learning their weights change to be activated as often as possible, while the error rate is minimized. This means that the neurons are starting to learn the input pattern and separate the signals into two groups.

In the utilized competitive neural network, there were two competitive neurons to separate the two groups. The learning rule was the Kohonen Learning rule and the network was trained for 1000 epochs. The input matrix was the selected two features for each single-period signal. The output vector contains the corresponding cluster for each single-period signal. I attempted to extend the number of considered features with the age and the BMI data, but the results did not changed significantly.

For evaluation the confusion matrix was used. In this case the statement was that the signal is hypertensive. The actual class was considered as the condition listed in the database and the predicted class was considered as the condition concluded by the

clustering algorithm. Using the confusion matrix, the following values were calculated:

$$\text{Sensitivity} = \frac{\text{number of true positives}}{\text{number of true positives} + \text{number of false negatives}} \tag{5.6}$$

$$\text{Specificity} = \frac{\text{number of true negatives}}{\text{number of true negatives} + \text{number of false positives}} \tag{5.7}$$

$$\text{Precision} = \frac{\text{number of true positives}}{\text{number of true positives} + \text{number of false positives}} \tag{5.8}$$

Here, sensitivity refers to the correctly identified signals as hypertensive signals. Selectivity refers to the correctly rejected healthy signals. Precision is the fraction of truly hypertensive signals among all the signals considered as hypertensive by clustering.

5.5 Results and discussion

First, it is important to know, whether the presented method is able to record signal types frequently discussed in the literature. In Figure 5.8. and 5.9., examples are shown for signal types presented in the literature that appeared in our measurements too. This proves that the presented method is capable to record distinguishable, common signal characteristics.
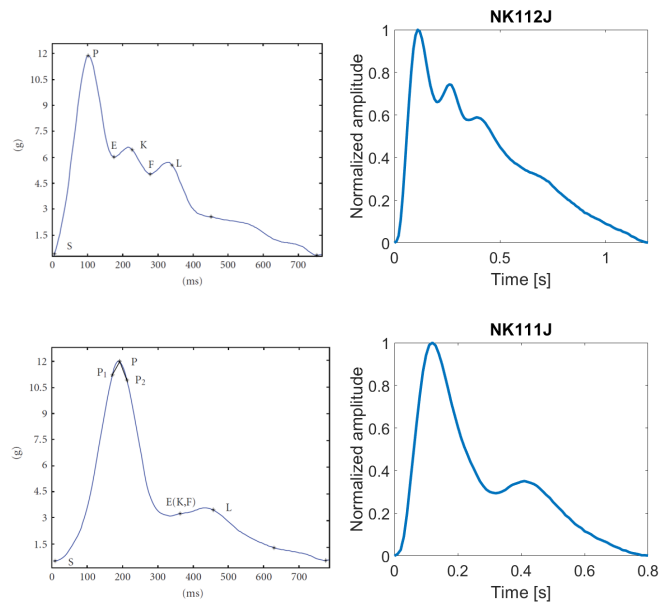
Figure 5.8: The graphics on the **left** are examples from [1] (x-axis is the time for a 100 Hz signal, y-axis is the measured amplitude), and the graphics on the **right** are our results.

The database, which was created, can be considered really valuable, but unfortunately it is not large enough to support truly proved statements. Assumptions can be made, which will require further studies, extended number of measurements. This should be considered in the statements below.
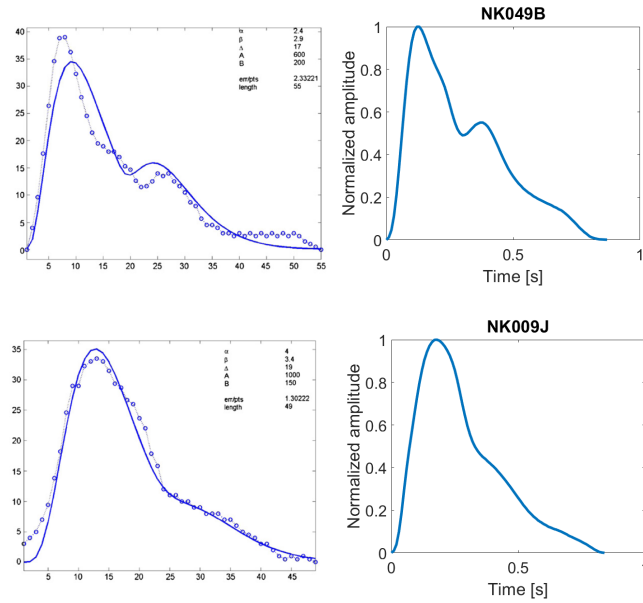
Figure 5.9: The graphics on the **left** are examples from [2] (x-axis is the time for a 100 Hz signal, y-axis is the measured amplitude) reprinted with permission from Elsevier, and the graphics on the **right** are our results.

The signal processing algorithm is robust, meaning it can process most of the measured signals. In around 70% of the measured signals, the default parameters were applicable, in the other 30% of the signals, the parameters had to be adjusted.

a Age group: 20–30

b Age group: 30–40

c Age group: 40–50

d Age group: 50–60
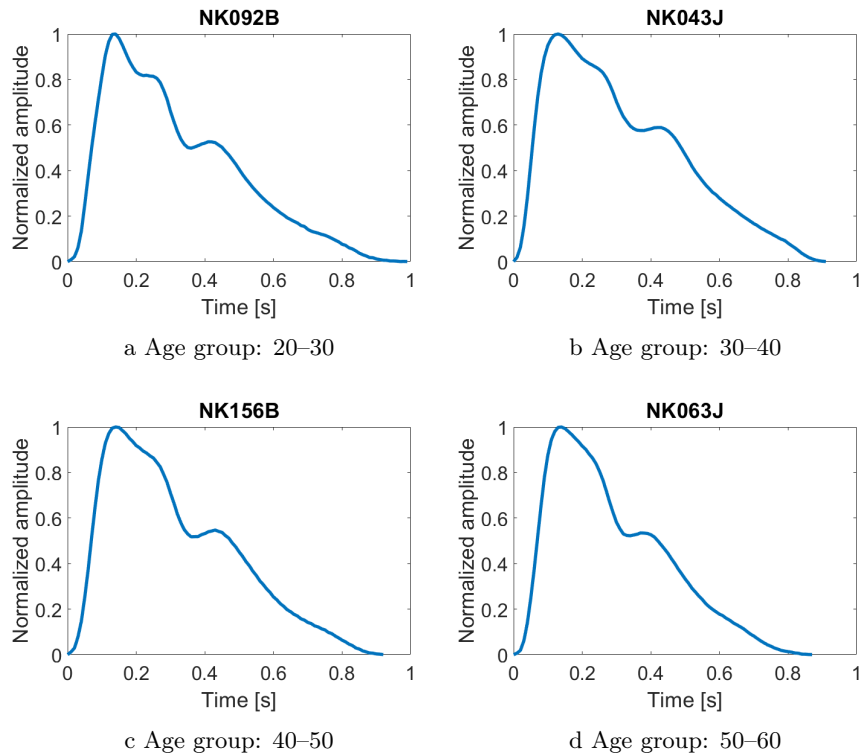
Figure 5.10: Healthy signals in different age groups.

One of the most important results was related to the measurement of the healthy pulse signal in women in different age groups. Figure 5.10. demonstrates the effects of ageing on the pulse signal. It can be recognized that as people get older the arteries get stiffer. In stiff arteries the wave propagation is faster, therefore the reflected wave arrives earlier. As it arrives earlier, it merges with the percussion wave. Similar observation cannot be made in the case of men, because in healthy men the three waves usually cannot be distinguished visually. The possible reason for this is the slight difference in arterial wall structure, usually for man the arteries are a bit stiffer.

a Healthy candidate signals.

b Hypertension candidate signals.

c Arteriosclerotic candidate signals.
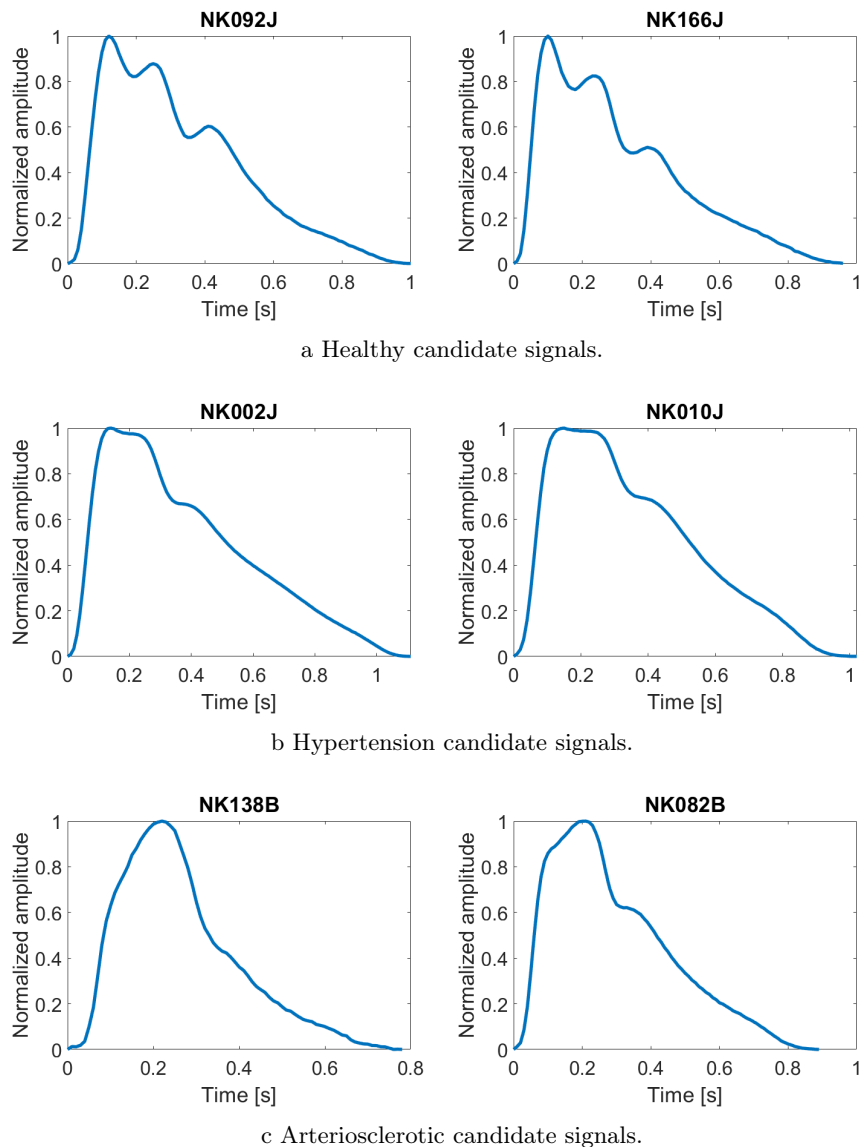
Figure 5.11: Different health conditions.

Another important result is related to signals with different health condition. Considering the medical history and the recorded signals, we could find candidate signals for hypertension and arteriosclerosis beside the healthy signal. These can be seen in Figure 5.11. The candidate signal for hypertension is a bit similar to the elderly healthy women's signal, but the reflected wave arrives with a much higher amplitude creating a plateau

between the percussion and the reflected wave. This higher amplitude arrival can be the effect of the stiffer arteries and the constantly high blood pressure which is accompanied. This hypertensive waveform shows risk for the patient, as high blood pressure during a longer period of time for each heart cycle means a much higher stress for the arterial wall.

In the case of arteriosclerosis, the artery wall is even stiffer than for hypertensive signals. Therefore, the wave propagation is much faster, thus the reflected wave could arrive earlier than the percussion wave, causing a less steep upward rising section in the initial phase of the single-period pulse signals. These patients are from the high cholesterol group, with BMI over the normal range and smoking habit.

a Number of true positives: 34   b Number of false positives: 79

c Number of false negatives: 14   d Number of true negatives: 129
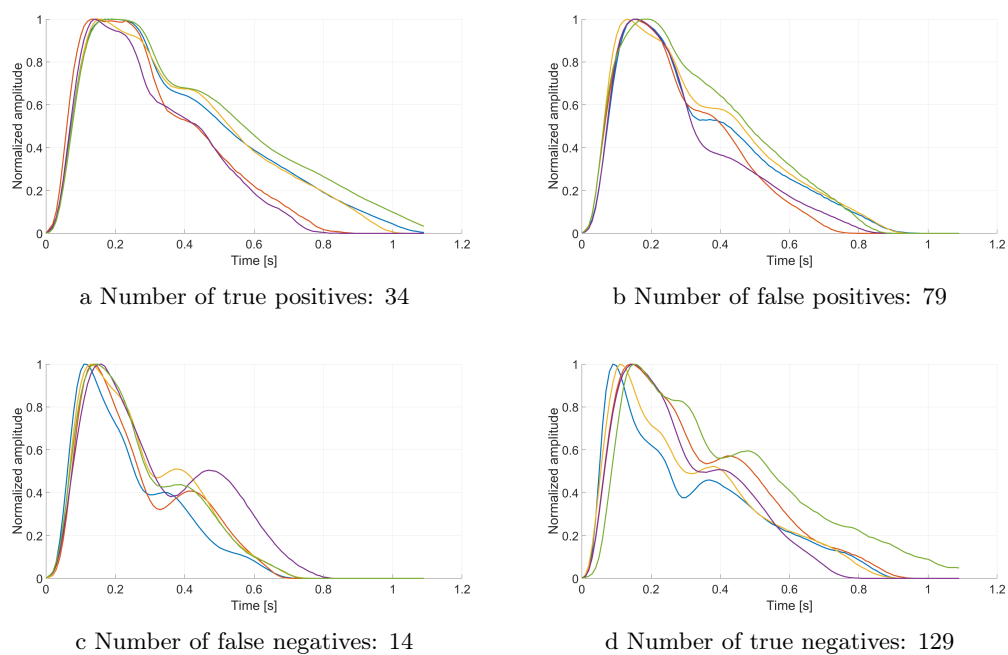
Figure 5.12: Results of the clustering algorithms with several example signals in each group.

The results of the clustering algorithm is shown in Figure 5.12. The sensitivity is 0.7083, the specificity is 0.6202 and the precision is 0.3009. Although at first glance these numbers do not look promising further clarification and discussion are required to evaluate these results. First, there are a great number of healthy signals in the hypertensive cluster. By visual inspection most of these signals would belong to the hypertensive cluster. As the database contains self assessed information, it has a relatively high chance that the given participant does not know about his/her disease. This observation supports even more the potential of this diagnostic technique at the preventative care. Considering the hypertensive signals clustered as healthy, it is important to know that almost all the hypertensive participants was on medication except one participant. This means that for those participants whose disease was diagnosed and treated in an early stage, the condition of their arteries could remain healthy, thus the shape of their signal can be

healthy too.

In summary, the database is too noisy and small to withdraw any strong conclusion. However, considering the limitation and inaccuracy of the dataset, these results are promising for initial proof of the diagnostic capabilities. Based on signal shape, the hypertensive signals could be found with significant sensitivity. Based on the results, further studies would be beneficial, since pulse diagnostics with the presented 3D force sensor based system is relevant and it has a great potential.

Chapter 6

Conclusions, new scientific results, applications

Author's publications

[I] **S. Földi**, T. Horváth, F. Zieger, P. Sótonyi, Gy. Cserey, "A novel non-invasive blood pressure waveform measuring system compared to Millar applanation tonometry," *Journal of Clinical Monitoring and Computing*, vol. 32, no. 4, pp. 717–727, 2018.

[II] **S. Földi**, T. Horváth, F. Zieger, P. Sótonyi, Gy. Cserey, "Comparison of a non-invasive 3D force sensor-based method and the invasive arterial cannula in postsurgery intensive care patients – a pilot study," *Blood Pressure Monitoring*, LWW, vol. 24, no. 6, pp. 310–314, 2019.

Conference publications

[III] **S. Földi**, "Framework for examination the changes of arterial pulse signal waveform in time and space," *PhD Poceedings Annual Issues of the Doctoral School Faculty of Information Technology and Bionics 2014*, pp. 87–90, 2014.

[IV] **S. Földi**, "Validation of a non-invasive arterial pressure waveform measuring system," *PhD Poceedings Annual Issues of the Doctoral School Faculty of Information Technology and Bionics 2015*, pp. 115–118, 2015.

[V] **S. Földi**, "Application areas of continuous non-invasive blood pressure measurements," *PhD Poceedings Annual Issues of the Doctoral School Faculty of Information Technology and Bionics 2016*, pp. 119–122, 2016.

[VI] N. Spulak, **S. Földi**, M. Koller, M. Niemier, J. Schmiedeler, Gy. Cserey, "Wrist pulse detection and analysis using three in-line sensors and linear actuators," *15th International Workshop on Cellular Nanoscale Networks and their Applications; Proceedings of CNNA*

2016, 2016.

[VII] E. Fodor, B. Huberth, A. Csörgő, B. Gellért, D. Lippai, M. Koller, **S. Földi**, L. Madácsy, Z. Tulassay, Gy. Cserey, "Computerized three dimensional mapping and robotic maneuvering through the human large intestine trajectory with magnetic capsule endoscopy using reference tracking control," *Zeitschrift für Gastroenterologie*, vol. 53, no. 05, p. A10, 2015.

Conference presentations

[VIII] **S. Földi**, F. Zieger, P. Sótonyi, Gy. Cserey, "Pulse diagnosis using arterial blood pressure waveforms," *Minisymposia at The 20th European Conference on Mathematics for Industry*, 2018.

[IX] **S. Földi**, F. Zieger, P. Sótonyi, Gy. Cserey, "Egy új lehetőség non-invazív vérnyomás mérésére," *Magyar Hypertonia Társaság XXVI. Továbbképző Kongresszusa Program és Absztrakt Kötet*, p. 30, 2018 (ISBN 978-615-00-2781-4), 2018.

6.1   Thesis group 1.

Thesis 1. *I have created a novel measurement method which can record non-invasive blood pressure characteristics from the radial artery using a 3D force sensor. I have defined the sensor attachment protocol to record non-invasive blood pressure characteristics. The designed wrist band and this protocol provides an easy to learn method with high repeatability. Signals from repetitive measurements by the same operator showed high (≈ 0.99) correlation. This novel method also has the advantage that it can measure approximately same quality signals on its surface in the $50°$–$130°$ angle range from the 3D force sensor's base plane.*

I have designed a wrist band, which can be used to attach the sensor to the wrist. It consist of a 3D printed sensor holder, its position can be adjusted on the band. An important design property is its adjustability, but still remaining fixed during the measurements (robust). This means that it was able to resist most of the patient's movements or other effects on the wrist band and hold the sensor in its initial position over the radial artery. My experiments proved that this sensor attachment solution has the above properties.

The protocol contains the following steps:

- The radial artery is attempted to be found at the wrist by palpation.

- At a strongly pulsating point the sensor is attempted to be attached. The tip of the sensor's dome is put over the strongest pulsating point, then the band is fixed using the buckle.

- A check should be done whether the amplitude of the signal is over 100 units for every channel and the 3D force vector is close to the $90°$, if so, the sensor placement is completed. Otherwise, the position of the sensor has to be adjusted by moving the sensor holder on the band or the band must be tightened. If the strongest pulsating point cannot be found the initial position of the sensor has to be changed, using palpation again to find the strongest pulsating point and trying to position the sensor over it.

The presented repeatability study proved that using the defined protocol the measurements are repeatable. Also, it is easy to learn, requires only several minutes of training.

Publication partially connected to this thesis: [I].

6.2   Thesis group 2.

Thesis 2.1. *I have compared this 3D force sensor-based method with another non-invasive continuous blood pressure monitoring method. Using a Millar tonometer as the validation device and making measurements in a young, healthy group, my results showed that the 3D force sensor-based method is within the AAMI criterion, which requires a bias within 5 mmHg and a standard deviation within 8 mmHg. After the calibration of both sensors by cuff BP measurement, for systolic, diastolic, incisura pressures and MAP the difference between the two methods were* 0.35 ± 1.75 *mmHg,* 0.02 ± 0.19 *mmHg,* 3.84 ± 3.90 *mmHg and* 2.88 ± 2.42 *mmHg, respectively.*

The Millar tonometer method is a validated and approved, commercially available continuous blood pressure waveform measurement method. A trained personal is required for the conduction of these measurements. The comparison of the 3D force sensor-based method and the Millar tonometer for continuously available BP values and also the continuous wave's shape was conducted. Both devices can measure relative BP changes, therefore they require calibration by a cuff BP measurement.

Publication related to this thesis: [I].

Thesis 2.2. *I have carried out validation measurements by an invasive arterial cannula to check the waveform similarity between the two methods. In this study the invasive and the non-invasive continuous blood pressure waveforms were compared. Simultaneous measurements were carried out on 9 participants with altogether 13 measurements. After signal processing for the waveforms the average correlation was* 0.9527 ± 0.0917. *To prove*

the repeatability, for 4 participants two consecutive measurements were conducted. The correlation values for each pair of measurements were: (0.939 ± 0.142, 0.971 ± 0.096); (0.968±0.055, 0.977±0.022); (0.986±0.024, 0.969±0.076); (0.935±0.073, 0.954±0.032)

It was crucial to compare the measurable continuous BP signal to the real BP waveform. For pulse diagnostics, the shape of the continuous BP signal is more important than the nominal BP values. Therefore, this study aims to compare the waveform of the invasive arterial cannula's signal and the non-invasive signal. Before comparison, the same signal processing steps were applied for each signal.

Publication related to this thesis: [IV].

Thesis 2.3. *I have compared the 3D force sensor-based method with an invasive arterial cannula studying the blood pressure values. The invasive system measured the absolute BP, the non-invasive system was calibrated to measure the relative BP changes. This validation study included 21 participants with altogether 26 simultaneously recorded non-invasive and invasive continuous blood pressure measurements. The average difference between the simultaneously recorded invasive and non-invasive systolic, diastolic and mean arterial pressure was −9.53 ± 4.69, −0.26 ± 3.06 and 1.25 ± 2.26 mmHg, respectively.*

The best practice to validate a continuous BP monitoring device is to compare with the gold standard invasive arterial cannula measurement that can measure the absolute BP. In this validation, the continuous BP signals from the two different devices were compared, so both the actual BP value and the continuous waveform were taken into consideration. The participants involved in this study were mainly elderly patients (the average age was 63.8 ± 11.2) who all underwent a serious cardiovascular system connected surgery.

The non-invasive system had to be calibrated to be able to measure the relative BP changes. The systolic and diastolic values of the invasive and non-invasive signals were contrasted. The diastolic values are equivalent to the momentary values of the continuous BP signal at each onset point. Similarly, the systolic values are equivalent of each single-period signal's global maxima point (between the current and the next onset points). The waveform similarity is taken into consideration by calculating the MAP using the integral of the waveform signal.

Publication related to this thesis: [II].

6.3   Thesis group 3.

Thesis 3. *A database was created by measuring on both arms of 175 people with the novel, 3D force sensor-based method and collecting data on the participants health condition. The measured signals showed agreement with common pulse waveforms presented in the literature of the related field. Using the presented database and the widely accepted observations of the related literature, I could demonstrate the frequently discussed signal types for the healthy and hypertensive group of the recorded signals. The effect of ageing in healthy people was also observable in the measured signals. I applied a k-means and a competitive neural network clustering method to separate the pulse waveforms into two groups, healthy and hypertensive, based on the waveform. The presented methods had the same result: 0.71 sensitivity, 0.62 specificity and 0.30 precision.*

The basic step of developing a pulse diagnostic device is to prove its capability of recording single-period signals commonly described in the literature of the related field. In the absence of online annotated database, we created a database with our measurements. These measurements included 175 people, 350 signals (measurements on both hands). Each signal was 3 minutes long. The database was recorded anonymously, it included antropometric characteristics of each participant, like age, height, weight, BMI, gender. For all participant it was noted, if he or she had an internal organ or cardiovascular disease and the smoking habits. All the data on the participants were self-assessment. The measurements included oscillometric blood pressure measurement before and after each pulse signal recorded. In data collection and database systematization, Flóra Zieger provided me a great help.

According to the database, there were 104 participants, 208 signals, who had not have any known disease at the time of the measurement and 24 hypertensive participants, 48 signals. For clustering two features were selected. The first feature is the numeric integral of the normalized averaged single-period pulse signal above the 0.9 line of its amplitude. The other feature is the amplitude of the dicrotic peak of the normalized averaged single-period pulse signal. To cluster the signals I used two different methods, the k-means clustering algorithm using the Euclidean distance and a competitive neural network based clustering method built-in in the Matlab R2019a software. Both algorithms concluded the same result. In the hypertensive cluster, there were 34 signals from participants with hypertension and 79 signals from healthy participants. In the healthy cluster, there were 14 signals from participants with hypertension and 129 signals from healthy participants. This means 0.7083 sensitivity, 0.6202 specificity and 0.3009 precision.

In the evaluation of these results several assumptions should be considered. The information on participants' condition was self-assessment, therefore it can be noisy. 23 of the 24 participants were taking medication for hypertension which could improve their condition. In the case of healthy participants, it is possible that they have hypertension,

but they did not know about it at the time of the measurements. And finally, the size of the database is low, much more data would be required to make more confident statement. However, the results showed that there is quantitatively describable difference between the healthy and the hypertensive pulse signals, which proves the potential of this novel method in pulse diagnostics.

Publication related to this thesis: [V, VI, VIII].

6.4 My participation in Theses as a co-supervisor

During my PhD process, I have supervised several thesis works connected to my dissertation. In this section, a short summary of these topics is presented.

6.4.1 Examination of physical stress caused morphological alterations on arterial pressure waveform from pulse diagnosis perspective

In this topic, the aim was to examine how the physical activity affects the pulse waveform. It is important in different aspects, like how the activity affects the measurable signal, thus the diagnostic strength. If the physical activity can change a signal in a way that it becomes a pathological signal, then it should be considered in diagnostic measurements. The other aspect is how the signal is distorted, it can also carry crucial information about the physiological condition of the studied person. It may also be useful in the survey of physical attributes. The result of this thesis showed similarity with the results found in the literature, meaning decrement in the amplitude of the dicrotic notch and the change in the time of the reflected wave. So, the physical activity should be considered in the diagnostic measurements, as it can distort the recordable signal significantly.

Reference: Flóra Zieger, '*Examination of changing morphology in arterial blood pressure wave caused by physical exercise in pulse diagnosis view*', MSc Thesis, 2015

6.4.2 Filtering motion artefacts during continuous blood pressure measurement

Motion artefacts are a great challenge in non-invasive continuous BP measurements. This topic tried to find a way of filtering motion artefacts using the 3D force sensor's capabilities. The idea of the Author was to examine all sensor channels individually and try to find connection between these signals and the motion artefacts. There were several promising observations and a trial was conducted to correct the part of the signal affected by motion. The main challenge is to generalize these observations, because much depends on the sensor's position above the artery, and the accuracy of the algorithm also depends on the attributes of the measured person. So, as will presented below, first a generalized

signal quality index is required, which can help in detection of motion artefacts and have a general assumption on how the signal quality can be improved.

Reference: Tamás Herkó, '*Filtering motion artefacts from non-invasive continuous blood pressure measurements*', BSc Thesis, 2016

6.4.3 Determination of pulse transit time with non-invasive pressure waveform and ECG

This thesis created the first steps in development of self calibration method of the presented 3D force sensor based system. In this study, we attempted to estimate the current BP using the simultaneously recorded continuous arterial pressure waveform measured by the 3D force sensor at the radial artery and an ECG. The estimated BP was compared to the BP values measured by an oscillometric cuff-based device. The trials showed promising results, but further studies are required. One limitation is the available ECG device, which has a sampling frequency of 250 Hz, which can lead to error in estimation as 1000 Hz would be the optimal sampling frequency. The other limitation is the parameter optimization of the estimation function. It was optimized on a small group of participants, but this optimization should be done on groups of people with different health characteristics and different age. The final goal would be to develop a personalized parameter optimization.

Reference: Zsófia Schramek, '*Feasibility study of Ankle-Brachial index determination using tactile sensors*', BSc Thesis, 2018

6.4.4 Non-invasive cuff-based blood pressure measurement using the 3D force sensor

This topic is about trying to create a new method for cuff-based blood pressure measurement. As mentioned, today the most frequently used method is the oscillometric method. It uses the small BP fluctuations to detect the mean arterial pressure to determine the systole and diastole values. The idea was, that by measuring the continuous BP signal at the wrist on radial artery, same side where the cuff is, there are signs in the continuous BP signal reflecting the systolic and diastolic BP while the cuff deflates. Unfortunately, the results were not strong enough, so a new idea, a new approach is required to make a viable combination of the arm cuff and the 3D force sensor for intermittent BP measurement.

Reference: Bonifác Olivér Tóth, '*Non-invasive blood pressure monitoring using tactile sensor*', BSc Thesis, 2016

6.4.5 Implementation of continuous non-invasive blood pressure monitoring with 3D force sensors and automatized sensor placement

This thesis is about the automation of sensor placement. The Author of this Thesis created a bracelet-like automatized sensor placement device. The device is capable of sensor placement in a two dimension plane parallel to the cross-sectional plane of the radial artery and also uses different touch depths. The design seems generalized enough as it was able to make measurements on participants with different physical characteristics. It was able to find the optimal measuring point on the radial artery in several trials. There are still many parts that can be improved, but it was a great step forward in automation of sensor placement. It is not only crucial for optimal sensor placement, but also for sensor position adjustment during recording to acquire good quality signals.

Reference:

- András Bakó, *'Feasibility analysis of automatized pulse diagnosis with 3D tactile sensor'*, BSc Thesis, 2016

- András Bakó, *'Automatized 3D tactile sensor positioning for non-invasive blood pressure waveform measurement'*, MSc Thesis, 2018

6.4.6 Determination of quantitative quality index for arterial pressure waveform

This is the most recent Thesis in this topic. Defining a quantitative quality index is a very hard task, but it is crucial in many-many fields of this topic. The difficulty of this task is to distinguish the signals affected by noise or having a low quality from those that are pathological, related to a disease, it is far not trivial. Moreover, defining what good quality means in the sense of continuous BP waveforms is difficult. The Author of this thesis defined a quality index using literature examples. This quality index merges and weights different quantitative statistical characteristics of the arterial pressure waveform found in the literature. The pilot results of this quality index showed better results than the individual quality indices, which is quite promising. This is still a studied topic, in still ongoing trials with the above mentioned automatized sensor placement device is merged with this quality index, improving its sensor positioning on radial artery. It is also planned to try its efficiency on signals related to diseases.

Reference: Anna Ignácz, *'Quantitative quality measure of arterial blood pressure signals'*, BSc Thesis, 2018

6.5   Future development ideas

The main challenge in continuous non-invasive BP measurement is sensor placement and robust measurements for a long period of time. These requirements define the future development areas.

First of all, as already mentioned above, the meaning of signal quality must be defined for continuous BP signals measured by the 3-axis sensor. This is a difficult task, because the diseased signals and the bad quality signals must be distinguished. Sometimes it is easy, it can be decided by just comparing the magnitude of the signal or the steepness of it. But determining the signal quality can also be quite challenging, for example in the case of deeply pressed signals. If the arteries are pressed down too deep, a distorted signal could be measured also in healthy case. This deeply pressed BP signal can be similar to the hypertensive BP signal. The main difference is the initial upward phase of the signal and the downfall after the percussion peak. The reflected part of the signal is usually absent. The defined quality index should also distinguish between different levels of good quality to be able to measure in the best signal acquiring position.

To make this non-invasive BP monitoring system more robust, and thus minimizing the number of bad measurements, the automatized sensor placement system should be developed. Utilizing the above mentioned quality index function, a completely automatized sensor placement device can be created. This device would be able to find the best measuring position on the radial artery at the wrist, with the best measuring depth. Also, during measurement, it would be able to compensate the noises occurred, by continuously compensating the patient's movements during the monitoring phase. Thus, it would greatly reduce the number of bad measurements.

Another idea to improve the robustness of the system is a noise detection sensor. This sensor can be another 3-axis sensor on an indifferent point at the wrist. This would measure the movements of the wrist. Using this sensor's signal, the movement noise could be compensated. The trials suggest that it is a challenging task, because it is hard to find an indifferent point that can measure similar movement signals as the BP signal measuring sensor. The other idea is to use another type of sensor for movement detection, like gyro sensors. This can identify the movement, but it cannot give any idea, how to compensate the 3-axis sensor's signal. Therefore, this noise detection sensor idea still requires a lot of research and development.

6.6   Applications

Bedside monitor The major application area is in critical care, anaesthetic procedure and ambulance monitoring. It could not substitute the invasive method for every situation, because in lot of the cases arterial blood tests are crucial which indicates the application of invasive arterial cannula. But in every other case it is capable to offer a great option for practitioners and patients. Also in ambulance it could be very effective, as there are not any continuous blood pressure monitoring options during patients' transportation, only the intermittent oscillometric cuff-based blood pressure monitor is available.

A business plan was created based on the presented non-invasive continuous blood pressure measuring system by Flóra Zieger. This was part of a combined project presented to the European Union's SME competition, where it reached over the threshold title. Which also proves the commercial potential of this measuring method.

Mobile BP monitoring device Due to its ease and safety of use, the non-invasive continuous BP monitoring can also be used at homes as a mobile device. Continuous BP signals measured at home in different day times would give a valuable tool for practitioners to conclude a particular diagnostic decision. During the day, the characteristics of the signal can change, collecting all the signal types, the patient specific signal waveform can be determined. So it can be a good alternative for the Ambulatory Blood Pressure Monitoring (ABPM), which is a 24 hours long intermittent BP monitoring method using a cuff-based BP measuring system. Event evoked changes, failures may also be detected easier and more detailed using the continuous BP signal waveform. Furthermore, it would be able to create a database to be used for study purposes and preventative care (effects of diseases, drugs, day cycle events on pulse waveform).

Supplemental parameter measuring This non-invasive continuous BP measurement method could be used as an additional parameter when measuring the physiological system with another diagnostic method, like ECG, MR or CT. Continuous blood pressure waveform could give an important additional (complementary) information, parameter. It can be used to follow important parameters, like blood flow velocity or augmentation index of the artery. Today, it is very rare to use continuous BP measurement during these non-invasive diagnostic methods, due to its invasive nature. However, based on discussion with practitioners, the continuous BP signal would give them a lot of parameters and sometimes crucial information about the patient, which they could use during surgery or treatment planning.

Diagnostics Using the continuous waveform, this measurement method could be a useful diagnostic device for several inner-organ or cardiovascular diseases. The waveform

analysis and its diagnostic capabilities were discussed in the Pulse diagnostics chapter. If this non-invasive continuous BP measuring method was widespread, and many data were collected then it is possible that a number of diseases could be diagnosed, and patients could be oriented which organ system is involved and so which specialist is most likely to give an answer if visited. It has also potential in medicine development, it could be a tool to follow the effects of several medicines, i.e. antihypertensive drugs. Measuring the pulse waveform during medical treatment would be a great tool to follow the drug effects. It could also lead to a device that can optimize the amount of drug intake, by detecting the effectiveness of the drug according to the changes in the pathological signal. So, if BP waveform suggests faster improvement in the condition of the patient then the doctor can decide whether dose of the drug intake can be decreased, therefore the side effects can be minimized.

Pulse transit time Extending the measurement with an ECG system, the Pulse Transit Time can be calculated. By Pulse Transit Time, the Pulse Wave Velocity can be determined, which is proportional to the blood pressure, therefore it is able to estimate the blood pressure non-invasively without a cuff-based measurement. This could lead to a cuffless calibration method for our non-invasive continuous blood pressure monitor.

Ankle-brachial index This continuous blood pressure monitoring device has also some potentials in ankle-brachial index (ABI) measurement. ABI is a diagnostic method mainly for the diagnosis of arteriosclerosis [96]. It takes the brachial systolic BP and the systolic BP measured at the ankle on the tibial artery and calculates their proportion. The normal range is between 1 and 1.2. If it is over 1.3, it refers to vessel hardening. If the ABI value is below 0.9 then it refers to different levels of vessel diseases. Measuring the blood pressure at the ankle is not an easy task. For that purpose nowadays a BP cuff is applied, but the oscillometric version is not that popular, because it is not robust enough, instead a device using ultrasound is applied to detect the start of the blood flow in the occluded artery and besides the systolic BP based on the cuff's current pressure. But still, the measured BP at the ankle is not as robust and accurate as in the case of brachial BP. The 3D force sensor is capable of recording the BP waveform at the ankle, therefore using the PTT method, it could provide an alternative technique for ankle BP monitoring. It requires development to create a robust device, but even the initial trials seemed viable.

It is also important in ABI, whether the continuous signal is present or not, because it can provide complementary information. Therefore, there is a chance of revolutionizing this ABI method, extending its diagnostic purposes. Also, it should be mentioned that using the PTT-based blood pressure estimation, better accuracy of ankle blood pressure could be reached compared to cuff-based measurements.

Fitness device As a potential commercial application, non-invasive continuous blood pressure monitoring could also be applied in fitness devices, like smart watches, fitness bracelets. By the continuous signal, it can also give a wider range of parameters, like blood flow velocity, augmentation index and estimation of arterial stiffness. It can also provide more information about the effects of the exercises on the body. It could support a personalized training plan. And it could be useful for sport clubs and trainers, to evaluate their players' stamina, physical preparedness.

Acknowledgements

References

[1] P.-Y. Zhang and H.-Y. Wang, "A framework for automatic time-domain character-istic parameters extraction of human pulse signals," *Eurasip Journal on advances in signal Processing*, vol. 2008, no. 1, p. 468390, 2007. (document), 2.3, 4.4.2.3, 5.8

[2] J.-J. Shu and Y. Sun, "Developing classification indices for chinese pulse diagnosis," *Complementary therapies in medicine*, vol. 15, no. 3, pp. 190–198, 2007. (document), 5.9

[3] E. Chung, G. Chen, B. Alexander, and M. Cannesson, "Non-invasive continuous blood pressure monitoring: a review of current applications," *Frontiers of medicine*, vol. 7, no. 1, pp. 91–101, 2013. 1, 2.2.1

[4] E. P. Widmaier, H. Raff, K. T. Strang, and A. J. Vander, *Vander's human physiology: the mechanisms of body function.* Boston: McGraw-Hill Higher Education,, 2008. 2.1.1, 2.1.2

[5] E. N. Marieb and K. Hoehn, *Human anatomy & physiology.* Pearson Education, 2007. 2.1.1

[6] C. Vlachopoulos, M. O'Rourke, and W. W. Nichols, *McDonald's blood flow in arter-ies: theoretical, experimental and clinical principles.* CRC press, 2011. 2.1.5

[7] E. J. Kroeker and E. H. Wood, "Comparison of simultaneously recorded central and peripheral arterial pressure pulses during rest, exercise and tilted position in man," *Circulation research*, vol. 3, no. 6, pp. 623–632, 1955. 2.2.1

[8] K. Lakhal, S. Ehrmann, and T. Boulain, "Non-invasive blood pressure monitoring in the critically ill: time to abandon the intra-arterial catheter?," *Chest*, 2017. 2.2.2, 4.4.2.7

[9] K. Lakhal, M. Martin, S. Ehrmann, and T. Boulain, "Noninvasive monitors of blood pressure in the critically ill: What are acceptable accuracy and precision?," *European Journal of Anaesthesiology (EJA)*, vol. 32, no. 5, pp. 367–368, 2015. 2.2.2

[10] K.-H. Smolle, M. Schmid, H. Prettenthaler, and C. Weger, "The accuracy of the cnap® device compared with invasive radial artery measurements for providing continuous noninvasive arterial blood pressure readings at a medical intensive care unit: a method-comparison study," *Anesthesia & Analgesia*, vol. 121, no. 6, pp. 1508–1516, 2015. 2.2.2

[11] C. Lawrence, "Physiological apparatus in the wellcome museum. 1. the marey sphygmograph," *Medical history*, vol. 22, no. 2, pp. 196–200, 1978. 2.2.2.2

[12] N. Langwieser, L. Prechtl, A. S. Meidert, A. Hapfelmeier, C. Bradaric, T. Ibrahim, K.-L. Laugwitz, R. M. Schmid, J. Y. Wagner, and B. Saugel, "Radial artery applanation tonometry for continuous noninvasive arterial blood pressure monitoring in the cardiac intensive care unit," *Clinical Research in Cardiology*, vol. 104, no. 6, pp. 518–524, 2015. 2.2.2.2

[13] Y. Yao, L. Wang, L. Hao, L. Xu, S. Zhou, and W. Liu, "The noninvasive measurement of central aortic blood pressure waveform," in *Blood Pressure-From Bench to Bed*, IntechOpen, 2018. 2.2.2.2

[14] P. Salvi, G. Lio, C. Labat, E. Ricci, B. Pannier, and A. Benetos, "Validation of a new non-invasive portable tonometer for determining arterial pressure wave and pulse wave velocity: the pulsepen device," *Journal of hypertension*, vol. 22, no. 12, pp. 2285–2293, 2004. 2.2.2.2

[15] M. W. Rajzer, W. Wojciechowska, M. Klocek, I. Palka, M. Brzozowska-Kiszka, and K. Kawecka-Jaszcz, "Comparison of aortic pulse wave velocity measured by three techniques: Complior, sphygmocor and arteriograph," *Journal of hypertension*, vol. 26, no. 10, pp. 2001–2007, 2008. 2.2.2.2

[16] B. Saugel, R. Dueck, and J. Y. Wagner, "Measurement of blood pressure," *Best Practice & Research Clinical Anaesthesiology*, vol. 28, no. 4, pp. 309–322, 2014. 2.2.2.2

[17] G. M. Janelle and N. Gravenstein, "An accuracy evaluation of the t-line® tensymeter (continuous noninvasive blood pressure management device) versus conventional invasive radial artery monitoring in surgical patients," *Anesthesia & Analgesia*, vol. 102, no. 2, pp. 484–490, 2006. 2.2.2.2

[18] P. Szmuk, E. Pivalizza, R. Warters, T. Ezri, and R. Gebhard, "An evaluation of the t-line® tensymeter continuous noninvasive blood pressure device during induced hypotension," *Anaesthesia*, vol. 63, no. 3, pp. 307–312, 2008. 2.2.2.2

[19] B. Saugel, A. Meidert, A. Hapfelmeier, F. Eyer, R. Schmid, and W. Huber, "Non-invasive continuous arterial pressure measurement based on radial artery tonometry in the intensive care unit: a method comparison study using the t-line tl-200pro device," *British journal of anaesthesia*, vol. 111, no. 2, pp. 185–190, 2013. 2.2.2.2

[20] R. Dueck, O. Goedje, and P. Clopton, "Noninvasive continuous beat-to-beat radial artery pressure via tl-200 applanation tonometry," *Journal of clinical monitoring and computing*, vol. 26, no. 2, pp. 75–83, 2012. 2.2.2.2, 4.4.2.7

[21] A. . Meidert, W. Huber, J. Müller, M. Schöfthaler, A. Hapfelmeier, N. Langwieser, J. Wagner, F. Eyer, R. Schmid, and B. Saugel, "Radial artery applanation tonometry for continuous non-invasive arterial pressure monitoring in intensive care unit patients: comparison with invasively assessed radial arterial pressure," *British journal of anaesthesia*, vol. 112, no. 3, pp. 521–528, 2013. 2.2.2.2, 4.4.2.7

[22] L. Wq, W. Hh, S. Cs, Y. Jt, Xiao, C. Yp, W. Xz, and C. Gz, "Comparison of continuous noninvasive blood pressure monitoring by tl-300 with standard invasive blood pressure measurement in patients undergoing elective neurosurgery.," *Journal of Neurosurgical Anesthesiology*, vol. 29, no. 1, pp. 1–7, 2017. 2.2.2.2, 4.4.2.7

[23] J. Sun, H. Chen, J. Zheng, B. Mao, S. Zhu, and J. Feng, "Continuous blood pressure monitoring via non-invasive radial artery applanation tonometry and invasive arterial catheter demonstrates good agreement in patients undergoing colon carcinoma surgery," *Journal of clinical monitoring and computing*, vol. 31, no. 6, pp. 1189–1195, 2017. 2.2.2.2

[24] G. Greiwe, P. Tariparast, C. Behem, M. Petzoldt, L. Herich, C. Trepte, D. Reuter, and S. Haas, "Is applanation tonometry a reliable method for monitoring blood pressure in morbidly obese patients undergoing bariatric surgery?," *British journal of anaesthesia*, vol. 116, no. 6, pp. 790–796, 2016. 2.2.2.2

[25] J. Fortin, W. Marte, R. Grüllenberger, A. Hacker, W. Habenbacher, A. Heller, C. Wagner, P. Wach, and F. Skrabal, "Continuous non-invasive blood pressure monitoring using concentrically interlocking control loops," *Computers in biology and medicine*, vol. 36, no. 9, pp. 941–957, 2006. 2.2.2.2

[26] C. Ilies, M. Bauer, P. Berg, J. Rosenberg, J. Hedderich, B. Bein, J. Hinz, and R. Hanss, "Investigation of the agreement of a continuous non-invasive arterial pressure device in comparison with invasive radial artery measurement," *British journal of anaesthesia*, vol. 108, no. 2, pp. 202–210, 2012. 2.2.2.2

[27] J. R. Martina, B. E. Westerhof, J. van Goudoever, E. M. H. de Beaumont, J. Truijen, Y.-S. Kim, R. V. Immink, D. A. Jöbsis, M. W. Hollmann, J. R. Lahpor, *et al.*, "Non-invasive continuous arterial blood pressure monitoring with nexfin®," *The Journal of the American Society of Anesthesiologists*, vol. 116, no. 5, pp. 1092–1103, 2012. 2.2.2.2, 2.2.2.2

[28] J. Y. Wagner, I. Negulescu, M. Schöfthaler, A. Hapfelmeier, A. S. Meidert, W. Huber, R. M. Schmid, and B. Saugel, "Continuous noninvasive arterial pressure measurement using the volume clamp method: an evaluation of the cnap device in intensive care unit patients," *Journal of clinical monitoring and computing*, vol. 29, no. 6, pp. 807–813, 2015. 2.2.2.2

[29] K. Ameloot, K. D. V. Van, N. R. Van, I. L. De, K. Schoonheydt, H. Dits, O. Broch, B. Bein, and M. Malbrain, "Validation study of nexfin® continuous non-invasive blood pressure monitoring in critically ill adult patients.," *Minerva anestesiologica*, vol. 80, no. 12, pp. 1294–1301, 2014. 2.2.2.2

[30] G. A. Kumar, A. Jagadeesh, N. G. Singh, and S. Prasad, "Evaluation of continuous non-invasive arterial pressure monitoring during induction of general anaesthesia in patients undergoing cardiac surgery," *Indian journal of anaesthesia*, vol. 59, no. 1, p. 21, 2015. 2.2.2.2

[31] J. R. Martina, B. E. Westerhof, N. de Jonge, J. van Goudoever, P. Westers, S. Chamuleau, D. van Dijk, B. F. M. Rodermans, B. A. J. M. de Mol, and J. R. Lahpor, "Noninvasive arterial blood pressure waveforms in patients with continuous-flow left ventricular assist devices.," *Asaio Journal*, vol. 60, no. 2, pp. 154–161, 2014. 2.2.2.2

[32] J. J. Vos, M. Poterman, E. A. Mooyaart, M. Weening, M. M. Struys, T. W. Scheeren, and A. F. Kalmar, "Comparison of continuous non-invasive finger arterial pressure monitoring with conventional intermittent automated arm arterial pressure measurement in patients under general anaesthesia," *BJA: British Journal of Anaesthesia*, vol. 113, no. 1, pp. 67–74, 2014. 2.2.2.2

[33] F. Balzer, M. Habicher, M. Sander, J. Sterr, S. Scholz, A. Feldheiser, M. MĂźller, C. Perka, and S. Treskatsch, "Comparison of the non-invasive nexfin® monitor with conventional methods for the measurement of arterial blood pressure in moderate risk orthopaedic surgery patients," *Journal of International Medical Research*, vol. 44, no. 4, pp. 832–843, 2016. 2.2.2.2, 4.4.2.7

[34] J. Heusdens, S. Lof, C. Pennekamp, J. Specken-Welleweerd, G. de Borst, W. van Klei, L. van Wolfswinkel, and R. Immink, "Validation of non-invasive arterial pressure

monitoring during carotid endarterectomy," *BJA: British Journal of Anaesthesia*, vol. 117, no. 3, pp. 316–323, 2016. 2.2.2.2, 4.4.2.7

[35] E. Weiss, E. Gayat, V. Dumans-Nizard, M. L. Guen, and M. Fischler, "Use of the nexfin device to detect acute arterial pressure variations during anaesthesia induction," *BJA: British Journal of Anaesthesia*, vol. 113, no. 1, pp. 52–60, 2014. 2.2.2.2

[36] A. Hohn, J. Defosse, S. Becker, C. Steffen, F. Wappler, and S. Sakka, "Non-invasive continuous arterial pressure monitoring with nexfin® does not sufficiently replace invasive measurements in critically ill patients," *BJA: British Journal of Anaesthesia*, vol. 111, no. 2, pp. 178–184, 2013. 2.2.2.2

[37] M. Fischer, R. Avram, I. Cârjaliu, M. Massetti, J. Gérard, J. Hanouz, and J. Fellahi, "Non-invasive continuous arterial pressure and cardiac index monitoring with nexfin after cardiac surgery," *BJA: British Journal of Anaesthesia*, vol. 109, no. 4, pp. 514–521, 2012. 2.2.2.2

[38] K. Lakhal, M. Martin, S. Faiz, S. Ehrmann, Y. Blanloeil, K. Asehnoune, B. Rozec, and T. Boulain, "The cnap finger cuff for noninvasive beat-to-beat monitoring of arterial blood pressure: an evaluation in intensive care unit patients and a comparison with 2 intermittent devices," *Anesthesia & Analgesia*, vol. 123, no. 5, pp. 1126–1135, 2016. 2.2.2.2

[39] J. D. Tobias, C. McKee, D. Herz, S. Teich, P. Sohner, J. Rice, M. Michalsky, *et al.*, "Accuracy of the cnap monitor, a noninvasive continuous blood pressure device, in providing beat-to-beat blood pressure measurements during bariatric surgery in severely obese adolescents and young adults," *Journal of anesthesia*, vol. 28, no. 6, pp. 861–865, 2014. 2.2.2.2

[40] K.-H. Smolle, M. Schmid, H. Prettenthaler, and C. Weger, "The accuracy of the cnap device compared with invasive radial artery measurements for providing continuous noninvasive arterial blood pressure readings at a medical intensive care unit: A method-comparison study.," *Anesthesia & Analgesia*, vol. 121, no. 6, pp. 1508–1516, 2015. 2.2.2.2

[41] A. Jagadeesh, N. G. Singh, and S. Mahankali, "A comparison of a continuous non-invasive arterial pressure (cnap) monitor with an invasive arterial blood pressure monitor in the cardiac surgical icu.," *Annals of Cardiac Anaesthesia*, vol. 15, no. 3, p. 180, 2012. 2.2.2.2

[42] C. Ilies, G. Grudev, J. Hedderich, J. Renner, M. Steinfath, B. Bein, N. Haake, and R. Hanss, "Comparison of a continuous noninvasive arterial pressure device with invasive measurements in cardiovascular postsurgical intensive care patients:

a prospective observational study.," *European Journal of Anaesthesiology*, vol. 32, no. 1, pp. 20–28, 2015. 2.2.2.2

[43] R. Hahn, H. RinĂśsl, M. Neuner, and S. Kettner, "Clinical validation of a continuous non-invasive haemodynamic monitor (cnap 500) during general anaesthesia," *BJA: British Journal of Anaesthesia*, vol. 108, no. 4, pp. 581–585, 2012. 2.2.2.2

[44] C. Jeleazcov, L. Krajinovic, T. Münster, T. Birkholz, R. Fried, J. Schüttler, and J. Fechner, "Precision and accuracy of a new device (cnap) for continuous non-invasive arterial pressure monitoring: assessment during general anaesthesia," *BJA: British Journal of Anaesthesia*, vol. 105, no. 3, pp. 264–272, 2010. 2.2.2.2

[45] Y. Ma, J. Choi, A. Hourlier-Fargette, Y. Xue, H. U. Chung, J. Y. Lee, X. Wang, Z. Xie, D. Kang, H. Wang, *et al.*, "Relation between blood pressure and pulse wave velocity for human arteries," *Proceedings of the National Academy of Sciences*, vol. 115, no. 44, pp. 11144–11149, 2018. 2.2.2.2

[46] Y. Chen, C. Wen, G. Tao, M. Bi, and G. Li, "Continuous and noninvasive blood pressure measurement: A novel modeling methodology of the relationship between blood pressure and pulse wave velocity," *Annals of Biomedical Engineering*, vol. 37, no. 11, pp. 2222–2233, 2009. 2.2.2.2

[47] S. S. Thomas, V. Nathan, C. Zong, P. Aroul, L. Philipose, K. Soundarapandian, X. Shi, and R. Jafari, "Demonstration abstract: Biowatch: a wrist watch based physiological signal acquisition system," in *Proceedings of the 13th international symposium on Information processing in sensor networks*, pp. 349–350, 2014. 2.2.2.2

[48] J. Baulmann, U. Schillings, S. Rickert, S. Uen, R. Düsing, M. Illyes, A. Cziraki, G. Nickering, and T. Mengden, "A new oscillometric method for assessment of arterial stiffness: comparison with tonometric and piezo-electronic methods.," *Journal of Hypertension*, vol. 26, no. 3, pp. 523–528, 2008. 2.2.2.2

[49] T. Pereira, C. Correia, and J. ao Cardoso, "Novel methods for pulse wave velocity measurement," *Journal of Medical and Biological Engineering*, vol. 35, no. 5, pp. 555–565, 2015. 2.2.2.2

[50] B. Flaws, *The Secret of Chinese Pulse Diagnosis*. Blue Poppy Press, 1995. 2.3

[51] S. Lukman, Y. He, and S. C. Hui, "Computational methods for traditional chinese medicine: A survey," *Computer Methods and Programs in Biomedicine*, vol. 88, no. 3, pp. 283–294, 2007. 2.3

[52] K. Bilton, L. Hammer, and C. Zaslawski, "Contemporary chinese pulse diagnosis: a modern interpretation of an ancient and traditional method," *Journal of acupuncture and meridian studies*, vol. 6, no. 5, pp. 227–233, 2013. 2.3

[53] Y. Chen, L. Zhang, D. Zhang, and D. Zhang, "Wrist pulse signal diagnosis using modified gaussian models and fuzzy c-means classification," *Medical engineering & physics*, vol. 31, no. 10, pp. 1283–1289, 2009. 2.3, 2.3

[54] D. Zhang, L. Zhang, D. Zhang, and Y. Zheng, "Wavelet based analysis of doppler ultrasonic wrist-pulse signals," in *2008 International Conference on BioMedical Engineering and Informatics*, vol. 2, pp. 539–543, IEEE, 2008. 2.3

[55] D. Zhang, W. Zuo, D. Zhang, H. Zhang, and N. Li, "Classification of pulse waveforms using edit distance with real penalty," *EURASIP Journal on Advances in Signal Processing*, vol. 2010, no. 1, p. 303140, 2010. 2.3, 2.3

[56] C.-S. Hu, Y.-F. Chung, C.-C. Yeh, and C.-H. Luo, "Temporal and spatial properties of arterial pulsation measurement using pressure sensor array," *Evidence-based Complementary and Alternative Medicine*, vol. 2012, pp. 745127–745127, 2012. 2.3, 3.2

[57] P. Wang, W. Zuo, and D. Zhang, "A compound pressure signal acquisition system for multichannel wrist pulse signal analysis," *Instrumentation and Measurement, IEEE Transactions on*, vol. 63, no. 6, pp. 1556–1565, 2014. 2.3

[58] Y.-W. Chu, C.-H. Luo, Y.-F. Chung, C.-S. Hu, and C.-C. Yeh, "Using an array sensor to determine differences in pulse diagnosis–three positions and nine indicators," *European Journal of Integrative Medicine*, vol. 6, no. 5, pp. 516–523, 2014. 2.3

[59] J.-H. Wu, R.-S. Chang, and J.-A. Jiang, "A novel pulse measurement system by using laser triangulation and a cmos image sensor," *Sensors*, vol. 7, no. 12, pp. 3366–3385, 2007. 2.3

[60] C. Xia, Y. Li, J. Yan, Y. Wang, H. Yan, R. Guo, and F. Li, "A practical approach to wrist pulse segmentation and single-period average waveform estimation," in *2008 International Conference on BioMedical Engineering and Informatics*, vol. 2, pp. 334–338, 2008. 2.3, 5.1

[61] K. Wang, L. Xu, L. Wang, Z. Li, and Y. Li, "Pulse baseline wander removal using wavelet approximation," in *Computers in Cardiology, 2003*, pp. 605–608, 2003. 2.3

[62] L. Xu, D. D. Zhang, and K. Wang, "Wavelet-based cascaded adaptive filter for removing baseline drift in pulse waveforms," *IEEE Transactions on Biomedical Engineering*, vol. 52, no. 11, pp. 1973–1975, 2005. 2.3, 4.4.1.1

[63] L. Xu, D. Zhang, K. Wang, N. Li, and X. Wang, "Baseline wander correction in pulse waveforms using wavelet-based cascaded adaptive filter," *Computers in Biology and Medicine*, vol. 37, no. 5, pp. 716–731, 2007. 2.3, 4.4.1.1, 4.4.2.3, 5.1, 5.1

[64] W. Zong, T. Heldt, G. Moody, and R. Mark, "An open-source algorithm to detect onset of arterial blood pressure pulses," in *Computers in Cardiology, 2003*, pp. 259–262, IEEE, 2003. 2.3, 4.1.3, 4.4.2.3, 5.1

[65] B. R. Ferro, A. R. Aguilera, and R. F. de la Vara Prieto, "Automated detection of the onset and systolic peak in the pulse wave using hilbert transform," *Biomedical Signal Processing and Control*, vol. 20, pp. 78–84, 2015. 2.3

[66] B. Thakker and A. L. Vyas, "Outlier pulse detection and feature extraction for wrist pulse analysis," *World Academy of Science, Engineering and Technology, International Journal of Medical, Health, Biomedical, Bioengineering and Pharmaceutical Engineering*, vol. 3, no. 7, pp. 127–130, 2009. 2.3

[67] L. Liu, W. Zuo, D. Zhang, N. Li, and H. Zhang, "Combination of heterogeneous features for wrist pulse blood flow signal diagnosis via multiple kernel learning," *international conference of the ieee engineering in medicine and biology society*, vol. 16, no. 4, pp. 598–606, 2012. 2.3, 5.3

[68] Y. Chen, L. Zhang, D. Zhang, and D. Zhang, "Computerized wrist pulse signal diagnosis using modified auto-regressive models," *Journal of Medical Systems*, vol. 35, no. 3, pp. 321–328, 2011. 2.3

[69] D.-Y. Zhang, W.-M. Zuo, D. Zhang, H.-Z. Zhang, and N.-M. Li, "Wrist blood flow signal-based computerized pulse diagnosis using spatial and spectrum features," *Journal of Biomedical Science and Engineering*, vol. 3, no. 4, pp. 361–366, 2010. 2.3

[70] C. Xia, Y. L. J. Yan, Y. Wang, H. Y. Rui, and G. F. Li, "Wrist pulse waveform feature extraction and dimension reduction with feature variability analysis," in *2008 2nd International Conference on Bioinformatics and Biomedical Engineering*, pp. 2048–2051, 2008. 2.3

[71] J. Gong, S. Lu, R. Wang, and L. Cui, "Pdhms: Pulse diagnosis via wearable healthcare sensor network," in *2011 IEEE International Conference on Communications (ICC)*, pp. 1–5, 2011. 2.3

[72] G. Zheng, Q. Huang, G. Yan, and M. Dai, "Pulse waveform key point recognition by wavelet transform for central aortic blood pressure estimation," *Journal of Information & Computational Science*, vol. 9, no. 1, pp. 25–33, 2012. 2.3

[73] L. Zhang, W. Yang, and D. Zhang, "Wrist-pulse signal diagnosis using icpulse," in *2009 3rd International Conference on Bioinformatics and Biomedical Engineering*, pp. 1–4, 2009. 2.3

[74] Y. Sun, B. Shen, Y. Chen, and Y. Xu, "Computerized wrist pulse signal diagnosis using kpca," in *ICMB'10 Proceedings of the Second international conference on Medical Biometrics*, pp. 334–343, 2010. 2.3

[75] G. Lu, Z. Jiang, L. Ye, and Y. Huang, "Pulse feature extraction based on improved gaussian model," in *2014 International Conference on Medical Biometrics (ICMB)*, pp. 90–94, 2014. 2.3

[76] D. Zhang, W. Zuo, D. Zhang, Y. Li, and N. Li, "Gaussian erp kernel classifier for pulse waveforms classification," in *2010 20th International Conference on Pattern Recognition*, pp. 2736–2739, 2010. 2.3

[77] D. Zhang, W. Zuo, Y. Li, and N. Li, "Pulse waveform classification using erp-based difference-weighted knn classifier," in *ICMB'10 Proceedings of the Second international conference on Medical Biometrics*, pp. 191–200, 2010. 2.3

[78] H. X. Yan, Y. Q. Wang, R. Guo, Z. R. Liu, F. F. Li, F. Y. Run, Y. J. Hong, and J. J. Yan, "Feature extraction and recognition for pulse waveform in traditional chinese medicine based on hemodynamics principle," in *IEEE ICCA 2010*, pp. 972–976, 2010. 2.3

[79] Q.-L. Guo, K.-Q. Wang, D.-Y. Zhang, and N.-M. Li, "A wavelet packet based pulse waveform analysis for cholecystitis and nephrotic syndrome diagnosis," in *2008 International Conference on Wavelet Analysis and Pattern Recognition*, vol. 2, pp. 513–517, 2008. 2.3

[80] L. Xu, M. Q.-H. Meng, and K. Wang, "Pulse image recognition using fuzzy neural network," in *2007 29th Annual International Conference of the IEEE Engineering in Medicine and Biology Society*, vol. 2007, pp. 3148–3151, 2007. 2.3

[81] L. Xu, K. Wang, and L. Wang, "Pulse waveforms classification based on wavelet network," in *2005 IEEE Engineering in Medicine and Biology 27th Annual Conference*, vol. 5, pp. 4596–4599, 2005. 2.3

[82] P. Wang, S. Hou, H. Zhang, W. Zuo, and D. Zhang, "Wrist pulse diagnosis using complex network," in *2014 International Conference on Medical Biometrics (ICMB)*, pp. 15–20, 2014. 2.3

[83] C.-Y. Chung, Y.-W. Cheng, and C.-H. Luo, "Neural network study for standardizing pulse-taking depth by the width of artery," *Computers in Biology and Medicine*, vol. 57, pp. 26–31, 2015. 2.3

[84] C.-C. Chiu, S.-J. Yeh, and C.-H. Chen, "Self-organizing arterial pressure pulse classification using neural networks: theoretical considerations and clinical applicability," *Computers in Biology and Medicine*, vol. 30, no. 2, pp. 71–88, 2000. 2.3

[85] A. C. Tang, J. W. Chung, and T. K. Wong, "Digitalizing traditional chinese medicine pulse diagnosis with artificial neural network," *Telemedicine Journal and E-health*, vol. 18, no. 6, pp. 446–453, 2012. 2.3

[86] X. Hu, H. Zhu, J. Xu, D. Xu, and J. Dong, "Wrist pulse signals analysis based on deep convolutional neural networks," in *2014 IEEE Conference on Computational Intelligence in Bioinformatics and Computational Biology (CIBCB)*, pp. 1–7, 2014. 2.3

[87] OnRobot, "Onrobot omd-20-se-40n datasheet," 2018. 3.1, 4.1.1

[88] A. Tar, *Low Resolution Infrared Proximity Array Based 3D Object and Force Reconstruction, and Modular Oscillatory Arrays*. PhD thesis, Faculty of Information Technology and Bionics, Pázmány Péter Catholic University, 2012. 3.1, 3.1

[89] A. Tar and G. Cserey, "Development of a low cost 3d optical compliant tactile force sensor," in *Advanced Intelligent Mechatronics (AIM), 2011 IEEE/ASME International Conference on*, pp. 236–240, IEEE, 2011. 3.1

[90] J. M. Bland and D. Altman, "Statistical methods for assessing agreement between two methods of clinical measurement," *The lancet*, vol. 327, no. 8476, pp. 307–310, 1986. 4.1.5, 4.4.2.5

[91] J. M. Bland and D. G. Altman, "Agreement between methods of measurement with multiple observations per individual," *Journal of biopharmaceutical statistics*, vol. 17, no. 4, pp. 571–582, 2007. 4.1.5, 4.4.2.5

[92] C. Hofhuizen, B. Lansdorp, J. G. van der Hoeven, G.-J. Scheffer, and J. Lemson, "Validation of noninvasive pulse contour cardiac output using finger arterial pressure in cardiac surgery patients requiring fluid therapy," *Journal of Critical Care*, vol. 29, no. 1, pp. 161–165, 2014. 4.4.2.7

[93] A. S. Meidert, W. Huber, A. Hapfelmeier, M. Schöfthaler, J. N. Müller, N. Langwieser, J. Y. Wagner, R. M. Schmid, and B. Saugel, "Evaluation of the radial artery applanation tonometry technology for continuous noninvasive blood pressure monitoring compared with central aortic blood pressure measurements in patients with multiple organ dysfunction syndrome," *Journal of Critical Care*, vol. 28, no. 6, pp. 908–912, 2013. 4.4.2.7

[94] P. Szmuk, E. Pivalizza, R. D. Warters, T. Ezri, and R. E. Gebhard, "An evaluation of the t-line tensymeter continuous noninvasive blood pressure device during induced hypotension," *Anaesthesia*, vol. 63, no. 3, pp. 307–312, 2008. 4.4.2.7

[95] G. M. Janelle and N. Gravenstein, "An accuracy evaluation of the t-line tensymeter (continuous noninvasive blood pressure management device) versus conventional invasive radial artery monitoring in surgical patients.," *Anesthesia & Analgesia*, vol. 102, no. 2, pp. 484–490, 2006. 4.4.2.7

[96] E. Mašanauskienė, S. Sadauskas, A. Naudžiūnas, A. Unikauskas, and E. Stanke-vičius, "Impedance plethysmography as an alternative method for the diagnosis of peripheral arterial disease," *Medicina*, vol. 50, no. 6, pp. 334–339, 2014. 6.6